THE DESIGN AND IMPLEMENTATION OF MICROWAVE RECEIVER FRONT END COMPONENTS

Vhudilangi P. Netshifhire

Thesis presented in partial fulfilment of the requirements for the degree of Master of Science in engineering at the University of Stellenbosch

Supervisor: Prof. Petrie Meyer

June 2005

Declaration

I, the undersigned, hereby declare that the work contained in this thesis is my own original work, unless stated otherwise, and that it has not previously in its entirety or in part been submitted at any university for a degree.

V. P. Netshifhire: Date:.

Abstract

Different types of RF and Microwave receiver systems architectures are investigated. The superheterodyne receiver characteristics are studied qualitatively. A three components system (LNA, Mixer and VCO) is selected and the components are first measured individually, and then measured as a single system. A monofilar axial mode helix antenna is designed, simulated using FEKO and constructed. A narrow band interdigital bandpass filter is designed using the capacitance network and its transformation, and it is simulated using two different simulation packages, CST Microwave Studio and AWR Microwave Office. Two filter prototypes are fabricated using cylindrical rods. An open circuited microstrip resonator oscillator is designed and implemented through the negative resistance method. Its performance is verified using the harmonic balance simulator in AWR MWO. A single balanced mixer is designed and implemented using 180^{o} hybrid junction (rat-race) and it is also fabricated using microstrip transmission line technology. All designed components performed well in comparison to their predicted performance. The LNA and three of the designed components (Filter, Oscillator and a Mixer) are connected together and characterized as a single four block system. The system performed well except for the IF signal which shift to a lower frequency due to oscillator load pulling.

Opsommming

Die argitektuur van verskeie RF en Mikrogolf ontvanger stelsels word ondersoek. Die "superheterodyne" ontvanger eienskappe is kwalitatief bestudeer. 'n Stelsel wat uit drie komponente bestaan (LNA, Menger en VCO) is bestudeer. Die individuele komponente is eers gemeet en daarna die stelsel as 'n eenheid. 'n "Monofilar" aksiale modus heliks antenna is ontwerp, gesimuleer met FEKO en gebou. Verder is 'n nouband inter-digitale banddeurlaat filter ontwerp met behulp van die kapasitiewe network metode en sy transformasie. Hierdie ontwerp is gesimuleer deur van twee verskillende sagteware pakette gebruik te maak, naamlik CST Microwave Studio en AWR Microwave Office. Twee filter prototiepes is gebou met silindriese stafies. 'n Oopgeslote mikrostrook ossilator is ontwerp en geimplementeer deur negatiewe weerstand te gebruik. Die stelsel se prestasie is bevestig deur gebruik te maak van 'n harmoniese balans simulator in AWR MWO. Verder is 'n enkelbalans menger ontwerp en geimplimenteer via 'n 180° hibriede verbinding ("rat-race"). Hierdie menger is gebou met mikrostrook transmisielyn. Al die ontwerpte komponente werk goed in vergelyking met die voorspelde resultate. Die LNA, filter, ossilator en menger word gekoppel en gekarakteriseer as 'n vier blok stelsel. Die stelsel werk goed behalwe vir 'n skuif in die IF-sein by laer frekwensies a.g.v. belasting.

Acknowledgements

During the course of these studies many people supported this work in many ways and their contribution made these studies to be at the state they are today: complete.

I would like to thank my supervisor Prof. Petrie Meyer for the guidance that is equal to none, for introducing me to Microwave Electronics since the early dark days to the now bright light, again for the support you gave me outside academic life.

Secondly thanks to my parents Mr. TW Netshifhire & Mrs. AP Netshivhilidulu, you are the pillars of my strength since you believed I can, sorry for being away so long, I will see you more often now.

DR Riana H. Geschke, Prof. JB de Swardt thanks for your valuable help, meetings and discussions. They were vital for me in many ways.

Mr Wessel and the team at SED thanks for the rush and another filter again.

Robert and Valpre`, Mr Martin Siebers, Andi, Rembu and all the E212 guys thanks for every input, help and suggestion.

Mmbangiseni, Elelwani, Rabelani, Rofhiwa, Rialivhuwa and others its your turn now

Lastly and most importantly thanks to the lord for providing me with the strength and ability to accomplish many challenges I faced during the course of these studies.

List of Abbreviations

UHF	Ultra High Frequency
RF	Radio Frequency
LO	Local Oscillator (Frequency)
IF	Intermediate Frequency (Signal)
RFID	Radio Frequency Identification
GPS	Global Positioning System
TRF	Tuned Radio Frequency Receiver
BPF	Band Pass Filter
LPF	Low Pass Filter
MDS	Minimum Detectable Signal
η_o	Characteristic impedance of free space
Z_o	Characteristic impedance in ohms
F	Noise Figure
P1dB	1 dB Compression Point
LNA	Low Noise Amplifier
VCO	Voltage Controlled Oscillator
AWR MWO	Applied Wave Research Microwave Office
dBm	Decibel with respect to 1 mW
HPBW	Half Power Beam width
BWFN	Beam width First Null
AUT	Antenna Under Test
HP	Hewlett and Packard
TL	Transmission Line
k_o	Wave Number
ε_r	Dielectric constant
ε_e	Effective Dielectric Constant
U.S	University Of Stellenbosch
μ_0	Permeability of free space
ω	Angular Frequency = $2\pi f$

Table of Contents

List of Figures

List of Tables

1. The Receiver Front End

1.1 Introduction

1.1.1 Receiver Review

Wireless communication using RF energy is known to have started with the theoretical work of Maxwell, followed by experimental verification by Hertz of electromagnetic wave propagation and the commercial development of practical radio systems by Marconi [1]. The receiver is often the most critical component of a wireless communication system where its main purpose is to recover a desired signal from a wide spectrum of transmitting sources, noise and interference [21]. The receiver must be selective and sensitive enough to detect even a weak signal among many other, possibly stronger signals [9]. A good receiver needs to cope with overload from in-band stronger signals, which lead to a concept of minimum detectable signal, dynamic range and automatic gain control [21]. UHF to millimeter wave receivers are now employed due to spectrum overcrowding and the need for high data rate receivers [1]. RF and microwave receivers offer wide bandwidth, and have the added advantage of penetrating dust, fog and even buildings to some extent [1]. Today wireless systems receivers are found in broadcast radio and television, Cellular telephone systems, Direct broadcasting satellite, Wireless local area networks, GPS, RFID and many more.

1.1.2 Thesis Overview

The aim of the project is to characterize a microwave receiver front end that can be used in a data link system, and design some of its components. The focus of this project is the superheterodyne architecture of microwave receiver front end and four components which are the Antenna, Filter, Oscillator and a mixer. The receiver architectures are mentioned and the superheterodyne receiver is briefly discussed. Dynamic range, frequency conversion, filtering and other performance parameters of the receiver front end are discussed and also the receiver specifications and power requirement. The thesis is further structured as outlined in the following page.

Chapter 2

In this chapter three off-the-shelf components, the Low noise amplifier, voltage controlled oscillator and a mixer were selected and characterised in comparison with their specified performance and were integrated and measured as a single subsystem.

Chapter 3

The chapter discusses a monofilar axial mode helix antenna design. It gives the general antenna definitions and helix antenna parameters. The helix antenna is designed with reference to the optimum performance criterion and the antenna is constructed and tested at University of Stellenbosch antenna chamber.

Chapter 4

The chapter gives a brief description of interdigital lines and their characteristics with respect to capacitance network transformation. A 5^{th} order interdigital filter is designed using the capacitance network transformation technique. Small in-house codes were used to realise the physical parameters of the filter and the filter is constructed and measured.

Chapter 5

A negative resistance model is used to design a fixed frequency oscillator. A careful look into biasing circuit and a simple resonator is performed. Nonlinear simulations are performed to verify the system performance. The oscillator is constructed and its parameters measured.

Chapter 6

A brief description of diode mixers is given with a more dedicated investigation to balanced mixers. A small signal approximation theory is outlined and is used to design a 180^{o} hybrid junction single balanced diode mixer. The mixer is simulated, constructed and measured.

Chapter 7

This chapter gives the performance measurements of the integrated system which consist of an amplifier (off-shelf), designed interdigital filter, oscillator and mixer. The linearity and the compression point of the system are given. The spurious rejection and radiation were also measured.

Chapter 8

This chapter gives thesis conclusion and recommendation.

1.2 Receiver Front End

1.2.1 Subsystems Description

Antenna

An antenna is a device that converts a guided electromagnetic wave on a transmission line to a plane wave propagating in free space. In its basic form one side of an antenna can be taken as an electrical circuit element, while the other side provides an interface with a propagating plane wave. Most antennas can be used as bidirectional, meaning they can be used to transmit and receive [9].

Filter

A filter is a two port network used to control the frequency response at a certain point in a communication system by providing transmission at frequencies within the passband of the filter and attenuation in the stopband of the filter [1 and 19]. Often filters on UHF to millimeter wave frequencies are passive.

Amplifier

It is a device that increases the voltage, current or power of the signal. They can be categorized as either weak-signal (small signal) or power amplifiers. Usually weak-signal amplifiers are primarily used in receiver systems while the power amplifiers are used in transmitting system.

Oscillator (LO)

A single port nonlinear subsystem which is used to convert dc signals to radio frequency (RF) signals. It also uses a nonlinear device like transistor or a diode. It can be used for carrier generation in transmitters and also in the local oscillator (LO) used for receiver signal processing.

Mixer

A three port frequency translation device or system used to down-convert the RF signal to the intermediate frequency (IF) for convenient signal processing [32]. It can also be used in up-

conversion if implemented in a transmitter. The circuit should be able to preserve the information contained in the RF signal.

1.2.2 Receiver architectures

The components mentioned in section 1.2.1 are virtually found in all RF and microwave analog receiver front ends. A well designed radio receiver must provide the following requirements [21]

- High gain to restore the low power of the received signal to a level where signal processing can be easily carried out.
- Good selectivity in order to receive the normally low desired signal while rejecting the adjacent channels, image frequencies and other interference.
- Down-conversion of the received RF frequency signal to an IF frequency signal for processing.
- Detection of the received information and isolation from transmitter to avoid saturation of the receiver (mostly in case of transceiver).

There are various types of receiver front ends, of which all of them use similar components with only difference in overall performance. They can be classified as outlined below [21]

Tuned Radio Frequency Receiver (TRF)

These are the earliest receiving circuits to be developed, and they are consist of several stages of amplification along with tunable bandpass filters to provide high gain and selectivity [21]. The tunability is accomplished by using mechanically variable inductors and capacitors. The disadvantages are the need to individually tune various components, poor selectivity due to broadband filters and a limit to the gain because amplification is performed at the RF frequency [21]. Today they are very costly and complex to design due to high performance requirements of modern systems. In microwave systems they are very costly due to high cost on tunable high frequency components and thus TRF are not often used. The block diagram of the TRF receiver is given in figure 1-1.

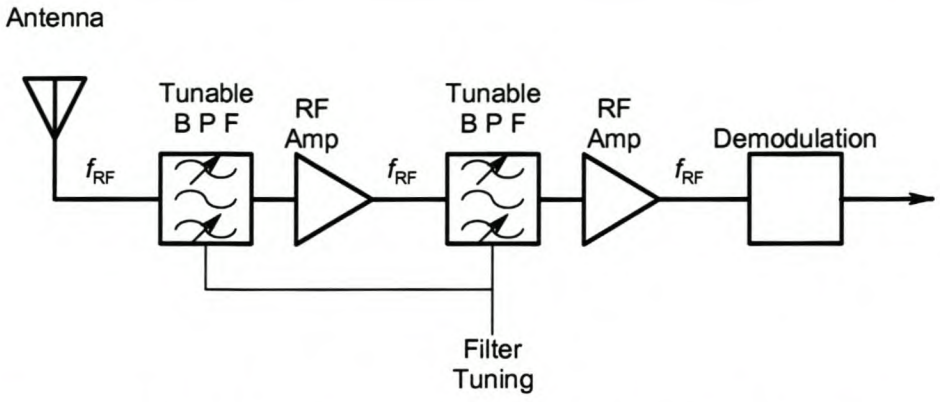

Figure 1-1: The block diagram of the tuned radio frequency receiver [21]

Direct Conversion Receiver (Homodyne)

This receiver uses a mixer and a local oscillator to perform frequency down conversion with zero IF frequency [21]. The local oscillator has the same frequency as the RF signal which is directly converted to baseband. Homodyne receivers offer more advantage as compared to TRF receivers such as better selectivity and that gain can be spread through RF and baseband stages [21 and 25]. Homodyne receivers are inexpensive compared to heterodyne receivers [explained in the next subsection], they don't suffer from image frequency problems and they have low power consumption [9]. The disadvantages are that the LO must be very precise and stable and they suffer from dc offset leakage from the LO [9]. These types of receivers find applications in Doppler radars where the exact LO can be obtained [21], new RF and Microwave systems in chip format also uses this architecture [33].

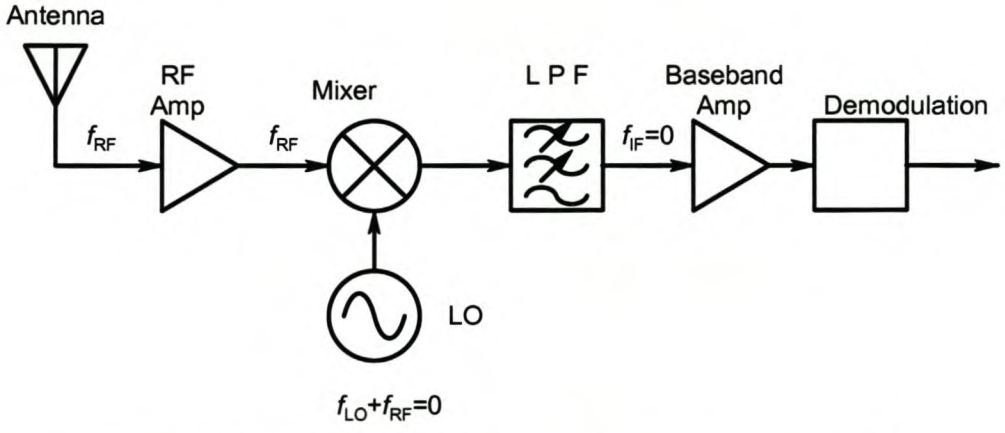

Figure 1-2: The block diagram of a homodyne receiver [21]

Superheterodyne Receiver

It is the most widely used form of receiving circuits in use today. In this receiver a signal from the antenna is first filtered and then amplified by a low noise amplifier (LNA). A frequency synthesizer generates an accurate LO signal and the mixer down-converts the signal to IF, where it is normally filtered and amplified before demodulation. In cases where the signal level may vary significantly, the IF gain is controlled with an automatic gain control (AGC) in order to avoid saturation [9]. The block diagram of the superheterodyne receiver is similar to the homodyne with a difference that the RF and LO signals are different and tuning in this receiving systems is accomplished by varying the LO frequency [1]. The mixing process of superheterodyne receiver between the input RF and the output LO signal can be described mathematically as [25]

$$f_{IF} = | f_{RF} \pm f_{LO} | \tag{1-1}$$

where f_{IF} is the output or Intermediate frequency, f_{RF} is the received frequency and f_{LO} is the local oscillator frequency. The process described above results in fundamental output terms at two frequencies which are the absolute sum and difference of f_{RF} and f_{LO} [25]. In practice often one is used and the desired signal is selected using the IF filter. Typically after the IF frequency the signal is demodulated and passed through another circuit for further processing depending on the final requirements of the information.

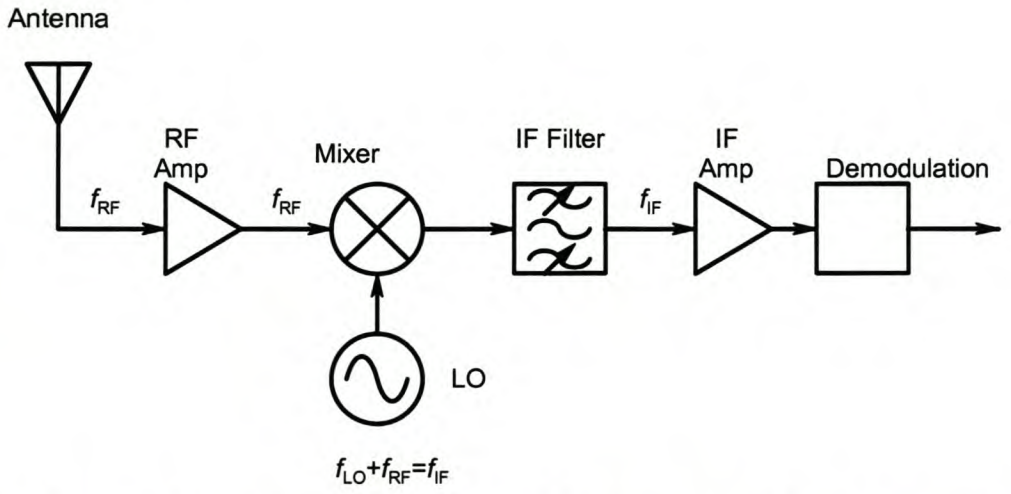

Figure 1-3: The block diagram of a typical single stage IF superheterodyne receiver [21]

1.2.3 System Performance Parameters

This section describes the fundamental performance parameters of a receiving system front end with reference to a superheterodyne down converting architecture.

Link Budget

Link budget is usually the first step in the analysis of a wireless communication system. To transfer a radio signal from point A to point B, it is necessary to transmit a signal of adequate power in the right direction [26]. The power level on the receive side of the system is determined using the Friis formula [27]

$$P_r = P_t G_t G_r \left(\frac{\lambda}{4\pi R}\right)^2 \tag{1-2}$$

where P_t and G_t are the transmitted power and gain respectively, while P_r and G_r are the received power and gain respectively, R is the distance between the two antennas and λ is the transmission wavelength. Figure 1-4 shows the setup assumed by the Friis formula.

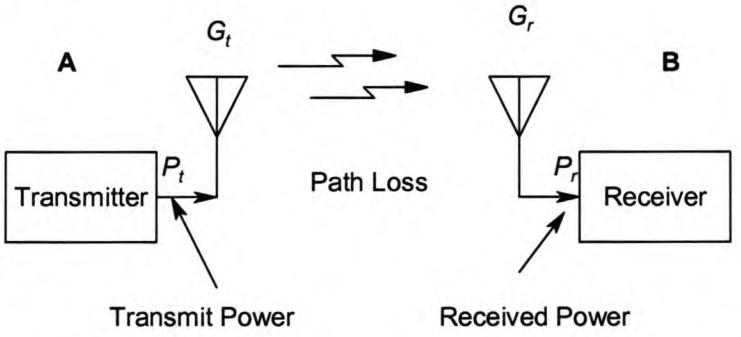

Figure 1-4: Elements of the wireless communication system [27]

From equation (1-2) the squared terms in brackets are sometimes termed path loss [27]. The Friis formula however is more accurate in point to point communications where there is no obstruction in the line of sight. For mobile and other systems which also rely on signal reflections from buildings and other obstacles the model can be more involved. In some systems reflection is good and in some it is not good. The system requirements determine the model which can be used to estimate the transmitted signal strength at the receiver. In some system more than one antenna can be used in a diversity scheme where the receiver chooses the antenna with the best quality signal at a given moment [9 and 26].

Minimum Detectable Signal (MDS)

Reliable communication requires a signal power equal or greater than a given minimum level. If the system noise power is known the MDS can be used to determine the signal to noise ratio (SNR) of the system at the demodulator of the receiver [21]. Minimum SNR is sometimes expressed in terms of SINAD which is the ratio of a wanted signal power plus noise plus distortion (SND) to the unwanted signal power which is noise plus distortion (ND) and is given by [21].

$$SINAD = \frac{S+N}{N} \tag{1-3}$$

where S and N are wanted signal and unwanted signal respectively. If it is assumed that the antenna delivers an input signal level S_i to the receiver including the noise characterized by antenna temperature T_A [21] and using the receiver's complete system power gain, G, and its noise figure, F, which is related to its effective noise temperature by [21]

$$T_e = (F-1)T_0 \tag{1-4}$$

together with the output signal to noise ratio defined as S_o / N_o applied to the input of the demodulator, the output signal power can be written as [21]

$$S_o = GS_i \tag{1-5}$$

The total output noise power can be written as [1 and 21]

$$N_o = kBG(T_A + T_e) \tag{1-6}$$

where B is the receiver bandwidth often set by the IF bandpass filter. The minimum detectable input signal is [21]

$$S_{i_{\min}} = kB[T_A + (F-1)T_o](\frac{S_o}{N_o})_{\min} \tag{1-7}$$

In a case where $T_A = T_o$ equation (1-7) reduces to [21]

$$S_{i_{\min}} = kBT_oF(\frac{S_o}{N_o})_{\min} \tag{1-8}$$

which can be expressed in dB as [21]

$$S_{i_{\min}} = -174dBm + 10\log B + F(dB) + (\frac{S_o}{N_o})_{\min}(dB) \tag{1-9}$$

The results of equation (1-8) and (1-9) are only valid when the antenna temperature is 290 K which is not often true in practice [21]. The actual minimum detectable signal is approximated by equation (1-7). If the MDS is converted into voltage using a given receiver impedance it is

referred to as voltage sensitivity or simply sensitivity. The relationship between MDS and the voltage sensitivity is [21]

$$V_{i_{\min}} = \sqrt{2Z_0 S_{i_{\min}}} \tag{1-10}$$

and is usually given in microvolts. MDS and sensitivity do not depend on the gain of the system since noise and input signal are equally amplified [32].

Dynamic Range

As mentioned earlier, receivers should be able to accept signals when they are very close to a transmitter. The power level of this signal is usually bigger than when the receiver is far away from the transmitter and the Friis equation is usually employed to estimate relevant power levels. The maximum allowable signal together with MDS set the receiver dynamic range, defined as [21]

$$DR_r = \frac{\text{maximum allowable signal power}}{\text{minimum detectable signal power}} \tag{1-11}$$

Dynamic range depends on the noise characteristics of the receiver, modulation type and the required minimum SNR. The maximum allowable signal is defined as the maximum input power level before the level where the intermodulation distortion becomes unacceptable or the RF amplifier or any element in the system becomes compressed.

Compression and Intermodulation distortion

A continuous increase of input power on the amplifier input port will result in a state where the output no longer responds linearly with the input. The P1dB is the power level for which the output power level has decreased by 1dB from ideal characteristics [21]. A receiver compression point may also be reached when one of its components is driven at or above its 1 dB compression point and that may lead to harmonic distortion. AGC circuits can also be employed in some RF amplifier to compensate for high level input signals, though are normally employed at IF stages. To avoid RF stage compression the received signal S_i has to satisfy equation (1-12) [21]

$$S_{i_{\max}} + G_{RF} < P1dB \tag{1-12}$$

where G_{RF} is the gain of the RF stage , and $P1dB$ is the 1 dB compression point at the output of the RF amplifier (G_{RF} and $S_{i_{\max}}$ are in dB). The P1dB can be replaced by the third order intercept point in an unusual situation where it is lower than the 1 dB compression power.

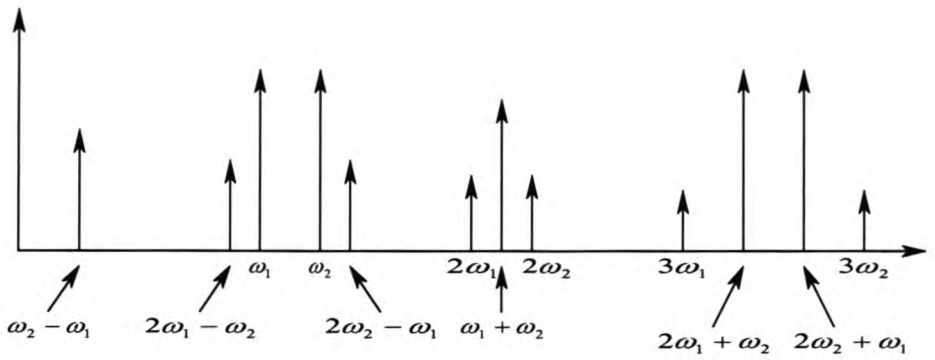

Figure 1-5: The output spectrum of second and third two-tone intermodulation products assuming $\omega_1 < \omega_2$

Figure 1-5 gives the first, second and third order intermodulation products which are often produced by a nonlinear circuit or system. The third order products are $3\omega_1$, $3\omega_2$, $2\omega_1+\omega_2$, $2\omega_2+\omega_1$, $2\omega_1-\omega_2$, $2\omega_2-\omega_1$ and the first four are located in higher frequencies, often outside the band [21]. The inband third order intercept point is usually caused by the difference third order intermodulation products ($2\omega_1-\omega_2$, $2\omega_2-\omega_1$). A given signal which consist of many frequencies with varying amplitude and phase, the resulting inband third intermodulation products will cause distortion of the output signal and this phenomenon is called third order intermodulation distortion [21 and 1].

Selectivity

This is the measure of a receiver to select the desired signal frequency and discriminate against the unwanted signals (usually from adjacent channels) [32]. From equation (1-1) and considering lower side band IF, the receiver responds to an RF image frequency separated by twice the IF frequency. The image frequency is given by [14 and 21]

$$f_{IM} = f_{RF} - 2f_{IF} \tag{1-13}$$

where f_{IM} denote image frequency. This signal can be removed from the band either using image rejection mixer or through filtering if it is out of the RF band.

Ensuring that the image frequency is out of the RF bandwidth it is necessary to have [21]

$$f_{IF} > \frac{B_{RF}}{2} \tag{1-14}$$

where B_{RF} is the RF bandwidth of the receiver. This requirement becomes impossible in wide band receivers where the IF has to be kept low for easy processing and components availability. Good selectivity is often achieved by a preselect filter placed between the antenna and the RF

amplifier, this filter rejects out of band signals and prevent strong signals from compressing the RF (LNA) amplifier. If the RF filter cannot reject the image frequency, an image reject filter is sometimes inserted after the preselect filter. Since the LO frequency is normally close to RF and its signal is normally higher, the image reject filter, amplifier reverse attenuation, preselect filter and mixer LO to RF isolation helps to prevent such signal from leaking back to the front end and get radiated by an antenna [21]. The IF filter is responsible for setting the overall noise bandwidth of the receiver and removing most of the unwanted mixer products and other spurious signal [21]

Spurious Free Dynamic Range

The nonlinear operation of a mixer or other nonlinear device result in the sum and differences of the input signals together with smaller levels of power at the intermodulation products at frequencies given by [1, 21 and 25]

$$f = | mf_{RF} - nf_{LO} | \tag{1-15}$$

where m and n are positive integers. Many of these products are found outside the band since they spread all over the spectrum, whence some may fall within the IF bandwidth [21]. These signals are referred to as spurious response and are unwanted because a receiver may respond to undesired signals at RF frequencies that produces spurs within the IF passband [21]. The power of these spurious responses normally decreases with an increase of the order of the spurious signal. The spurious free dynamic range is the maximum output signal power for which the third order intermodulation product is equal to noise level of the component [21]. Double balanced mixers reject all spurious responses where either m or n is even and singly balanced mixer may also reject some spurious response, though not as much as the double balanced mixer [21].

Noise Figure

Noise in the receiver is often due to thermal noise, where a single element noise is modeled as a resistor with an absolute temperature of T Kelvin and is given by [27]

$$N = kTB \tag{1-16}$$

where k is Boltzmann's constant, T is the absolute temperature of the input noise source and B is the effective noise bandwidth of the system [27]. Noise figure is a measure of the amount by which an element or system increases the given noise power relative to signal power. It is expressed in dB and it is sometimes referred to as noise factor if given in linear scale [27]. Here it is referred to as noise figure.

$$F = \frac{N_{out}}{N_{in}} \tag{1-17}$$

where N_{in} is the input noise power and N_{out} is the output noise power of the two port element. A complete system is characterized by a cascade of two port elements where each element has its own gain and noise figure.

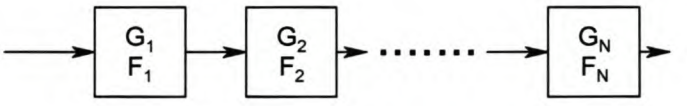

Figure 1-6: A cascade of two port elements

The gain of the complete system is given by

$$G = G_1 \times G_2 \times .... \times G_N \tag{1-18}$$

and the overall noise figure is given by [27]

$$F = F_1 + \frac{F_2 - 1}{G_1} + \frac{F_3 - 1}{G_1 G_2} + ... + \frac{F_N - 1}{G_1 G_2 .....G_{N-1}} \tag{1-19}$$

The noise figure of the first element is added directly to the noise figure of the complete system, while subsequent contributions are added and divided by the gains of the prior elements [27]. The noise figure of the first element should be minimized while increasing its gain since its noise dominates the system noise figure. In practice by trying to lower the noise figure of an element usually its gain is reduced, often a balance between a gain and a noise figure must be achieved [27]. The noise figure of the passive components can be approximated to be their insertion loss if they don't contain many resistive elements.

1.2.4 Proposed Front End Requirements

In the proposed receiver front end, only five components are considered which are Antenna, Filter, RF amplifier (LNA), Oscillator and a Mixer. The proposed receiver front end had to receive a 1 watt power transmitted 10 kilometers away using 12 dB gain antenna which is identical to the transmitter antenna. The receiver is to have an RF and IF bandwidth of 100 MHz and 10 MHz respectively and an IF system with a sensitivity of approximately -60 dBm. The receiver front end power requirements were determined using equation (1-2) and the receiver block diagram is given in figure 1-7.

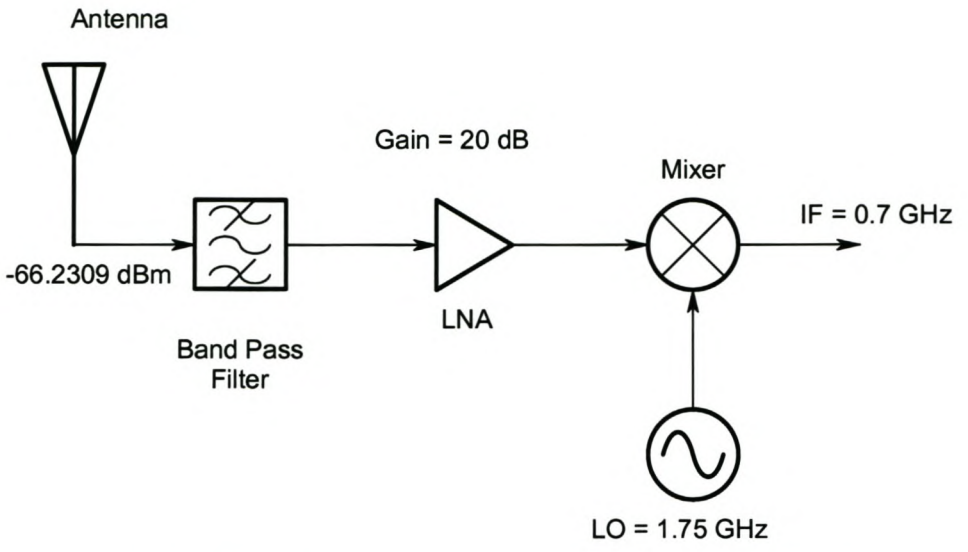

Figure 1-7: The ideal block diagram of the proposed receiver front components

Parameter	Performance Measure
Transmission Frequency	2.45 GHz
Estimated Received Power	-66.2309 dBm
Antenna Gain	12 dBi
Preselect Filter bandwidth	100 MHz
LNA Gain	20 dB
Intermediate Frequency	0.7 GHz
Local oscillator frequency	1.75 GHz
MDS at IF (Sensitivity)	-60 dBm (0.22 mV)

Table 1-1: Receiver requirements summary

2. Receiver Using Commercially Available Components

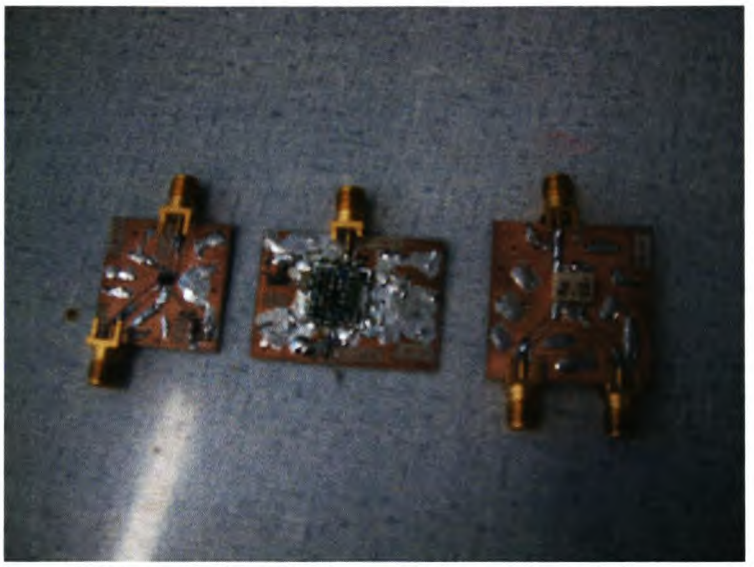

From left to right are LNA, VCO and Mixer selected for measurements

2.1 Introduction

Three commercial components namely a Low Noise Amplifier (LNA), Voltage controlled Oscillator (VCO) and a Mixer were measured and their characteristics were compared to their published specifications. These components were integrated and measured as a small receiver front end system without a filter, where spurious radiation, linear range, compression point, image and IF rejection were measured.

2.2 LNA (HMC286)

The HMC286 LNA was selected from Hittite Microwave Corporation and is specified to operate between 2.3 and 2.5 GHz for spread spectrum applications, provides 17 dB of gain, 1.8 dB noise figure and has an input reflection coefficient of better than -15 dB across the 100 MHz band from a single positive +3V power supply that consumes 8mA. In addition, a typical output 1 dB compression point of 0 to 5 dBm and the output third order intercept point of 10 to 13 dBm is specified. The 17 dB gain of the LNA is lower than proposed for the system, but was deemed acceptable due to its low noise figure as compared to other available packages.

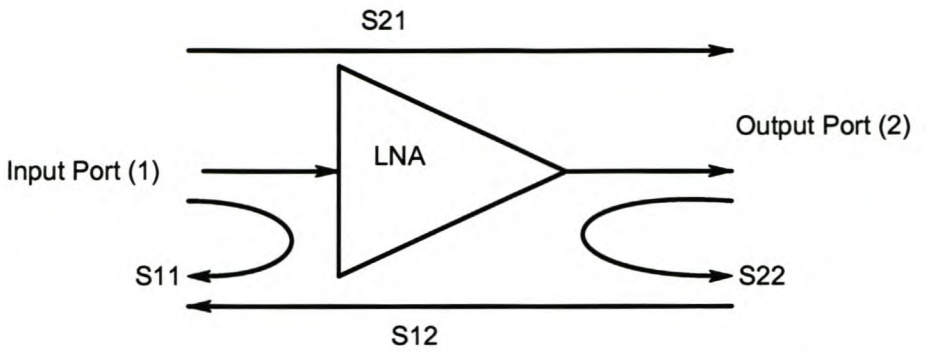

Figure 2-1: The amplifier measurement parameters model

The model in figure 2-1 represents parameters used to characterize the amplifier's operation using the Network Analyser. S21 is the gain of the amplifier and sometimes the gain is bigger than S21 if the measured component incorporates to further matching. S11 and S22 are the input and output reflection coefficients respectively. S12 is referred to as reverse signal isolation and is usually very low. Amplifiers with zero or very low S12 are called unilateral amplifiers, which is rarely true in practice.

The LNA Spectrum Analyzer Measurements

In order to evaluate the linear range of the LNA, the power sweep is performed and its measurement setup is shown in figure 2-2.

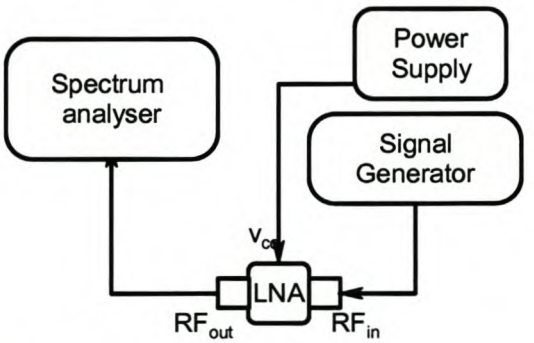

Figure 2-2: The LNA Spectrum analyzer measurement set up

The signal generator power was swept from -90 dBm to -10 dBm at the RF center frequency of 2.45 GHz. The span and resolution bandwidth were 100 MHz and 100 KHz respectively. The gain of the amplifier is given by the gradient of figure 2-3.

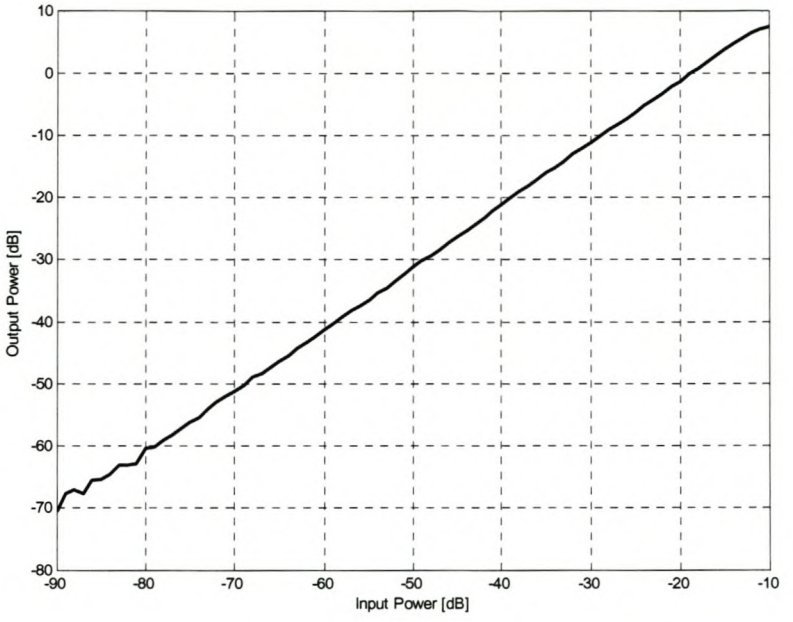

Figure 2-3: The Input power versus output power plot of the amplifier's response

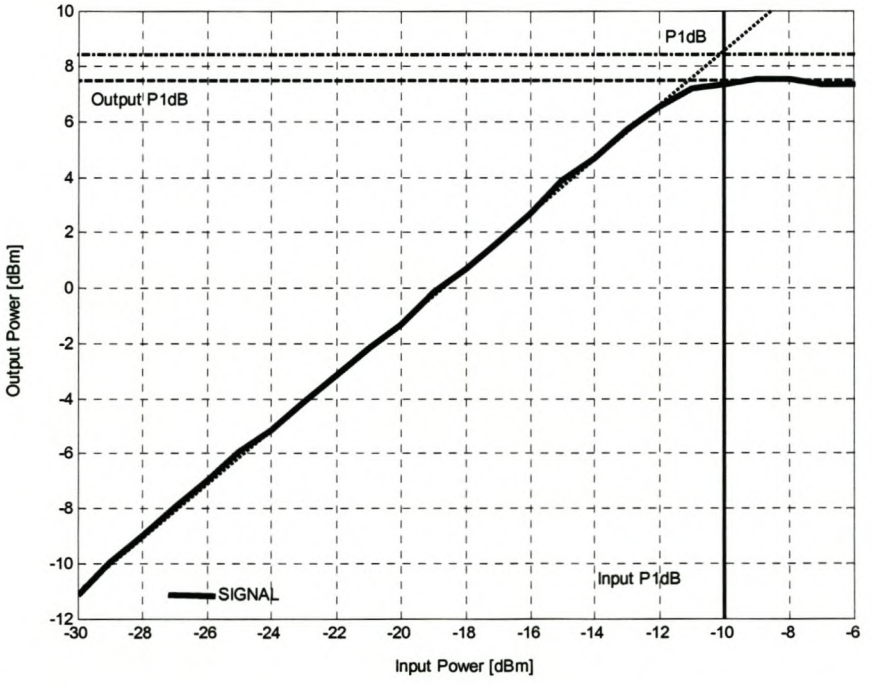

Figure 2-4: The curve showing maximum power to achieve linear gain and compression point of the LNA

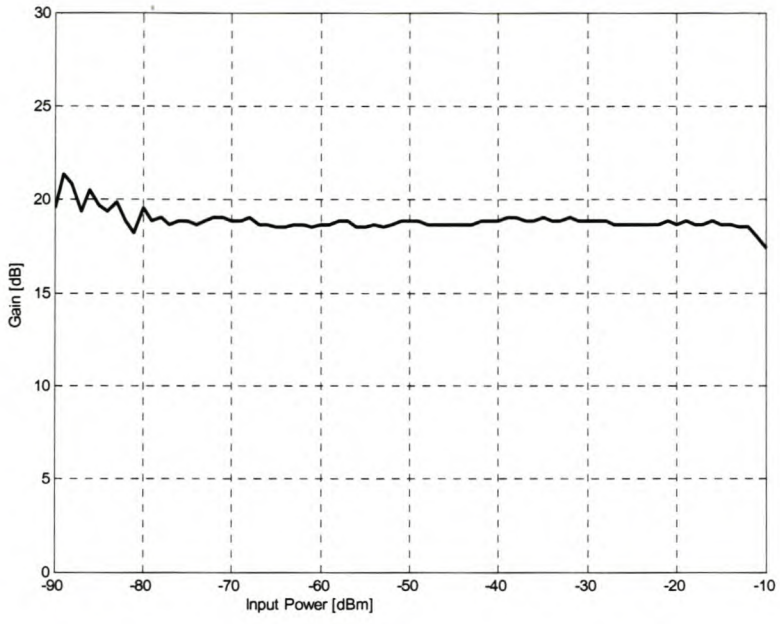

Figure 2-5: The gain of the amplifier determined from the gradient of the input versus output power curve in figure 2-3

From figure 2-3, the amplifier is linear until -10 dBm input power. The gain is obtained by subtracting input power from the output from figure 2-3 and it is about 18.6 dB. Figure 2-4 is measured from a power swept from 30 dBm to -5 dBm in order to completely reach the amplifier's 1 dB compression point. The span and resolution bandwidth of the spectrum analyzer were 10 MHz and 100 KHz respectively. The input 1 dB compression point is -10 dBm and the output 1 dB compression point is 7.5 dBm. Figure 2-5 gives the input versus gain of the amplifier. The gain flatness with respect to input power remains within ±0.5 dB.

The LNA Network Analyzer Measurements

From the linear range measurement setup using a spectrum analyzer, the gain and the compression points of the LNA is obtained but the reflections of the amplifier remain unknown. The network analyzer is used to measure such reflections and also the amplifier gain. The parameters which are measured by the network analyzer are as provided by figure 2-1.

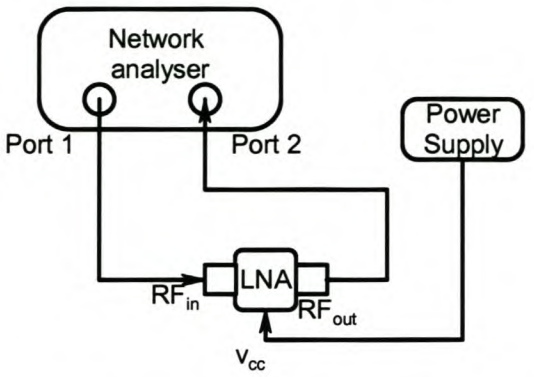

Figure 2-6: The LNA vector network analyzer measurement setup

The LNA was measured using an HP8753C network analyzer over a 2 to 2.9 GHz frequency band using +3V power supply. Figure 2-7 gives the amplifier's measured gain (S21), which is 19.2 dB at 2.45 GHz and it is between 18.4 and 19.5 dB across the 100 MHz RF bandwidth of interest. The input reflection coefficient is less than -13 dB within the RF bandwidth, while the output reflection coefficient is -4.8 dB. Figure 2-8 compares the amplifier at different bias conditions. The higher voltage bias condition has a better gain and output return loss but worsen the input return loss and noise figure at the frequency of interest. Poor return losses were tolerated to satisfy the minimum noise figure requirement.

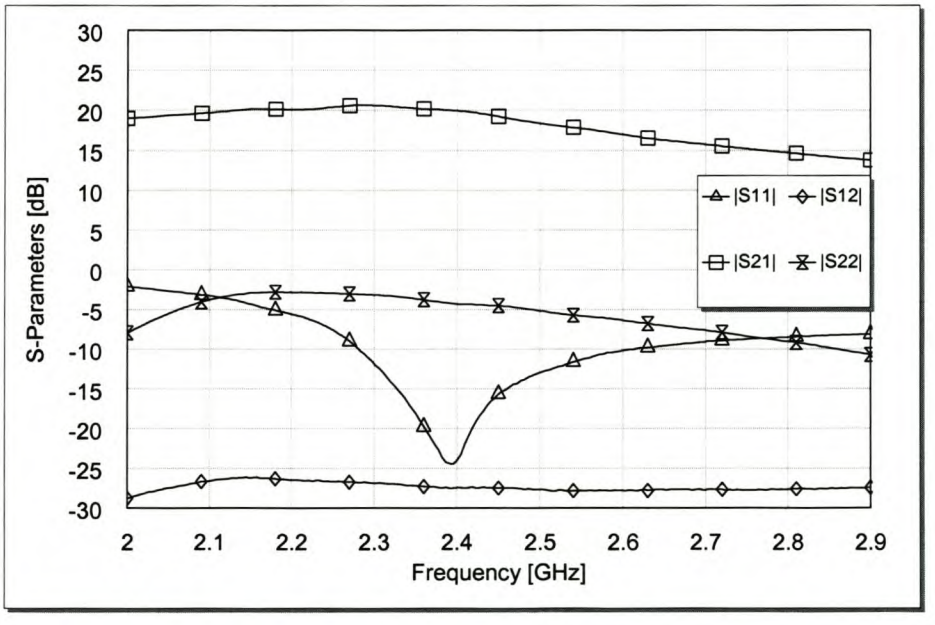

Figure 2-7: The amplifier response measured with 3V power supply

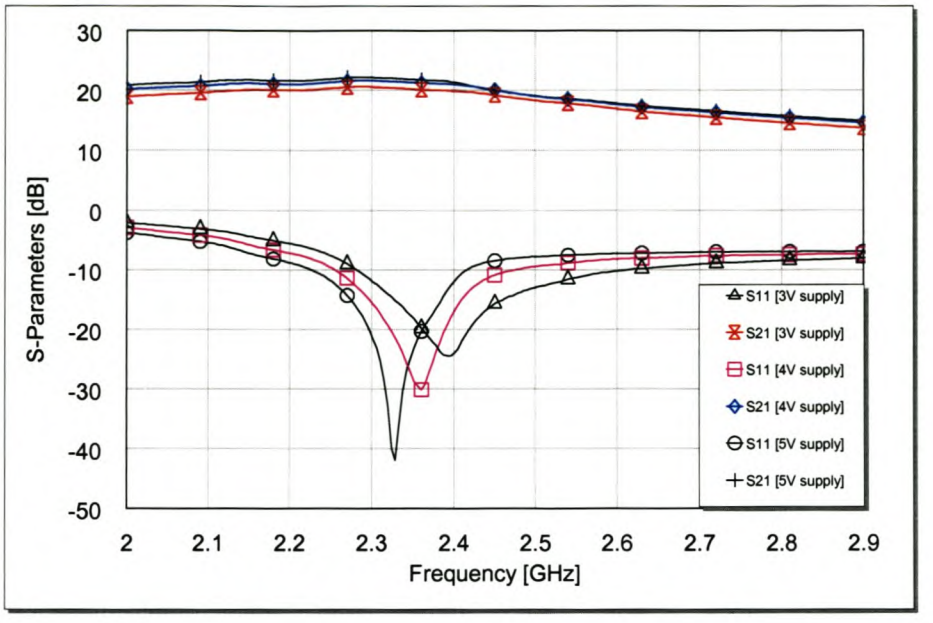

Figure 2-8: The comparison between different power supply conditions

The amplifier's noise figure was also measured using an agilent N8975A noise figure analyzer. The frequency swept was 2 to 2.9 GHz and the measured noise figure remains less than 1.95 dB in the RF frequency passband which is 100 MHz centered at 2.45 GHz.

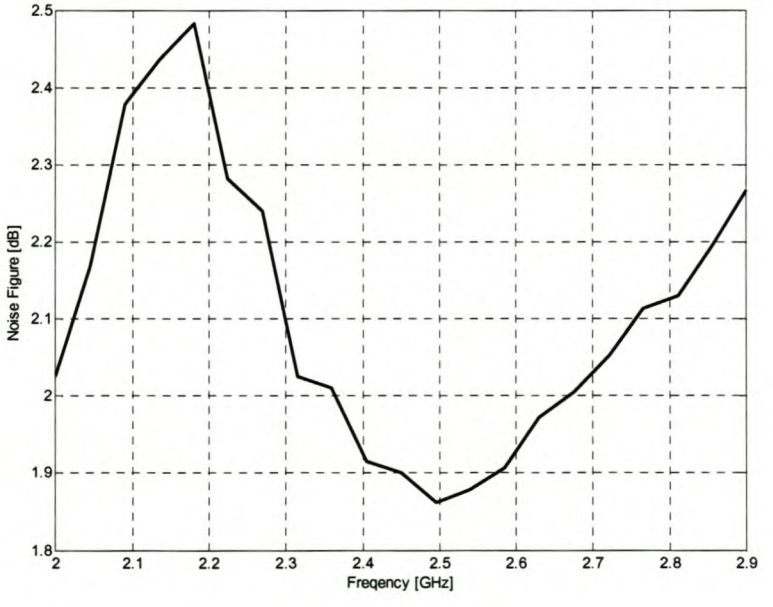

Figure 2-9: The measured noise figure of the amplifier

Parameters from the data sheet		Measured
Parameters	Typical Performance	Performance
Frequency Range [GHz]	2.3 – 2.5	2.3 – 2.5
Gain [dB]	17	18.6
Gain Flatness [dB]	±0.5	±0.5
Output P1dB [dB]	5	7.5
Noise Figure [dB]	1.8	1.95 dB
Input return Loss	10	13 dB
Output Return Loss	6-9	4.8

Table 2-1: The summary of amplifier specified and measured performance

The measured response agrees well with the specified performance except the output return loss which is poor. The gain and the P1dB are much greater than expected, hence the amplifier can be used for the intended application. The amplifier measurements were successfully accomplished.

2.3 Mixer

The mixer selected for measurements is a mini-circuits ADE-28 passive down conversion mixer. It is specified to operate with RF and LO frequencies of between 1500 MHz to 2800 MHz, an IF frequency of DC to 1000 MHz, a typical conversion loss of 5.1 dB and a maximum of 8.2 dB. It is further specified that the typical LO to RF port isolation is 30 dB (minimum is 21) and the typical LO to IF isolation is 27 dB (minimum is 17 dB). The mixer is also specified to operate with 7 dBm LO power and to have 8 dBm third order intercept point.

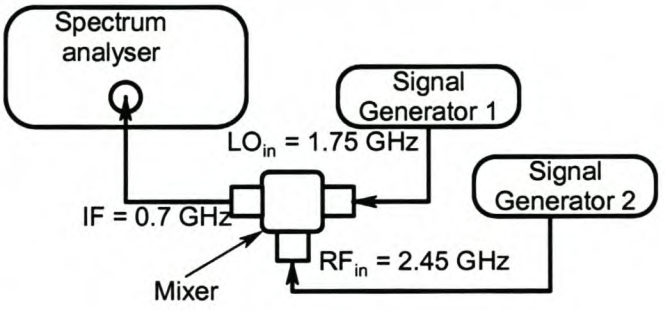

Figure 2-10: The mixer conversion loss Measurement setup

The RF input power was swept from -65 to 0 dBm and the LO input power was at 7 dBm, with the span and resolution bandwidth of the spectrum analyzer at 1 MHz and 3 KHz respectively. The output power responded linearly through out the swept power scale. The conversion gain is obtained by subtracting input from the output power from the graph in figure 2-11.

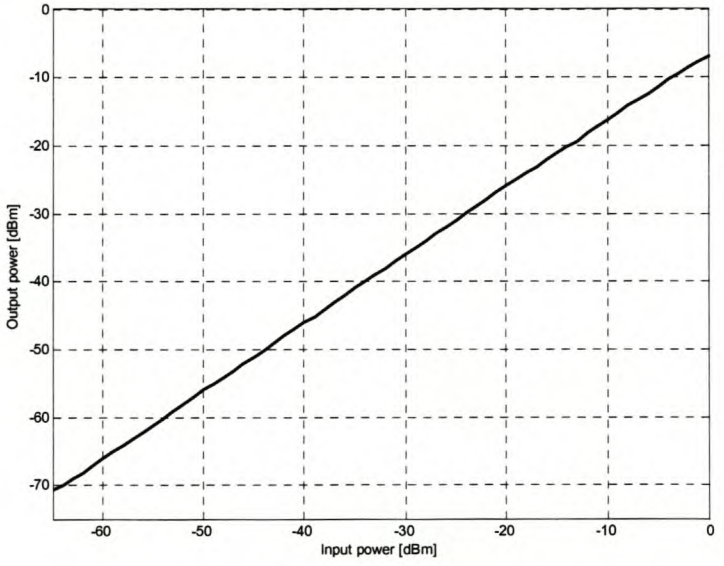

Figure 2-11: The input (RF) versus output (IF) power from the mixer

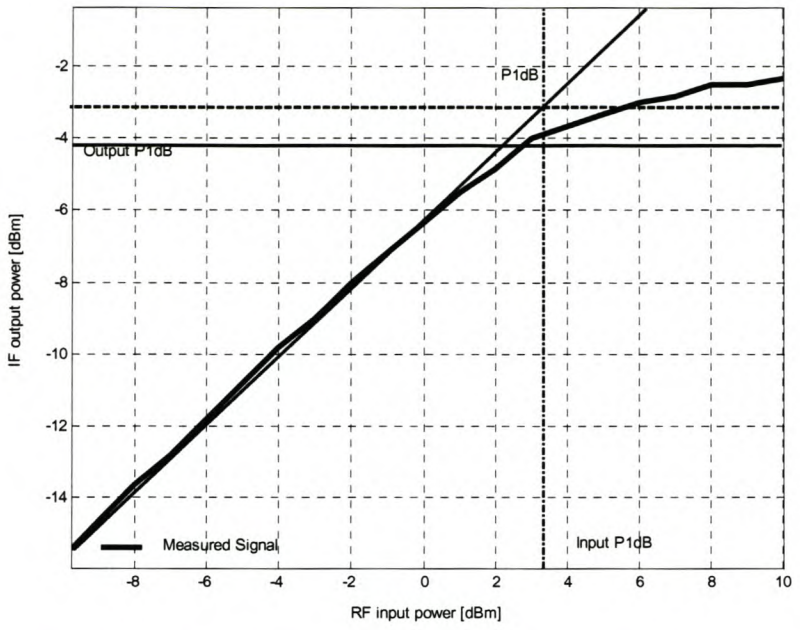

Figure 2-12: The 1 dB compression point curve of the mixer

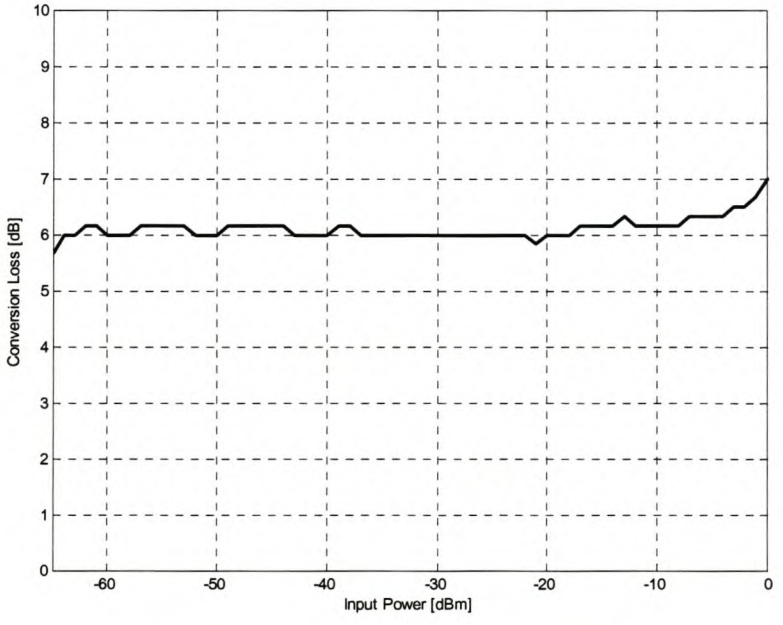

Figure 2-13: The measured conversion loss of the mixer

Figure 2-12 gives the measured input P1dB as 3.1 dBm and the output P1dB is -4.2 dBm. Figure 2-13 gives the measured conversion loss of the mixer, which is approximated to an average of 6.1 dB determined by subtracting the output from the input power in the graph of figure 2-11.

Isolation Measurements

Different isolation measurements were performed as shown in the setup schematics that follow. The LO to IF and LO to RF isolations were measured with LO power at 7 dBm.

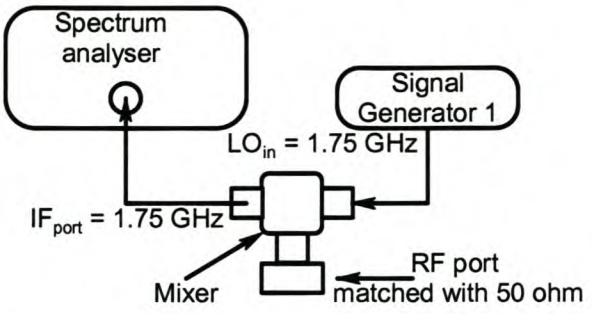

Figure 2-14: The measurement setup of the LO port to IF port isolation

In the LO to IF Isolation the RF port is matched to 50 ohm load and the spectrum analyzer center frequency is set to LO frequency. The LO to IF isolation is given by subtracting the LO power at the IF port from the LO power at the LO port and it was found to be 28.87dB.

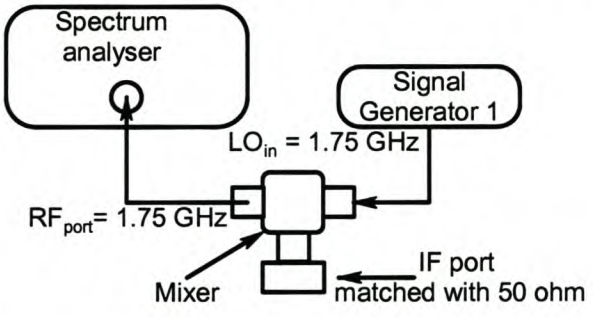

Figure 2-15: The measurement setup of the LO port to RF port isolation

The LO to RF port is performed by matching the IF port with 50 ohm and measure the LO signal coming out of the RF port. The signal level measured is subtracted from the LO signal level at the input of the LO port. The LO to RF isolation was found to be 34 dB.

The RF to IF is measured using similar setup to figure 2-10, except the spectrum analyzer center frequency is set to RF frequency (2.45 GHz). Again the RF level at the IF port is subtracted from the RF level at the RF port and it was found to be 14 dB. The RF to IF isolation is not a very important factor which affect the system, since its amplitude is normally low and is often located at much higher frequency as compared to the IF signal.

Parameters	Specified from datasheet	Measured
RF/LO frequency Range	1500 MHz – 2800 MHz	2450 MHz and 1750 MHz
Intermediate Frequency	0 – 1000 MHz	700 MHz
Conversion Loss	5.9 – 8.2 dB	6.0 - 6.1 dB
LO to RF Isolation	Typically 30 dB	34 dB
LO to IF Isolation	Typically 27 dB	28.87 dB
RF to IF Isolation	Not specified	14 dB
Input P1dB	Not specified	3.2 dBm

Table 2-2: The summary of specified and measured mixer performance

The mixer specified the third order intercept point (IP3) at 8 dB and approximate guess suggests that IP3 is usually 10 dB higher than P1dB. The obtained output P1dB is -4.2 dBm and if 10 dB is added to -4.2 it adds up to almost 6 dB which is a good approximation for IP3. The mixer measurement was successful and the mixer performs as specified.

2.4 Voltage Controlled Oscillator (VCO)

A mini-circuits ROS 1900 voltage controlled oscillator was selected for measurements. It is specified to operate from 1450 MHz – 1900 MHz frequency range with a 10 V power supply that consumes 25 mA and a tuning voltage of 0.5 to 20 V. It is further specified to give an output power of 7 dBm, a single sideband phase noise of 146 dBc/Hz at 1 MHz offset frequency, and harmonics level of between 10 - 18 dBc. It is also specified to have a tuning sensitivity of 22 to 33 MHz/V.

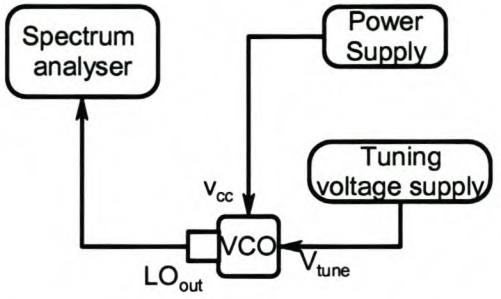

Figure 2-16: The measurement setup of the voltage controlled oscillator

The supply voltage of the VCO was set at 10V and the tuning voltage was varied between 0.0 – 20 V observing the frequency response.

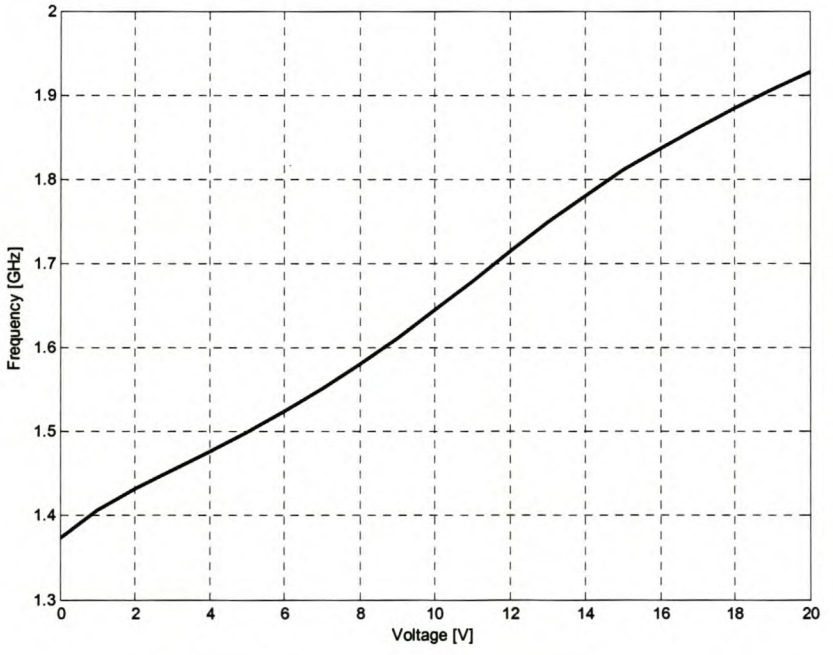

Figure 2-17: The measured tuning voltage versus output frequency of the VCO

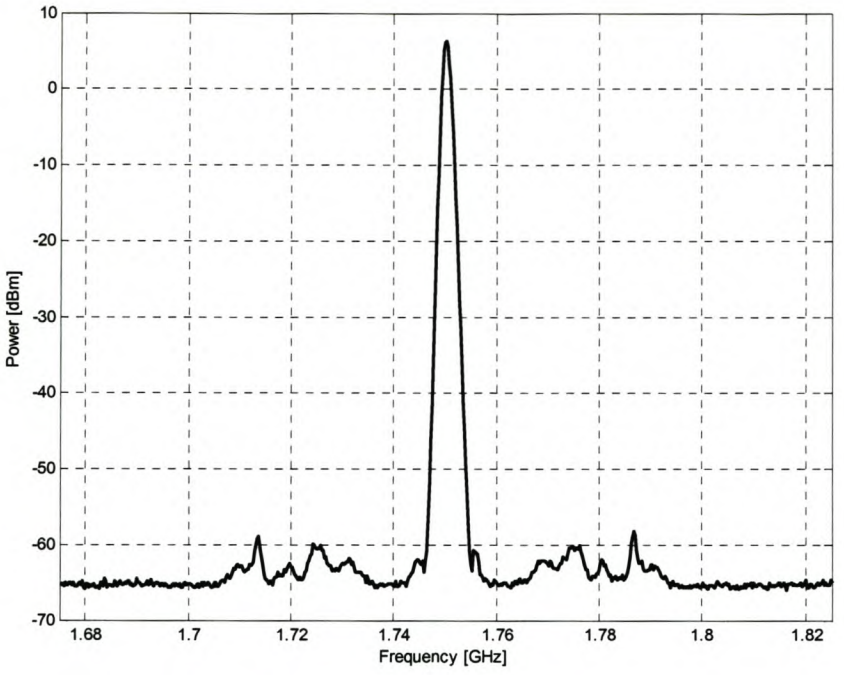

Figure 2-18: The measured VCO output signal with 13.054 V tuning voltage and 150 MHz span, 1 MHz spectrum analyzer resolution bandwidth and 3 KHz video bandwidth from the HP 8562 spectrum analyzer

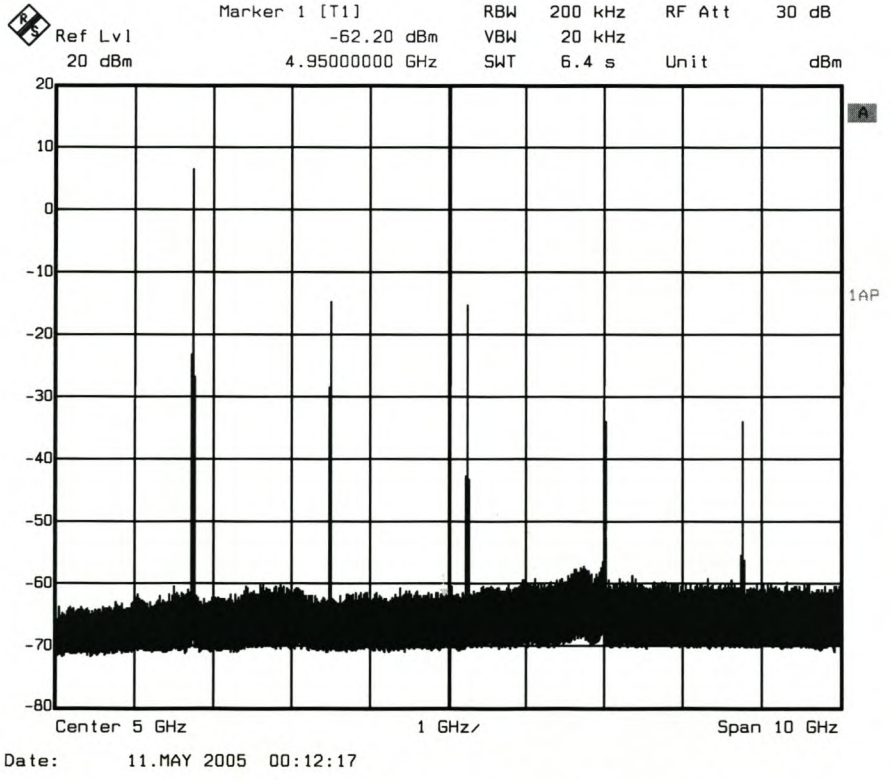

Figure 2-19: The measured output spectrum of the VCO with a large span using Rhode & Schwarz FSEK 30

Figure 2-17 shows the VCO frequency response with the tuning voltage, and it was measured from Rhode & Schwarz FSEK 30 spectrum analyzer and two Agilent power supplies. The VCO frequency varied from 1.375 GHz to 1.92 GHz and the power decreased from 7.3 dBm to 6.8 dBm respectively. The oscillator generates a signal at 1.75 GHz frequency with 6.83 dBm power level and a tuning voltage of 13.054.

VCO Parameters	Specified Performance	Measured Performance
Power Supply	10 V and max 25 mA	10 V and 20 mA
Frequency range [MHz]	1450 - 1900	1.375 – 1.9273
Output Power [dBm]	+7	6.83 at 1.75 GHz
Tuning Voltage [V]	0 - 20	0 - 20
Phase Noise [dBc/Hz]	146 at 1MHz offset	97 at 1 MHz offset
Harmonics [dBc]	10 - 18	21.8
Tuning Sensitivity [MHz/V]	22 - 32	20 - 36

Table 2-3: The summary of specified and measured VCO parameters

The voltage controlled oscillator performs as specified except the decrease in output power as the oscillation moves to higher frequencies and the power remains satisfactorily high. Also the measured phase noise is very poor but proper oscillation was observed. The oscillator measurements were successful.

2.5 The Three Block System Measurements

Linear Range Measurements

The subsystems components i.e. LNA, VCO and the Mixer were connected together and measured as a single system.

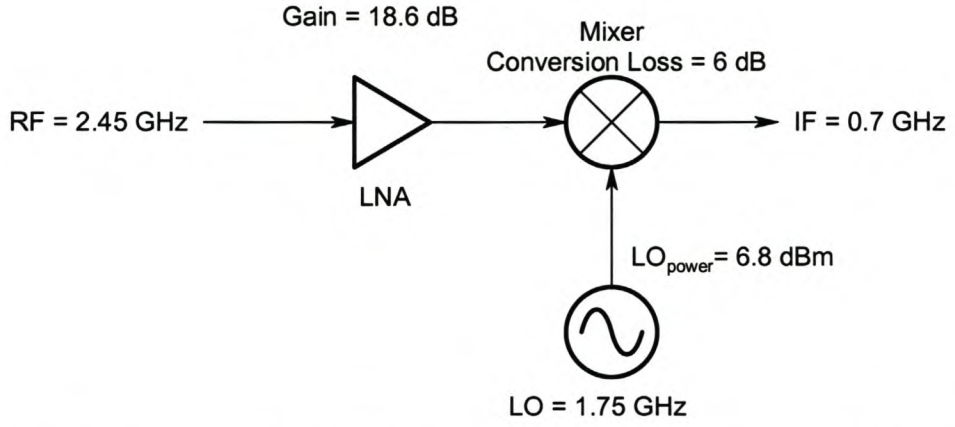

Figure 2-20: The different components connected together to form a small system

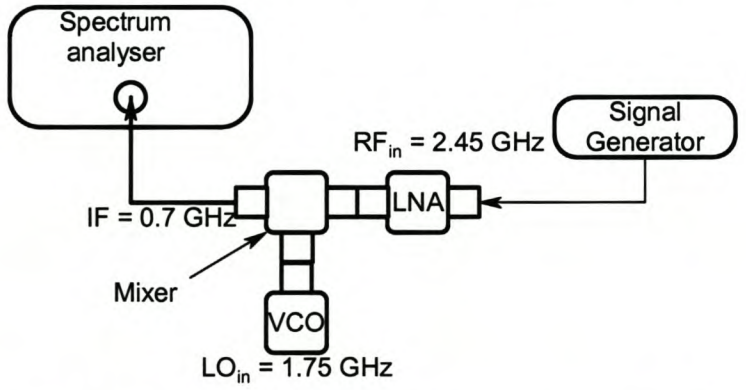

Figure 2-21: The small system linear range measurement setup

The signal from the signal generator was input on the RF input port of the LNA. The RF signal was swept from -75 to -10 dBm to measure the linear response of the system. This measurement setup gives gain and 1dB compression point of the system. Knowing the minimum SNR required, it allows the dynamic range to be determined using the system noise figure.

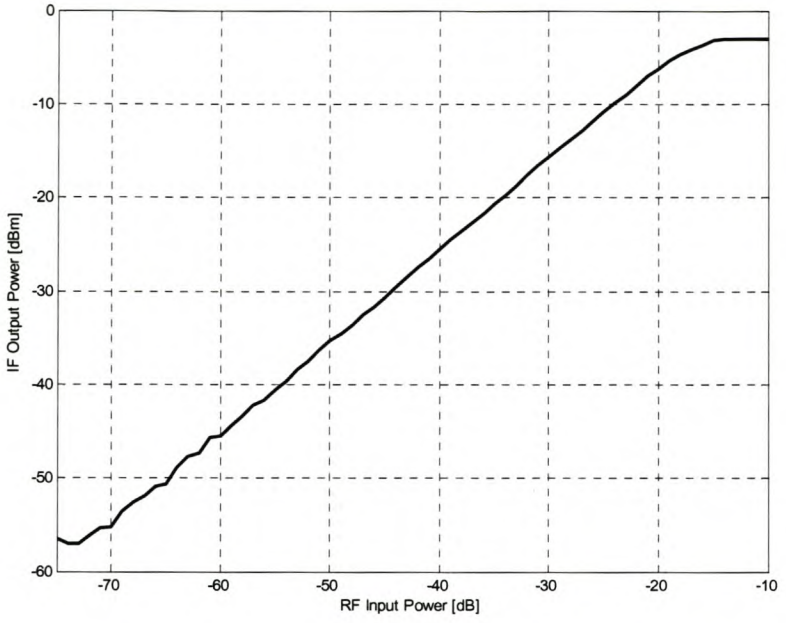

Figure 2-22: The input versus output power response of the system with 10 MHz span and a resolution bandwidth of 30 KHz

Figure 2-22 shows the linear range of the system measured where IF is 700 MHz and the RF is at 2.45 GHz. The P1dB of the system is given in figure 2-23.

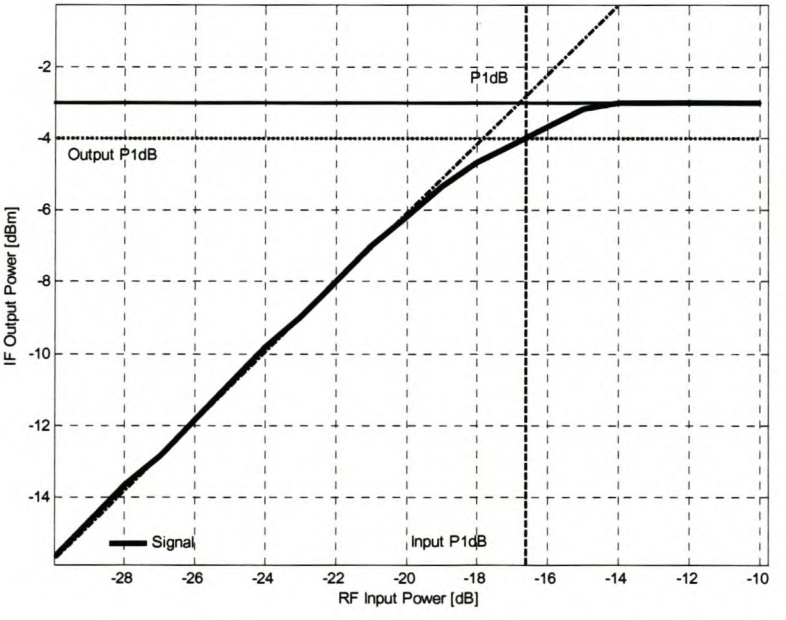

Figure 2-23: The measured input and output 1 dB compression point of the system

Spurious Response Rejection

In this subsection spurious response rejection refers to IF and image frequency rejection. These signals can desensitize the receiver and it may fail to receive wanted signals.

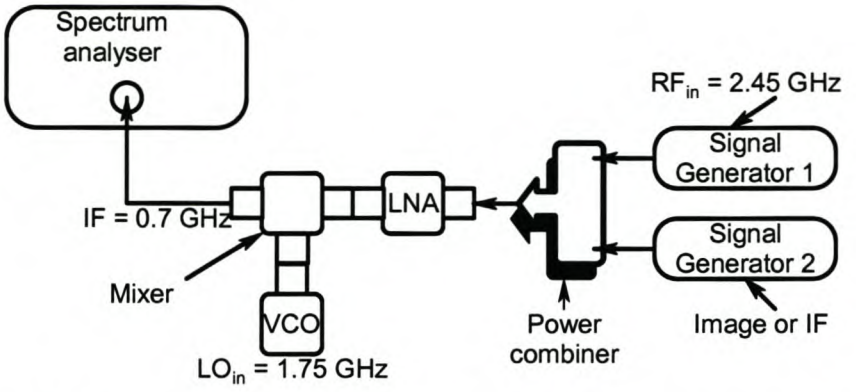

Figure 2-24: The setup for measuring image and IF frequency rejection

The image rejection is measured by combining RF and image signal with a combiner from two signal generators, and increase the power of the image signal until the RF which is converted into IF signal falls by 3 dB. The IF rejection is measured using the same technique except that the image signal is replaced by IF signal. The RF level was -60 dBm and the image and IF power levels distorting the signal were obtained as -30 and -10 dBm respectively.

LO and Spurious Radiation

Spurious radiation refers to the radiation of signals from the receiver back to the antenna.

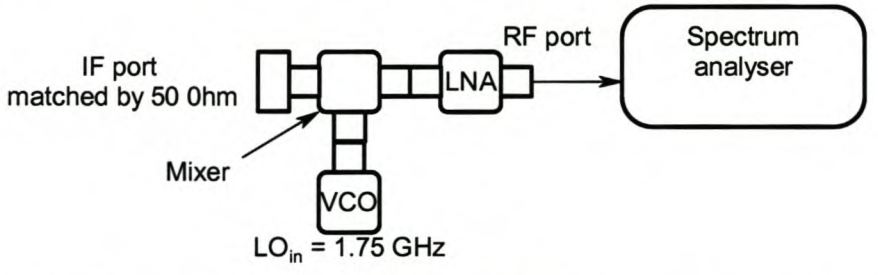

Figure 2-25: The measuring setup for LO and other spurious radiation

The measured radiated spurious signal is the LO at 1.75 GHz and it had -55 dBm power level from the LO output of 6.8 dBm.

Parameters	Specified	Measured
Dynamic Range	N/A	Max input Level ~ -16.5 dBm
Input P1dB	N/A	-16.5 dBm
Noise Figure	N/A	2.0138 dB
Image Rejection		30 dB
IF rejection		50 dB
Spurious Rejection		61.8 dB

Table 2-4: The summary of system measured parameters

The fundamental performance parameters of the system were measured and the P1dB of the system is less than the amplifier and mixer's P1dB and it is suspected to be due to the low power of the oscillator, which might have caused the reduced linear range of the system. The system IF and image rejection and spurious signals radiation are poor since no filter is included in the system. The dynamic range is not completely determined since the minimum detectable signal also depends on the demodulator technology plus its sensitivity (Minimum SNR). The amplifier's noise figure was measured and the mixer's noise figure was approximated to its conversion loss to determine the system noise figure.

3. The Monofilar Axial Mode Helix Antenna

3.1 Introduction

Helix antennas were first used as waveguides for electron beam amplification, overlooking the radiative nature of these structures and only modeled as antennas by John Kraus in 1946 [3]. The monofilar (one wire) helix is simple to construct from inexpensive materials. It allows fairly wide tolerances. It offers higher gain and broader bandwidth compared to the patch antenna. The wide bandwidth comes from the fact that the impedance is almost constant and resistive over a wide range of frequencies. The helix antenna operates in two modes, i.e. the normal and axial mode. The modes are controlled by the size of the winding circumference of the antennas as compared to the wavelength, with the normal mode obtained with a helix circumference very small compared to the wavelength, (typically less than a half wavelength). It operates in a similar way as an isotropic antenna with elliptical field polarization [9], with the maximum of the directional pattern perpendicular to the axis of the helix. The axial mode helix has a circumference of around one wavelength and it is a directional antenna. The main beam is along the axis of the helix and the field is circularly polarized, as illustrated in figure 3-1. The axial mode of the helix antenna was chosen to satisfy the high gain specification of the proposed receiver. By choosing the high gain from the antenna the beam width was thus allowed to be narrow, making the antenna more directional, which is ideal for a point to point communication.

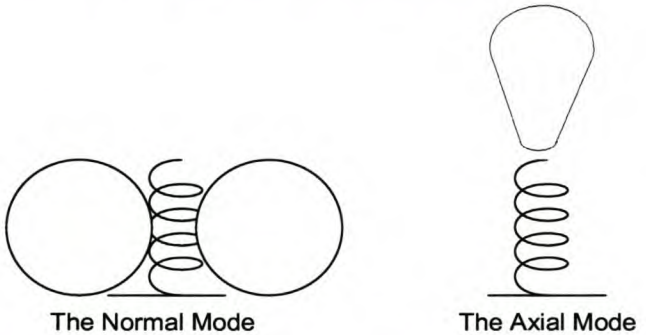

Figure 3-1: The illustration of different operation modes of monofilar helix antenna

The axial mode helix antenna has found wide applications in telephones, satellite, televisions and radar systems where-as the normal mode helix is used in mobile data and voice communication

systems. Such systems are cellular telephones and WLAN communicating devices. They are also widely employed in remote sensing. In this section a monofilar axial mode helix antenna is designed and fabricated.

3.2 The Antenna System Parameters

3.2.1 General Antenna Parameters

As defined in the first chapter the antenna is a device that converts a guided electromagnetic wave on a transmission line to a plane wave propagating in free space. This part of the system links the transmitter to the receiver in a wireless communications system [21]. There are a lot of antenna types and geometries, but all antennas can be described with respect to the parameters given below [22].

Radiation Pattern

It is the power radiated or received by the antenna as a function of angular position and radial distance from the antenna. At electrically large distances, the power density drops off as $1/r^2$ in all directions. Receive and transmit patterns of an antenna are identical provided the antenna does not contain any nonreciprocal material. The radiation pattern functions may be plotted for the azimuthal or the elevation plane and are dependent on the antenna polarization [21].

Far Field

This is described as the region far away from the antenna where the radiated wave takes the form of a plane wave. The commonly used criterion is a distance of $2D^2/\lambda$ from the antenna where D is the maximum linear dimension of the antenna and λ is the operating wavelength.

Directivity

Some antennas have the ability to transmit or receive maximum power in a given direction. The ratio of such maximum power to the average radiation intensity over all space is the directivity of the antenna [21], and is usually denoted by D. It is a dimensionless ratio of power and is usually given in dB and its value is solely dependent on the radiation pattern relative to an isotropic radiation pattern.

Efficiency

Antenna efficiency is defined as the ratio of total power radiated by the antenna to the input power of the antenna, and it is sometimes referred to as the radiation efficiency and is given by the relation $e_{rad} = P_{rad} / P_{in}$ where P_{rad} is the power radiated by the antenna and P_{in} is the power supplied to the input of the antenna [21].

Gain

The gain of the antenna is the product of efficiency and directivity and it is either less or equal to directivity. It is expressed as $G = e_{rad} D$, where e_{rad} and D are the antenna efficiency and directivity respectively and is usually expressed in dB [21].

Impedance

This is usually the driving point impedance which the antenna presents to the circuit it is connected to. If it is not matched it can reflect more power and degrade the antenna performance.

Bandwidth

The range of frequencies with which the performance of an antenna, with respect to some characteristic, conforms to a specified standard (or requirements) [4]. In most cases 3dB bandwidth is widely used as a specification.

Polarization

This refers to the polarization of the electric field vector of the radiated wave. It can either be vertical, horizontal or circularly polarized. Circular polarization can be right hand circular polarized (RHCP) and left hand circular polarized (LHCP).

3.2.2 Helix Antenna Parameters

The helix is a basic three dimensional geometrical form, which combines the geometric forms of a straight line, a circle and a cylinder. Its 3D form is seen when unwound, on the end-on and on the sides respectively, this is shown in figure 3-3. The Helix antenna is circularly polarized and it can be either left or right hand circularly polarized depending on the direction in which it is wound along the helical direction.

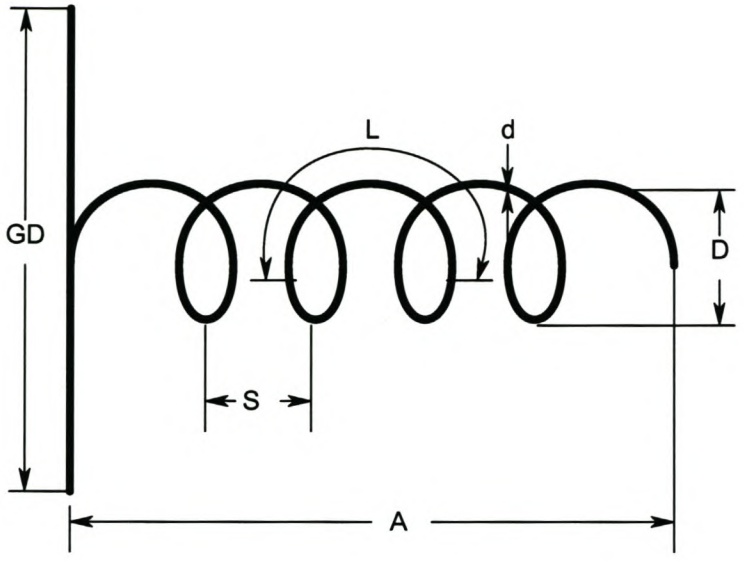

Figure 3-2: A monofilar Helix with its associated dimensions

The monofilar helix is shown in figure 3-2 with

D = helix diameter

C = circumference of Helix = πD

S = spacing between turns

α = pitch angle

L = length of one turn

N = number of turns

A = axial length =NS

d = diameter of Helix conductor

GD = diameter of the ground plane

The helix pitch angle for optimum performance is given by [3],

$$\alpha = \arctan(\frac{S}{\pi D}). \tag{3-1}$$

L represents the length of one turn of a helix when it is unrolled on a flat plane and the relation between the spacing S, circumference C, turn length L and pitch angle α are as illustrated by the triangle in figure 3-3.

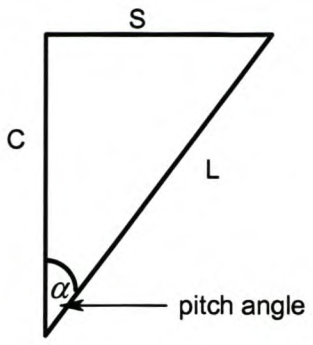

Figure 3-3: Relation between circumference, spacing, turn length and pitch angle of helix.

From figure 3-3 when the spacing is zero, pitch angle equals zero and the helix becomes a loop. When the diameter becomes zero, the pitch angle becomes 90 degrees and the helix becomes a linear conductor or a dipole antenna depending on the length.. The spacing, circumference and length can be given in terms of electrical length and it is achieved by dividing actual parameter values by one wavelength as in equation (3-2).

$$C_\lambda = \frac{C}{\lambda},\ S_\lambda = \frac{C}{\lambda} \text{ and } L_\lambda = \frac{L}{\lambda} \tag{3-2}$$

3.3 Design Considerations

The following parameters are the most important for design consideration in designing the proposed antenna.

- Beam width (HPBW)
- Gain (G)
- Impedance (Zin)
- Axial Ratio (AR)

Half Power Beam width is the angle between the two directions in which the radiation intensity is one-half the maximum value of the beam [4]. The axial ratio is a measure of how circular is the polarization of the antenna, with zero being the most circular. In most antennas gain and beam width are inversely proportional. In the proposed antenna the above mentioned parameters

(HPBW, G, Zin and AR) are all dependent on the number of turns, frequency and the turn spacing which affect the pitch angle. These parameters often determine the useful band of the antenna. For optimum performance of the monofilar helix, the circumference should be approximately one wavelength [3]. For a given bandwidth to be completely useful, all four parameters must be satisfactory over the entire bandwidth. The parameters also depend on the ground plane size, shape, the helical conductor diameter, the helix support structure and feed arrangement. The ground plane may be a flat square, round or cup shape with a diameter or side dimension of at least three quarter wavelength [3].

Another design consideration is the technique to be used in winding the antenna. The helix is usually modeled as a self supporting structure which is true for short designs. The self supporting property creates a serious challenge for long antenna, especially thin wire fabrication. Support in the form of radial insulators, metal rods or tubes are normally used [3]. It can also be supported by one or more longitudinal dielectric rods mounted peripherally or by a thin wall dielectric on which the helix is wound. The latter arrangement has the effect of shifting the operation bandwidth to lower frequencies, which results in a smaller antenna for a given frequency [3].

Another important design parameter to consider is the feed. The helix maybe fed axially or peripherally or from any convenient location on the ground plane. From [3] the axial feed resistive impedance is approximated within twenty percent accuracy by

$$R = 140C_\lambda \tag{3-3}$$

The peripheral feed real impedance is approximated within ten percent accuracy by equation (3-4) [3].

$$R = \frac{150}{\sqrt{C_\lambda}} \tag{3-4}$$

The relations given in equations (3-3) and (3-4) apply only when the following restrictions hold $0.8 \le C_\lambda \le 1.2$, $12 \le \alpha \le 14$ and the number of turns should be equal or greater than four ($N \ge 4$), [3]. The terminal impedance of the antenna can be made any desired value, from just below 50 ohm to approximately 180 ohm [3].

It is usually attained by a properly designed matching. In a peripheral feed, the matching can be achieved by bringing the last quarter turn of the helix parallel to the ground plane in a gradual

manner. Thus a tapered transition between the 150 ohm or more helix impedance and a 50 ohm coaxial line can be accomplished. The method can also be used in an axially feed helix but it is not convenient in comparison with the peripheral feed helix [3].

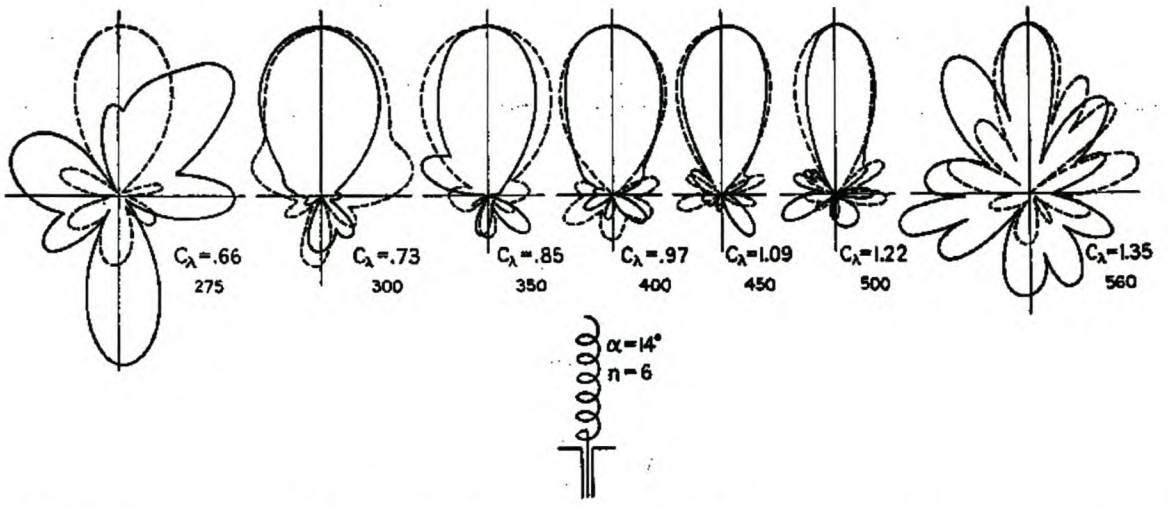

Figure 3-4: Measured field patterns of 14^0, 6 turn Helix. Patterns are characteristic of the axial mode of radiation over a range of circumference from about 0.73 to 1.22 wavelengths. Both the circumference and frequency in MHz are indicated. The solid patterns are for the Horizontal polarized field component and the dashed are for the vertically polarized. Both are adjusted to the same maximum [3].

Based on the large number of these pattern measurements shown in figure 3-4 which were performed during the early years of Helix existence, the beam widths were found to be given by the following quasi-empirical relations [3]

$$\text{HPBW (Half power beam width)} \approx \frac{52}{C_\lambda \sqrt{nS_\lambda}} \text{ in degrees} \quad (3\text{-}5)$$

$$\text{BWFN (Beam width between first nulls)} \approx \frac{115}{C_\lambda \sqrt{nS_\lambda}} \text{ in degrees, [3]} \quad (3\text{-}6)$$

Where C_λ and S_λ are the circumference and spacing with respect to wavelength respectively and n as the number of turns (see equation 3-2). The effect of the number of turns in the helix is shown in figure 3-5 with more turns creating a more directive antenna.

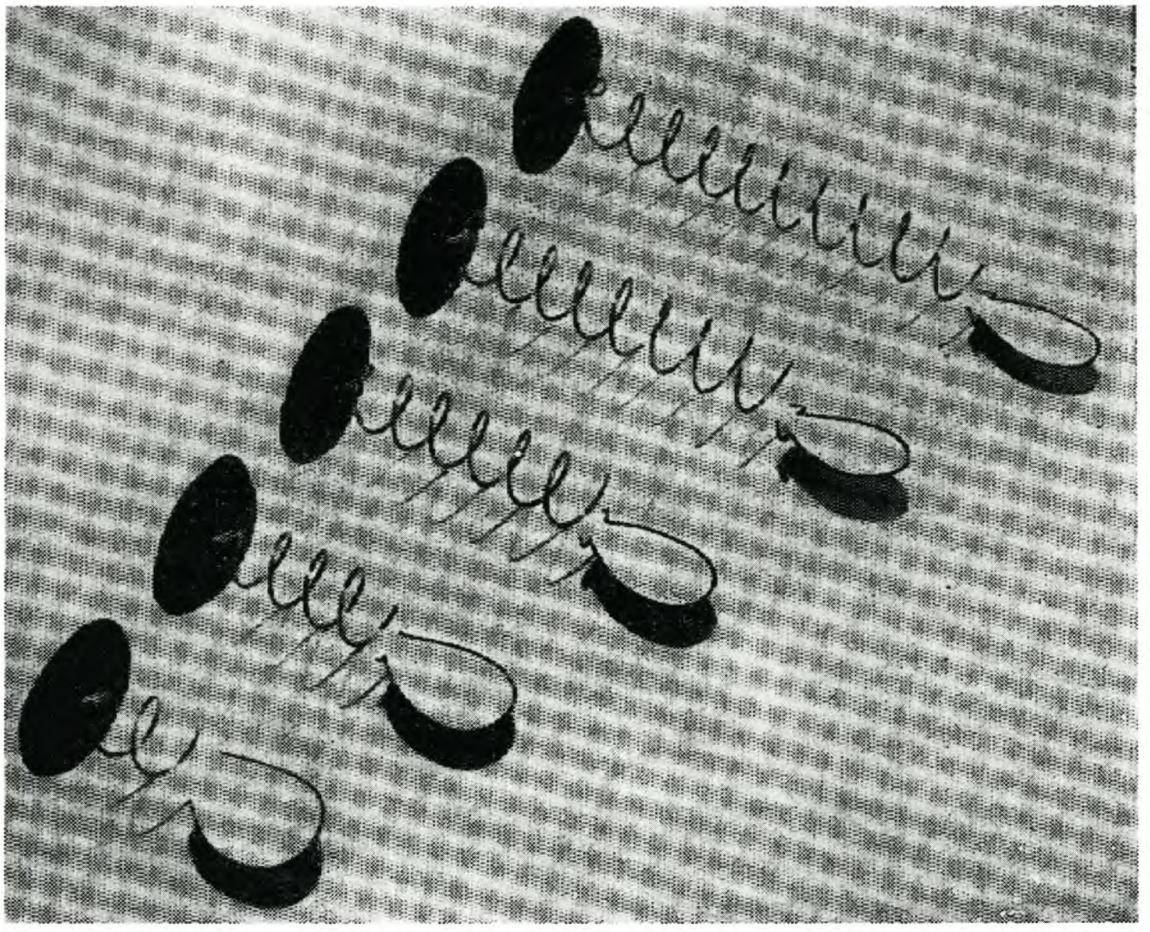

Figure 3-5: Models showing effect of number of turns on measured field patterns. Helices have 12.2° pitch angle and 2, 4, 6, 8 and 10 turns. Patterns shown are average of measured E_θ and E_Φ patterns [3]

Dividing the square of the half power beam width (equation 3-5) into the number of square degrees in a sphere (41253) yields an approximate directivity relation as [3]

$$D \approx 15 C_\lambda^2 n S_\lambda \tag{3-7}$$

Equation (3-7) disregards the effect of minor lobes and the details of the pattern shape. A more realistic relation is [3]

$$D \approx 12 C_\lambda^2 n S_\lambda \tag{3-8}$$

For equation (3-5) to equation (3-8) to be valid, the following restriction on circumference, pitch angle and number of turns should be true: $0.8<C_\lambda<1.15$, $12^\circ<\alpha<14^\circ$ and $N>3$ [3].

The relation given in equation (3-8) is equivalent to gain provided the antenna is lossless. The Helix can be constructed with pitch angle from 2° to 25° but the angles between 12° and 14° are

optimum [3]. The small optimum pitch angle (around 12°) can have a 1dB higher gain than the larger optimum pitch angle (around 14°), but it will have a narrow bandwidth [3]. The gain is directly related to directivity in a one to one relationship, with gain taking into effect the antenna efficiency. The gain can be increased by 3 dB if the number of turns is doubled. The helix antenna has good resistive terminal impedance and comparable smaller imaginary component of the impedance in the band, the resistive nature of the helix antenna can also be enhanced by a spiral termination of a helix antenna [2]. The more turns the helix the narrower the bandwidth. The resistive nature of the helix antenna slowly fades away as more turns are wound. The axial ratio of the axial mode helix is theoretically given by [2] as

$$|\mathrm{AR}| = \frac{2N+1}{2N} \tag{3-9}$$

The formula indicates that the quality of circular polarization increases with number of turns [2]. The axial ratio formula is an approximate and measured data shows that it is best with $0.8 \leq C_{\lambda} \leq 1.2$, [3].

3.3.1 Antenna Specification

Center Frequency	= 2.45 GHz
Polarization	~ Left hand circular polarization
Bandwidth	= 0.1 GHz (2.4 to 2.5 GHz)
Gain	≥ 12 dB
Reactance Impedance	≈ 0 Ω
Resistive Impedance	< 180 Ω
Reflection (Over the Bandwidth)	< -15 dB
Axial Ratio	< 3 dB
Size	< 0.35 m
Complexity	- Simple and use of inexpensive materials

3.4 Design and Simulations

The first antenna prototype was designed using theories from [3] and [2]. A small Matlab code was written to evaluate different properties of the antenna simultaneously. The antenna designed was more based on theory suggesting optimum performance in [3]. The following conditions were considered in designing the antenna

- Pitch angle $12<\alpha<14$
- Circumference $0.8<C_\lambda<1.15$
- Spacing $0.2<S_\lambda<0.3$
- Number of turns ≥ 4 (Only for terminal Impedance)

A number of designs were performed using various major parameters of the helix in the design space shown above including equation (3-1) and axial length relation (A = NS). For the requirements given in the specifications the following dimensions are obtained and the peripheral feed was preferred in this design because it is convenient to taper it into a matching section.

- $C_\lambda = 1.05$
- $N = 12$
- $\alpha = 12.5^0$
- $A = 0.3418$ m
- $r = 0.0205$ m (radius of helix)

From these parameters the most important parameters of the monofilar axial mode helix antenna were determined. They are gain (3-9) assuming a lossless antenna, input impedance (3-5), beam width (half power and first nulls) (3-6 and 3-7), axial ratio (3-10), turns spacing (3-2) and the ground plane diameter ($3/4\lambda$). The numbers in brackets represent the equation used in determining the given parameter except the ground plane diameter where inside the brackets is the minimum ground plane diameter with respect to the wavelength.

The parameters obtained are listed below

Gain (Lossless)	: G = 15.6 dB
Impedance	: Zin = 146.4 Ω
Half Power Beam width	: HPBW = 30°
Beam width First Null	: BWFN = 65.5°
Axial ratio	: AR = 1.0417
Turns Spacing	: S = 0.0285 m
Ground Plane diameter	: GD ≥0.0918 m

The physical parameters of the antenna were entered into FEKO electromagnetic simulation software. In the simulation the conducting material (wire) was varied from one through to two millimeters. In these simulations a thin wire was chosen because it is easy to wind in a prototype antenna. It had also displayed a better performance with respect to the antenna reflections. The ground plane was also made double the size required as minimum ground plane.

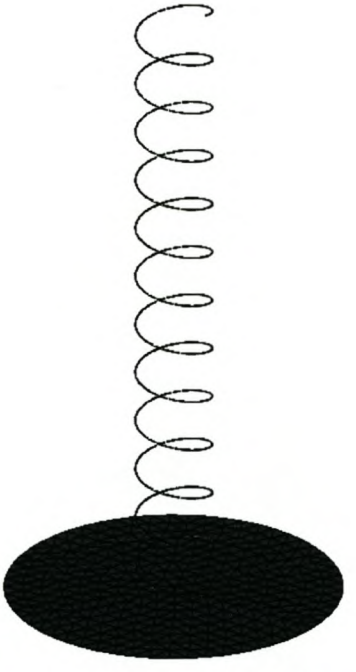

Figure 3-6: The antenna parameterized model in the active window of FEKO electromagnetic simulation software

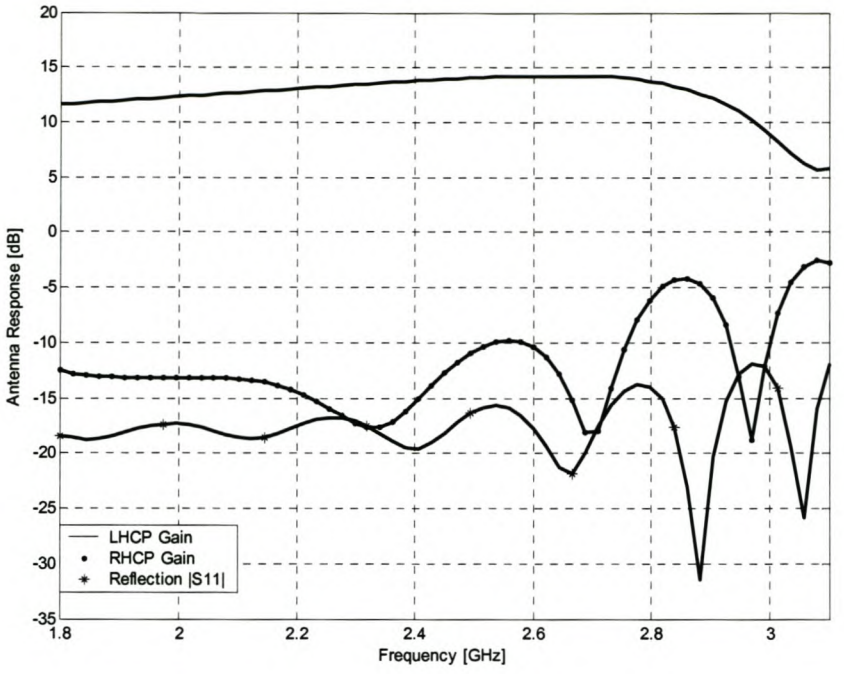

Figure 3-7: The LHCP, RHCP and reflections simulated response of Helix

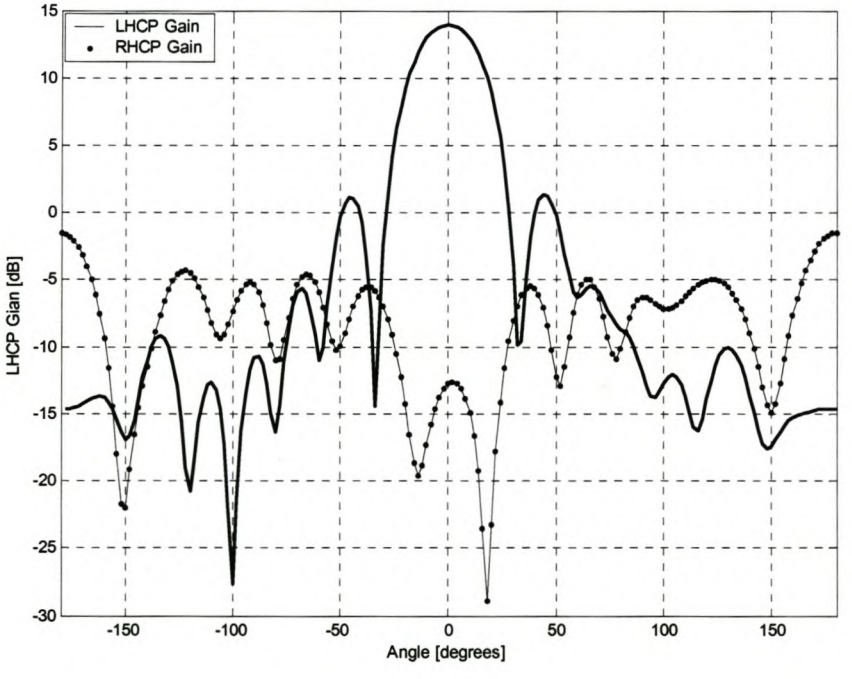

Figure 3-8: The simulated antenna gains given in a radiation pattern plot.

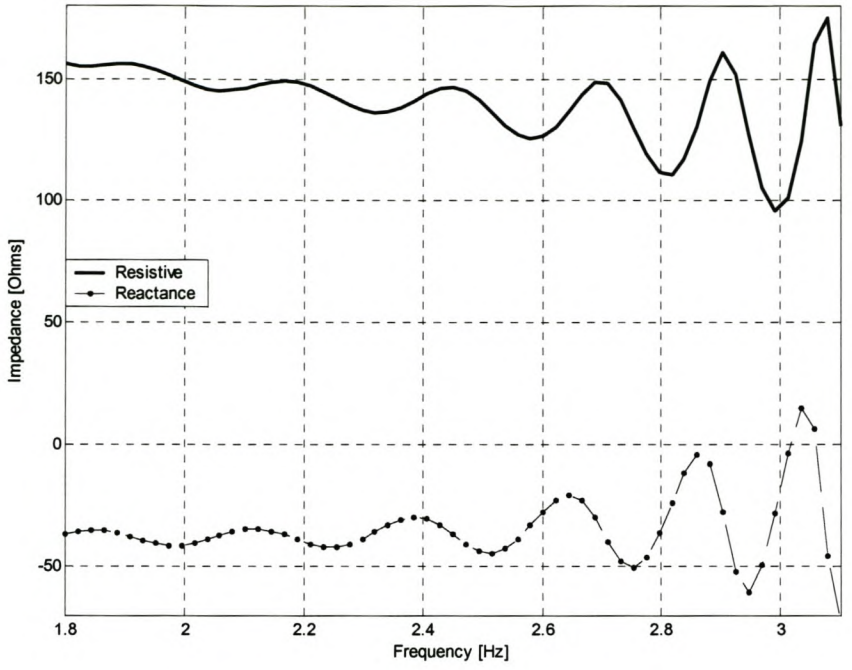

Figure 3-9: The simulated impedance of the antenna

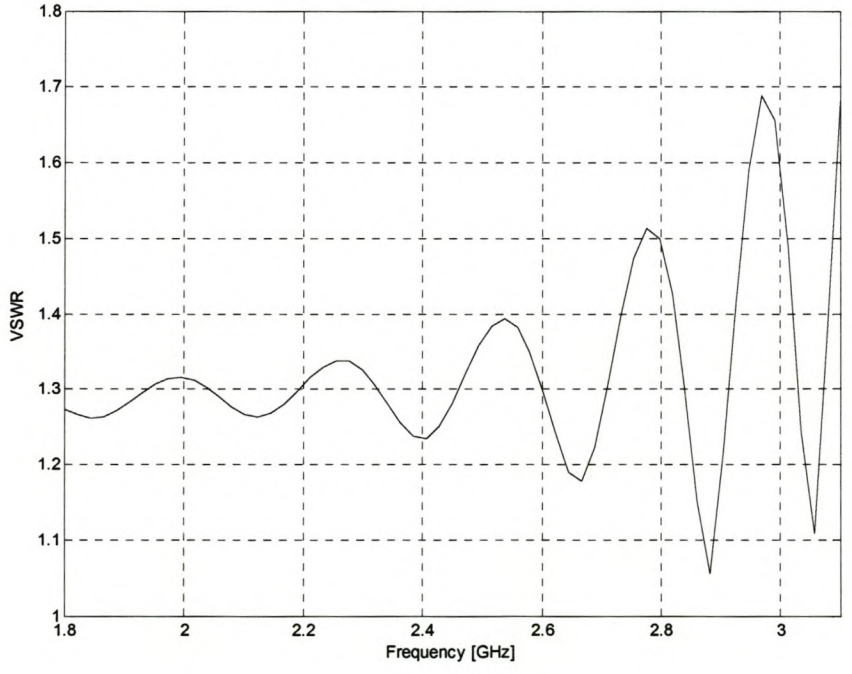

Figure 3-10: The simulated standing wave ratio with a system impedance of 147 Ω

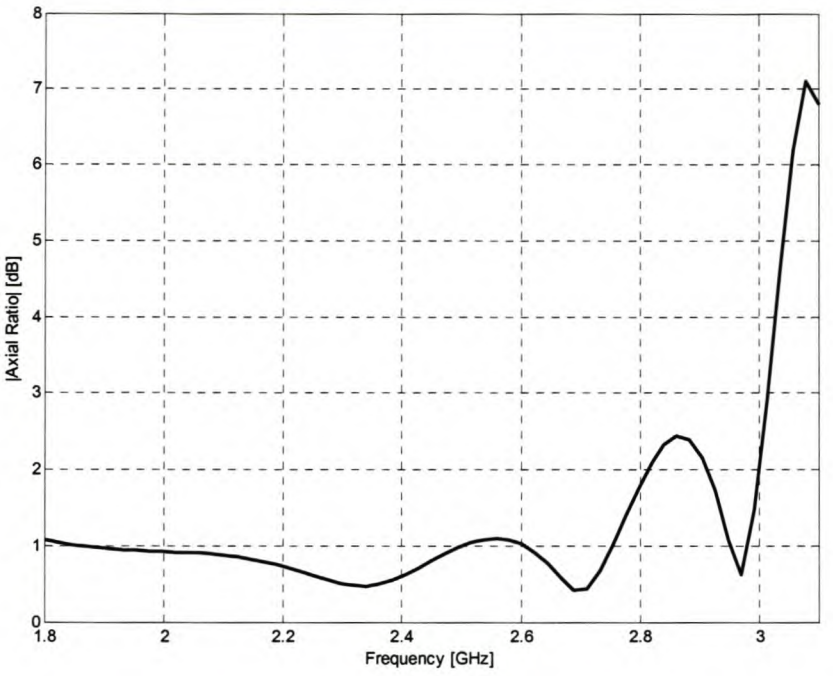

Figure 3-11: The Simulated axial ratio of the antenna

The simulations results are given starting from figure 3-7 through to figure 3-11. The left hand circular polarization gain of the antenna is 14 dB at the frequency of interest, it is above 13.8 dB in the proposed frequency range which is from 2.4-2.5 GHz. The right hand circular polarized gain is below -10 dB in the bandwidth of interest and it remains below 0 dB throughout the measured range. The magnitude of reflections (|s11|) at the proposed center frequency is just below -18 dB and it remains below -16 dB in the proposed bandwidth. It also remains -10 dB through out the whole measured range. The gain of the antenna in a radiation pattern plot shows the LHCP at 14 dB and RHCP show a gain of less than -10 dB in the HPBW range of the LHCP gain. The resistive impedance is 147 ohm, and the reactance impedance is -37 ohm. Both these impedances remain almost in the same range in the bandwidth of interest. The voltage standing wave ratio is less than 1.29 at the center frequency.

It remains less than 1.36 for the rest of the bandwidth. The simulated axial ratio is 0.8 dB at the frequency of interest and remains less than 1 dB within the proposed bandwidth, while it remains less than 3 dB until 3 GHz. The simulated gain is less by 1.6 dB compared to the lossless gain calculated. The calculated impedance agrees well with the calculated value. The simulations gave the performance within the proposed requirements.

3.5 Construction and Measurements

The antenna was wound on a cardboard tube which was 0.0401 m in diameter. The conductor used is a 1 mm diameter insulated copper wire. The center of the wire has a radius of approximately 0.0205 m including the winding radius with a 0.342 m of height. The ground plane was doubled in size compared to the minimum required and was done to prevent the field from coupling from the antenna to the feed bypassing the ground plane, and also to ensure proper support of the antenna due to its large size. The peripheral feed was fabricated and the antenna was matched by gradually bringing the last quarter turn of the helix closer to the ground plane. In that manner it is approximated to a quarter wave matching transformer. After wounding the antenna it was then connected to a small network analyzer (HP8753C), and using the Smith chart display format it was optimized until the impedance at the proposed center frequency is as close as possible to the center of a smith chart. After obtaining satisfactory results, the antenna was ready for complete measurements. Various methods of antenna measurements exists and in this case only three were evaluated,

- Gain transfer (or comparison) method
  It requires an antenna whose gain is exactly known and the set up and power levels should not be changed while exchanging transmits to receive antenna and vice versa [8].
- Two antenna method (known as absolute Gain measurements)
  It is based on the Friis equation and needs two identical test samples (two antennas under test, AUT) [8].
- Three antenna measurements (also known as absolute Gain measurements)
  Also based on the Friis equation, it needs only one sample (AUT) antenna. Any other two can be used to perform the measurements [8].

The three antenna method was chosen because all the requirements for the method were met. It allows the calculation of the gain of all three antennas and it is not necessary to identify if the antenna is transmitting or receiving [8]. The method was accomplished by using two linearly polarized horn antennas. The antenna to be measured was a circularly polarized antenna using linearly polarized antennas.

The magnitude and phase of horizontal and vertical polarization field components of the antennas were measured. The horizontal and vertical field components of the antenna under test (AUT) are usually given in terms of real and imaginary components [7].

- $H = x_r + jx_i$
- $V = y_r + jy_i$ (3-10)

The left hand circular polarized (LHCP) wave is given by [5]

$$L = H - jV$$

The right hand circular polarized (RHCP) wave is given by [5]

$$R = H + jV \quad (3\text{-}11)$$

The two linearly polarized horizontal and vertical instantaneous E-field phasor values Eh and Ev may be combined to form a left and right hand circularly polarized field.

The effective field strength values are preferred and they take the following form [5]

$$E_L = \frac{1}{\sqrt{2}}(Eh + jEv) \quad (3\text{-}12)$$

$$E_R = \frac{1}{\sqrt{2}}(Eh - jEv) \quad (3\text{-}13)$$

The above equations were used to determine the antenna under test's circularly polarized S_{21}-parameters. Using the three antenna method and assuming the antennas are well matched according to polarization and impedance the gain of each antenna can be deduced from Friis power transmission equation [2]

$$P_r = \frac{P_t G_t G_r \lambda^2}{(4\pi R)^2} \quad \text{(Friis)} \quad (3\text{-}14)$$

where R is the distance between the antennas under test and G_t and G_r are two antenna gains. If two identical sample antennas were being measured then their gains would be equal and no need to specify G_t and G_r. The relationship between the antenna s-parameters with the received and transmitted power is given by [1]

$$\frac{P_r}{P_t} = \frac{|S_{21}|^2}{(1-|S_{22}|^2)(1-|S_{22}|)} \quad (3\text{-}15)$$

Since each antenna is assumed to be well matched, $|S_{11}|$ and $|S_{22}|$ can be ignored and thus equations (3-14) and (3-15) becomes

$$|S_{21}|^2 = \frac{G_t G_r \lambda^2}{(4\pi R)^2} \quad (3\text{-}16)$$

The three equation describing the measurements are given by equation (3-17, 3-18 and3-19)

$$|S_{21}|^2 = \frac{G_1 G_2 \lambda^2}{(4\pi R)^2} \quad \text{(Between two horns)} \tag{3-17}$$

$$|S_{21}|^2 = \frac{G_1 G_{AUT} \lambda^2}{(4\pi R)^2} \quad \text{(Between horn1 and helix)} \tag{3-18}$$

$$|S_{21}|^2 = \frac{G_2 G_{AUT} \lambda^2}{(4\pi R)^2} \quad \text{(Between horn2 and helix)} \tag{3-19}$$

Where G_1 is the gain of the first horn and G_2 is the gain of the second horn. G_{AUT} is the gain of the AUT, a helix antenna. Solving these equations (3-17, 3-18 and 3-19) simultaneously give each antenna's gain.

The antenna was measured at Stellenbosch University anechoic chamber with the antennas under test positioned 5 m apart. The data processing was performed using a small Matlab code to determine the LHCP and RHCP s-parameters for the helix from the measured horizontal and vertical S-parameters. From the measured data the axial ratio was computed using the relation given below [5]

$$AR = \frac{(|E_R| - |E_L|)}{(|E_R| + |E_L|)} \tag{3-20}$$

The measured impedance of the helix antenna was also computed from equation (3-21) using parameters extracted from the measurements [1]

$$Zin = Zo\frac{1+\Gamma}{1-\Gamma}, \tag{3-21}$$

where Zo and Γ are the characteristic impedance of the transmission line connecting the antenna to the system and the reflection coefficient of the antenna respectively. The voltage standing wave ratio was also computed, from equation (3-22) [1]

$$VSWR = \frac{1+|\Gamma|}{1-|\Gamma|} \tag{3-22}$$

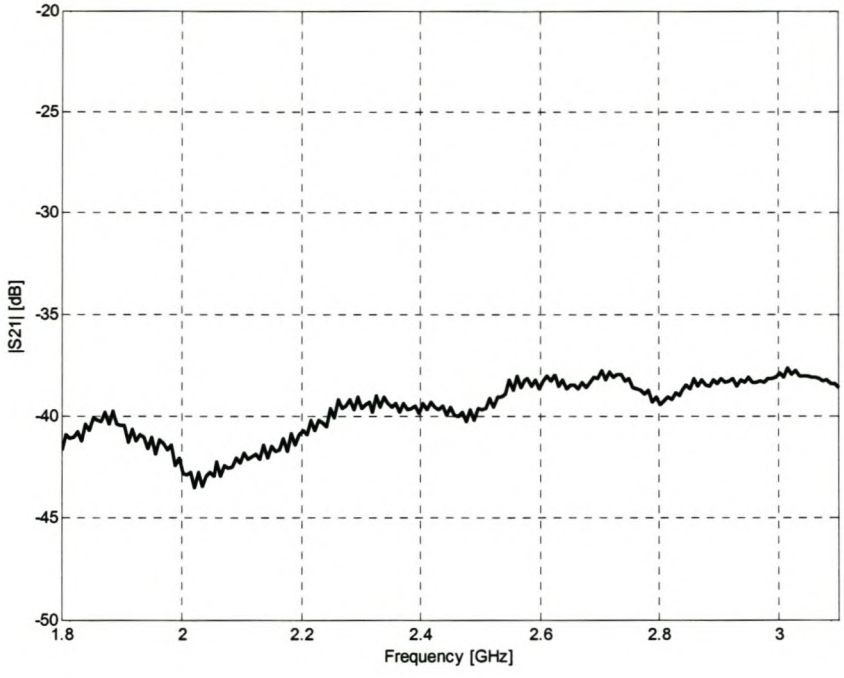

Figure 3-12: The s21 between the two horns in a co polarized set up

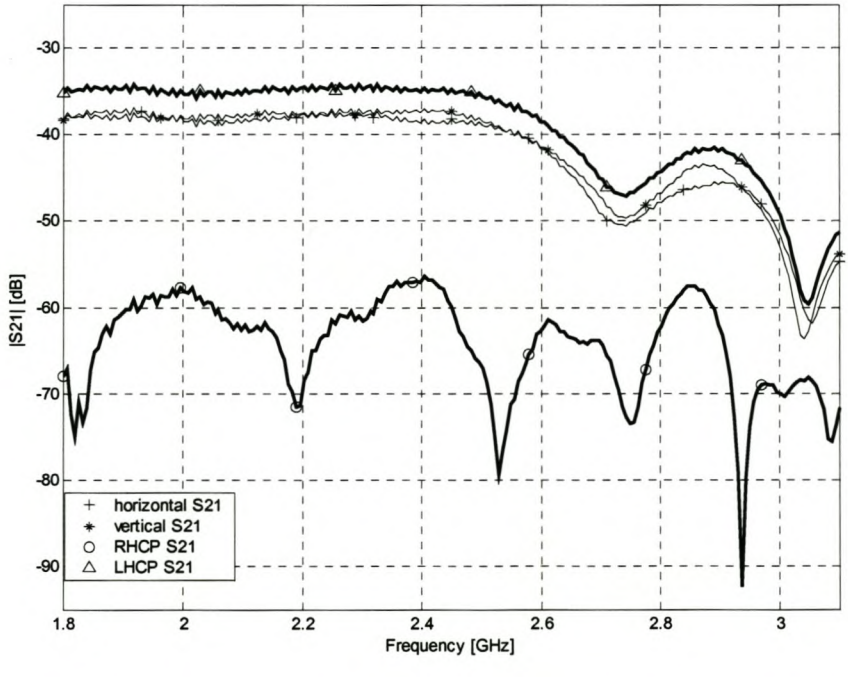

Figure 3-13: Measured horizontal and vertical S_{21} magnitude together with the calculated RHCP S_{21} and LCHP S_{21} from the measurements of the horn1 and the helix.

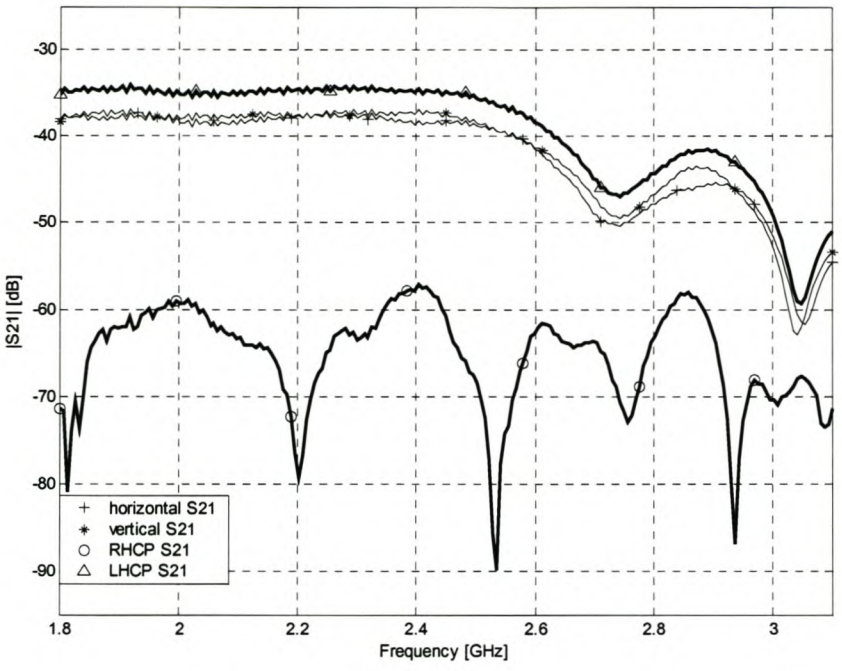

Figure 3-14: Measured horizontal and vertical S_{21} magnitude together with the calculated RHCP S_{21} and LCHP S_{21} from the measurements of the horn2 and the helix.

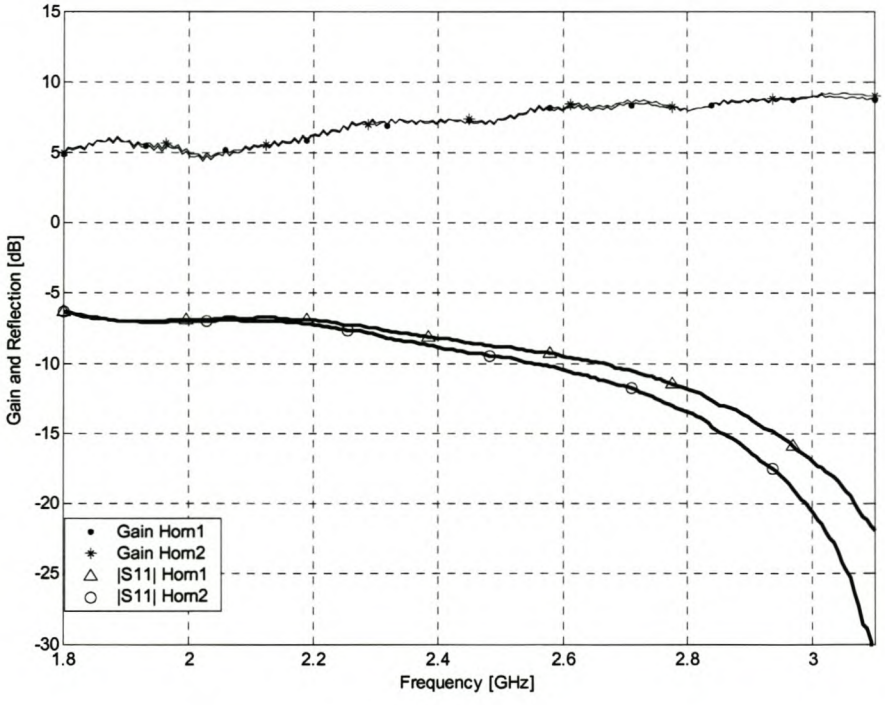

Figure 3-15: The measured responses of both horn antennas

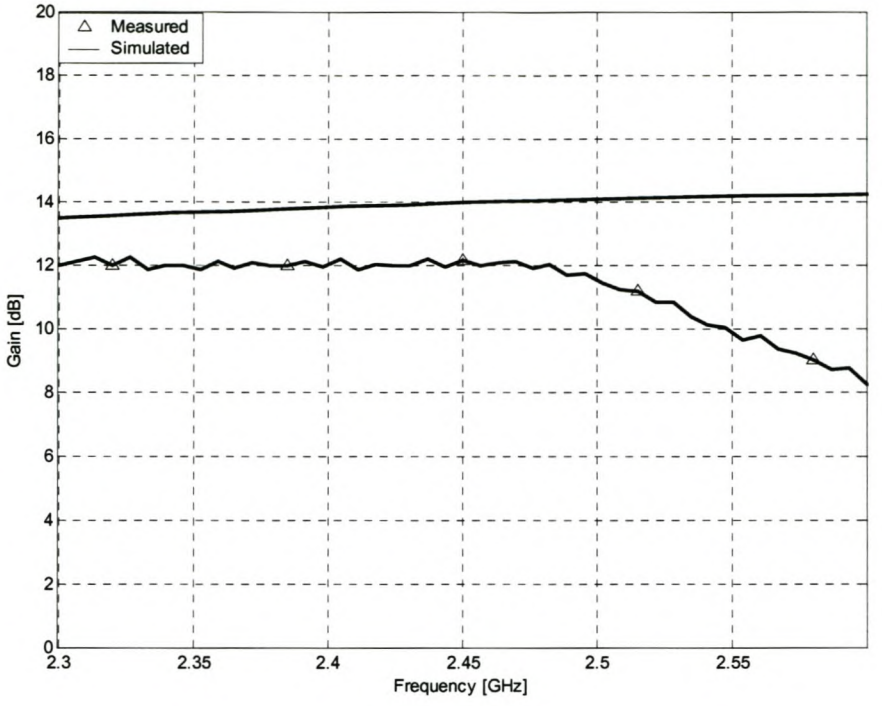

Figure 3-16: The comparison of measured and simulated LHCP gain of the helix.

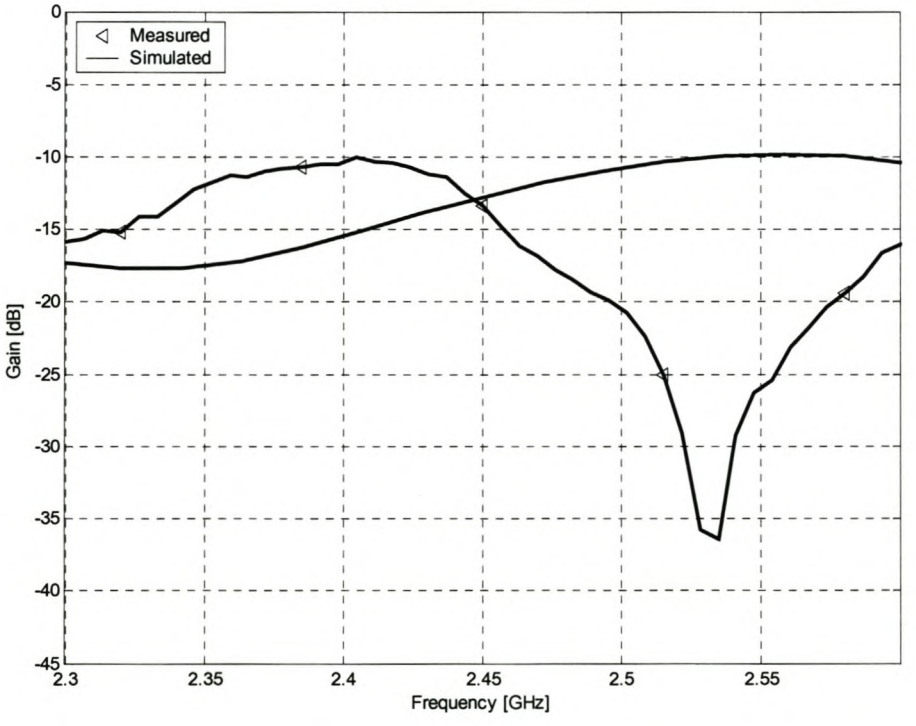

Figure 3-17: The comparison of measured and simulated RHCP gain of the helix

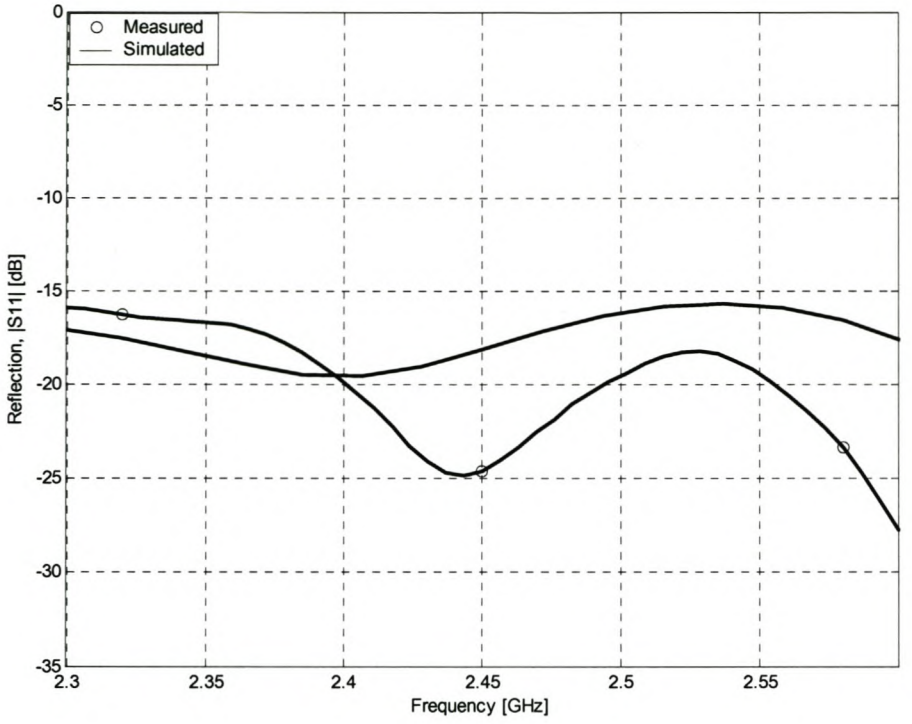

Figure 3-18: The measured and simulated reflection coefficient of the helix

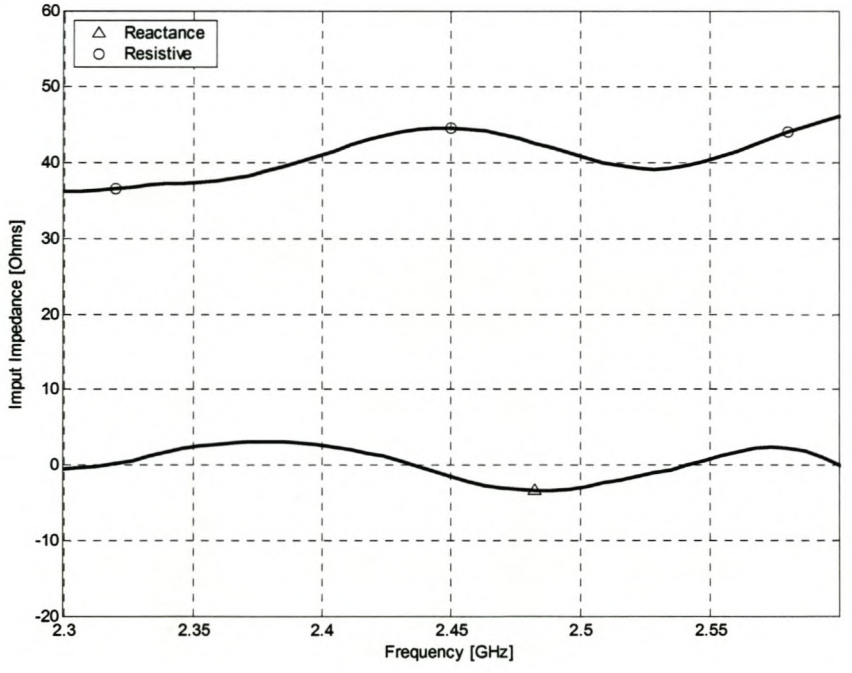

Figure 3-19: The measured resistive and reactive input impedance of the helix

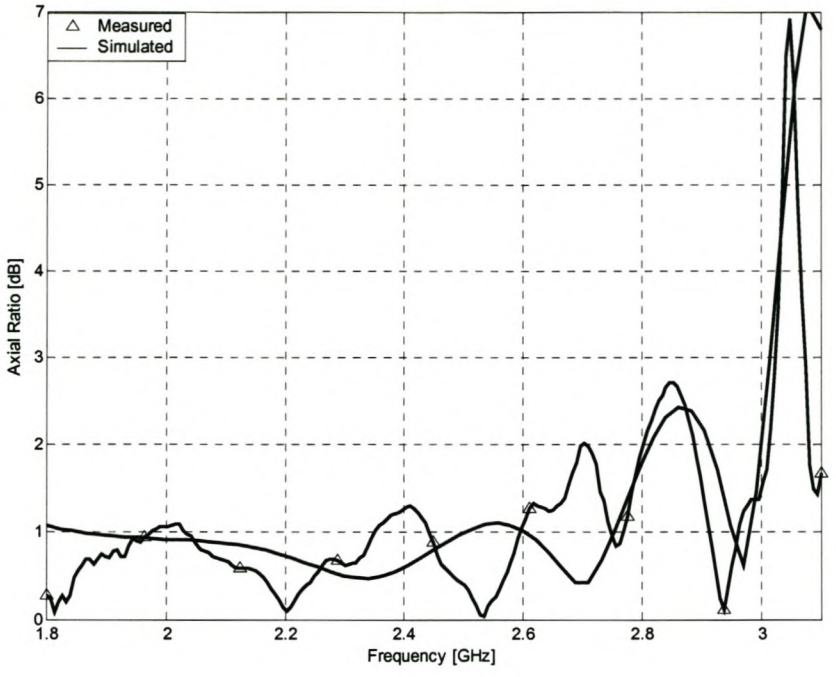

Figure 3-20: The simulated and measured axial ratio of the helix

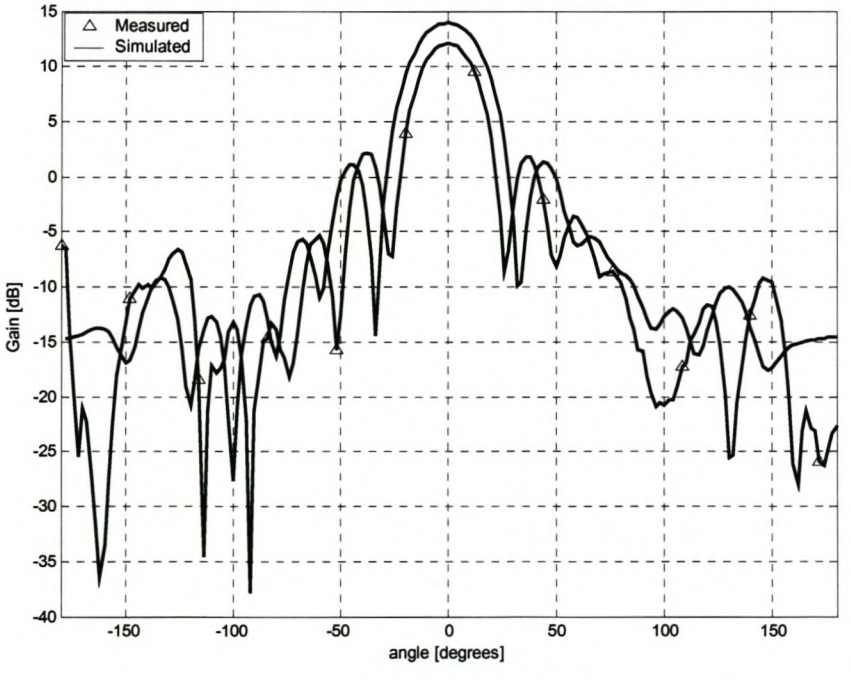

Figure 3-21: The measured and simulated LCHP gain radiation pattern of the helix

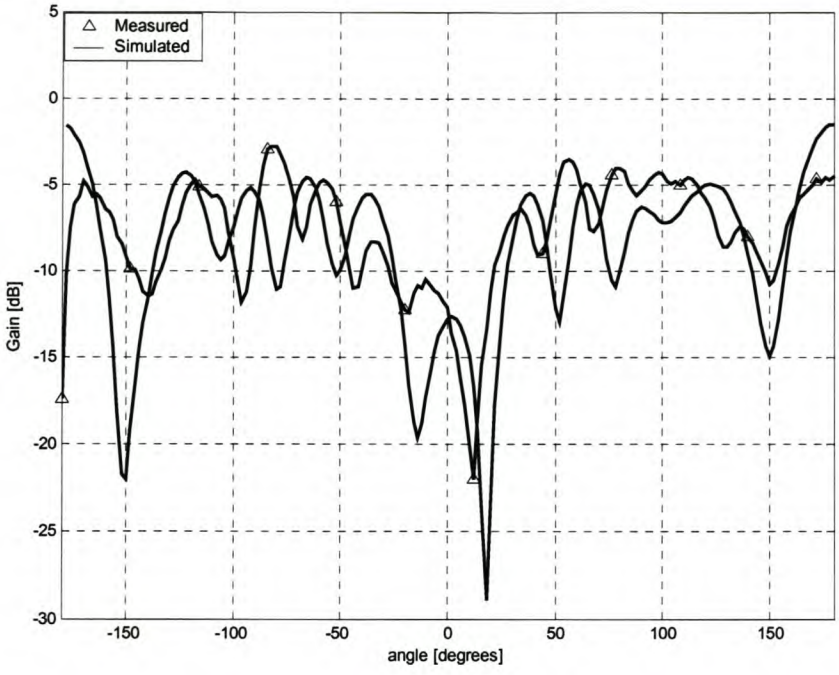

Figure 3-22: The measured and simulated RHCP gain radiation pattern of the helix

3.6 Discussion and Conclusions

The S_{21} between two linearly polarized horn antennas is given in figure 3-12; it was measured while the antennas were co-polarized avoiding losses through cross polarization. The horizontal and vertical S_{21} components of both horns each against the helix were used to determine LHCP and RHCP S_{21} components. The gain and reflections (S_{11}) of both horns were measured. The horns antennas show poor S_{11} and gain at lower frequencies (below 2.5 GHz). The simulated and measured gains of the helix antenna were compared and the simulated LHCP gain is 2dB higher than the measured gain along the bandwidth of interest. The measured gain has less bandwidth, it falls quickly at the upper edge of the bandwidth of interest. The RHCP gain matches the simulated gain at the center frequency, though the measured gain is a bit lower in average.

The reflection coefficient of the antenna and the impedance which are closely related were also determined. The obtained S_{11} is better than the simulated response. The reason behind this is that the matching circuit of the antenna was not modeled because a thin wire was used and accurate tapering distance could not be easily achieved and the antenna had to be optimized manually. In determining the simulated reflection response, the system impedance used was as calculated in

the first design and then optimized while carefully checking the response. From the simulation optimization, 147 ohms was obtained to be the best. In practical antenna the matching was optimized until a good matching was obtained using a vector network analyzer. From the measurements the reactive part of the impedance was 2 ohms at the frequency of interest and was in between 5 and -5 ohms through out the bandwidth of interest. The resistive part of the impedance was close to a complete match, approximately 45 ohms. The magnitude of the axial ratio was obtained to be 0.75 dB at the frequency of interest and it remains less than 1.3 dB throughout the required bandwidth. The measured gain response is lower by 2 dB as compared to the simulated gain from the radiation pattern. The simulated radiation pattern is also wider by about 8^{o}. The HPBW of the measured response is 28^{o}, while the simulated response is approximately 36^{o}. The measured beam width first null is approximately 50^{o} and the simulated is almost 58^{o}. The measured radiation pattern also showed strong side lobes which are 1 dB higher than the simulated side lobes. The measured RHCP radiation pattern is a little bigger than the simulated response. The measured pattern is bigger than -5dB within -150^{o} to 150^{o}, while simulated response is less than -5dB in the given range. The antenna measurements agreed with the simulations and it satisfied the proposed minimum specifications. The measured antenna showed a narrow bandwidth compared to simulations, which was accounted largely to the supporting structure [3]. The 2 dB loss incurred was also accounted to supporting materials and also the measurement setup, measuring components including the two horn antennas. The test antennas displayed reflections bigger than -10 dB at frequencies below 2.45 GHz, which is not very good to work with. The gain and reflections comparison with bigger span is given in chapter appendix.

3.7 Recommendations

A simple monofilar helix antenna is a potentially cost effective antenna which is still less exploited. It could be good for future designs to be completely modeled in the simulation software, which will improve predictability and probably reduce design time. To attain such and other high gain antennas it will require a consistent construction technique. The technique will have to be as accurate as possible to avoid disparities in the matching and supporting structure for long high gain helix. The separate matching section can also be considered to improve future designs predictability. There is a need for a simple antenna supporting structure that does not

influence the gain or matching of the antenna. Most of the above suggestions may require computer machined antenna for precision as compared to hand wound prototypes meaning more resources are needed.

3.8 Chapter Appendix

3.8.1 Complementary figures

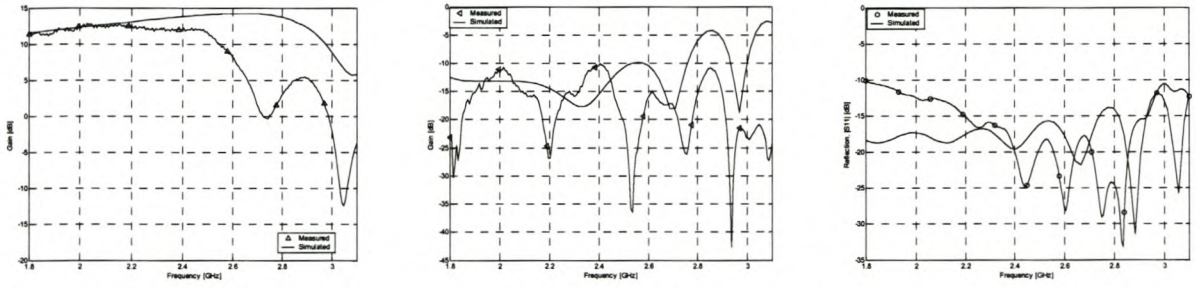

Figure 3-23: The simulated and measured LHCP gain, RHCP gain and reflections of the helix shown in large spans.

Figure 3-24: The measured helix antenna mounted on the U.S antenna chamber turn table

4. Interdigital Filter

4.1 Introduction

A microwave filter is a two port network used to control the frequency response at a certain point in a microwave system by providing transmission at frequencies within the passband of the filter and attenuation in the stopband of the filter [1, 9 and 29]. Typical frequency responses are low-pass, high-pass, band-pass and band-reject characteristics. In this case the response of interest is a bandpass filter. An interdigital filter was proposed to be designed and constructed because these filters are popular in the low GHz range and they work well. This filter can be fabricated on different mediums, for example microstrip, stripline, or using round and square rods. The proposed filter was implemented using cylindrical rods. The spacing of the rods, height and width of the closing material are determined from the capacitance matrix. A carefully designed filter of this type can result in a very small insertion loss.

These type of filters have a number of very attractive features [10]

- They are relatively compact
- The tolerances required in their manufacture are relatively relaxed as a result of relatively large spacings between resonator elements.
- In a properly designed filter the second pass band is centered at three times the center frequency of the first pass band, and no spurious response in between.
- The rates of cutoff and the strength of the stop bands are enhanced by multiple-order poles of attenuation at dc and at even multiples of the center frequency of the first pass band.
- It can be fabricated in structural forms which are self-supporting so that dielectric material is not required, eliminating dielectric loss.

A fifth order interdigital filter is designed in this chapter using the capacitance network and its transformation.

4.2 Filter Design

4.2.1 Design Theory

The design theory of an interdigital line is given and the basic filter design procedure is dealt with on the implemented design. Defining an interdigital filter requires the understanding of interdigital lines. The exact equivalent circuit for the interdigital line is the 2N port consisting of an array of N parallel conductors between ground planes [11] as shown in figure 4-1. In the early days the interdigital lines were used in slow wave structures to suppress unwanted harmonics and sometimes used as delay lines [10 and 31]. The characteristics impedance Zo of a lossless uniform transmission line operating in the TEM mode is related to its shunt capacitance by [11]

$$Zo = \frac{\eta_0}{\sqrt{\varepsilon_r}(c)} \tag{4-1}$$

The dimensionless ratio $c = c^{'} / \varepsilon$ can be used directly to obtain the physical dimensions.

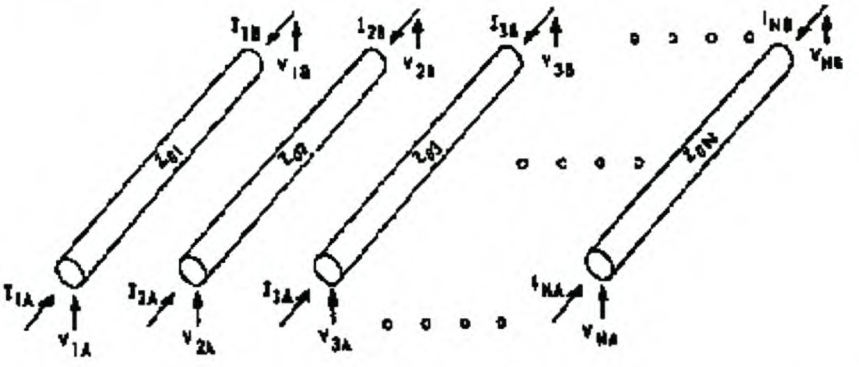

Figure 4-1: The basic parallel coupled line array which forms interdigital lines [10]

The array in figure 4-1 becomes an interdigital structure by shorting and leaving open alternative opposite ends of each conductor, as shown in figure 4-2. The array can begin with either open or short circuited line [11]. The input and output ports are on the same side of the array for N odd and on opposite sides for N even [29]. The interdigital filter with open circuited terminating lines has a third order pole at dc corresponding to three L-C elements, and the interdigital filter with short circuited terminating lines has a first order pole at dc corresponding to one shunt L element. The remaining N-3 for the N-line network with open circuited terminating lines and N-1 elements for the short circuited terminating lines are unit elements [11]. A brief description of unit elements is given by Wenzel in [12].

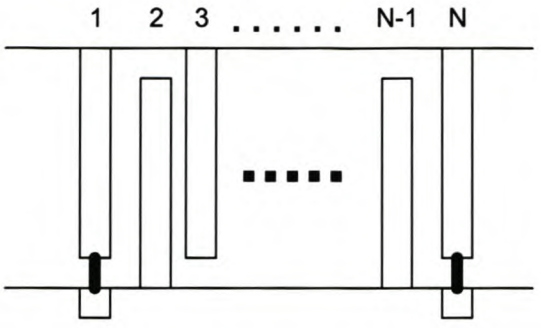

Figure 4-2: Odd number of rods interdigital network with alternating shorted lines, seen from the top

The focus of this work will be on the method used in the design and fabrication of the proposed filter which is the capacitance network method. The parallel coupled line array in figure 4-1 can be represented by the capacitance array as provided by figure 4-3. This representation assumes that no significant coupling exist between nonadjacent lines; if it were the case extra capacitance would be required between nonadjacent lines [11]. Extra coupling could cause the synthesis of the structures to be complex and the technique used here would not be applicable. In these structures each line element serves as a resonator, except for the input and output lines that have an impedance matching function.

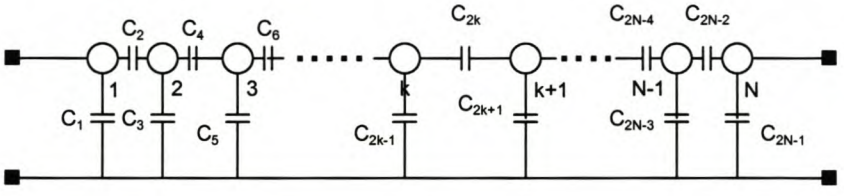

Figure 4-3: Two dimensional capacitance array of the interdigital line

The generalized capacitance matrix of the capacitance network in figure 4-3 can be given as provided by figure 4-4.

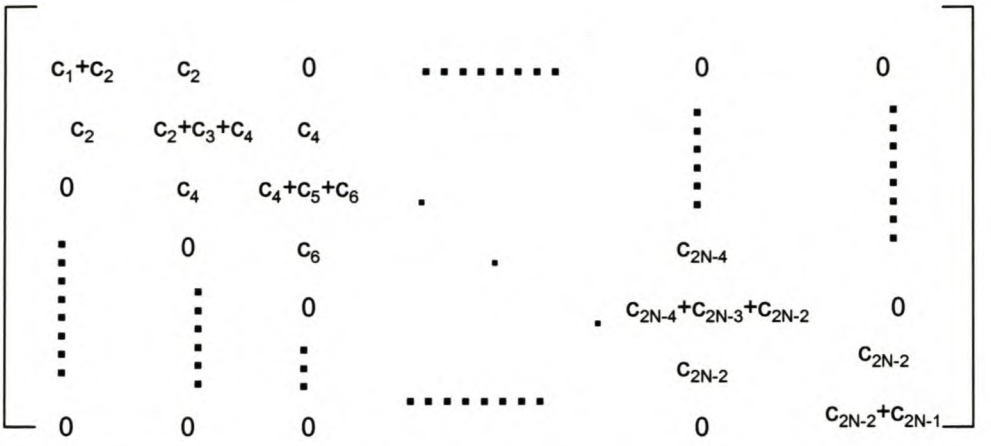

Figure 4-4: The capacitance matrix deduced from the generalized capacitance array of interdigital network

Multiplying the k th row and column of this matrix by any factor n' corresponds to multiplying the admittance level of the k th node by the square of n' and the transfer admittance between nodes adjacent to the k th node by the multiplying factor, n'. If this transformation is performed on any interior row and column, the two port performance of the network is unchanged. If the transformation is performed on the end row and column, the admittance level of the corresponding port is multiplied by the square of the factor (n'^2) [11]. Performing multiple transformations allows an infinite number of equivalent networks and port impedance level to be attained [11]. After the entire transformation the final circuit must not contain negative elements. The sum of the elements of any row or column should be greater or equal to zero. This condition ensures realizability of the circuit and also limits the choice of the multiplying factor. In performing the transformation the capacitors are treated as static capacitance [11]. The capacitance network which represents static capacitance can also be used to obtain dimensions for the a physical realization of the interdigital structure.

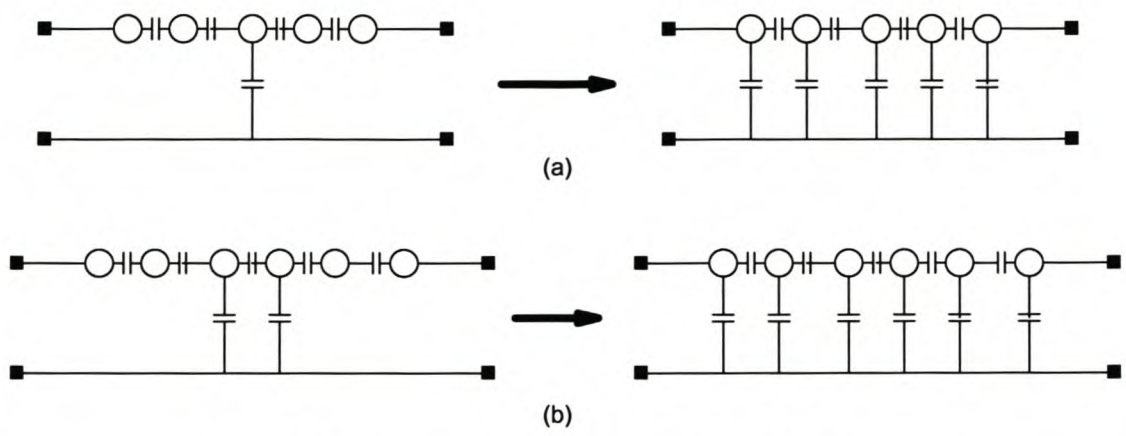

Figure 4-5: Capacitance network equivalent [11]

A capacitance network containing both self and mutual capacitance can be obtained by transformation from a capacitance network having an odd number of nodes containing all series capacitors and one shunt capacitor from the center line to the ground plane, see figure 4-5(a). Similarly, a capacitance network containing both self and mutual capacitors can be obtained by transforming a capacitance network having an even number of nodes containing all series capacitors and shunt capacitors from the two nodes nearest the center, see figure 4-5(b), [11]. The capacitance network containing the simplest form is used because the nature of the coupling between lines is readily found in terms of S-plane elements. The form shown in figure 4-5 is particularly useful for symmetric networks and can often be used for asymmetric networks without the addition of ideal transformers.

4.2.2 Filter Specification

Equal ripple chebyshev filter response

Center frequency	: 2.45 GHz
Bandwidth	: 5% (0.1225 GHz)
S_{11}	: $\leq$-20 dB
Insertion Loss	: $\leq$ 2 dB
Filter Order	: 5th order (7 lines including two transformers).
Passband Ripple	: 0.05 dB

4.2.3 Implemented Design

The interdigital filter uses highpass filter prototype and it offers an advantage of having a second passband at three times the first passband frequency as compared to a low pass prototype that has the second passband at two times the first passband frequency and also short line lengths.

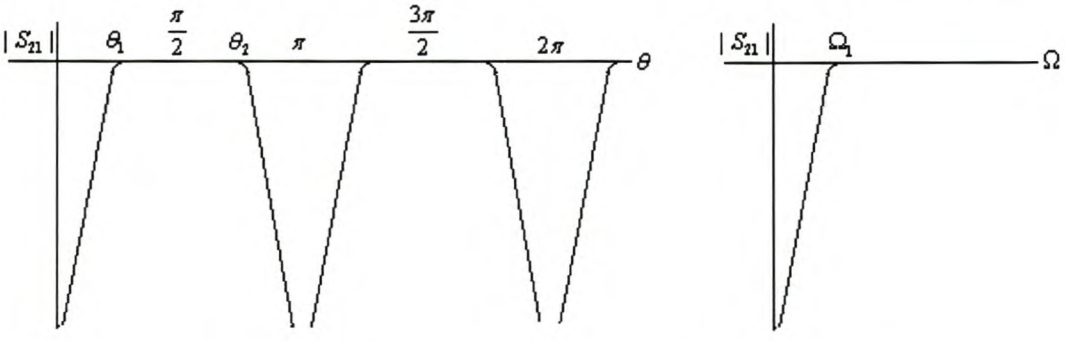

Figure 4-6: The highpass prototype transformation

From the specifications the bandwidth is 5 percent and using figure 4-6 and Richards's transformation, the following relations holds

$$\frac{\theta_2 - \theta_1}{\theta_0} = 0.05 \tag{4-2}$$

where θ_1, θ_2 and θ_0 represents the length at the first and second cutoff, and the center frequency respectively. From the high pass prototype, $\theta_0 = \pi/2$ and

$$\theta_2 - \frac{\pi}{2} = \frac{\pi}{2} - \theta_1 \tag{4-3}$$

where equations (4-2) and (4-3) lead to the following equation

$$\Omega_1 = \tan(\theta_1)$$

$$\Omega_2 = \tan(\theta_2) \tag{4-4}$$

where $|\Omega_1| = |\Omega_2| = 25.4517$.

From the s_{11} specification and assuming lossless and reciprocal network, the s_{21} ripple can be determined from

$$|s_{11}|^2 + |s_{21}|^2 = 1 \tag{4-5}$$

where the ripple is found to be , ripple = 0.0436 dB

The short circuited end lines were chosen to satisfy narrow bandwidth, as it is known to work much better with a bandwidth of 30 percent or less [9]. The supporting structure (side rods or transformers if added) is also fairly rigid, increasing dimension stability. From the specifications (5^{th} order) and table II in [11], the s-plane equivalent circuit takes the form shown by figure 4-7.

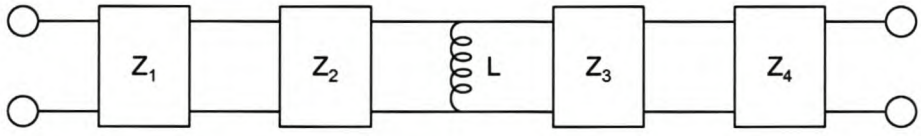

Figure 4-7: The s-plane equivalent circuit of a fifth order filter

The elements values on figure 4-7 were obtained from an in-house z-plane network synthesis program as follows.

$$Z_1 = Z_4 = 4.0338119 \times 10^{-2}$$

$$Z_2 = Z_3 = 4.659243 \times 10^{-5}$$

$$L = 2.908402318 \times 10^{-8}$$

Two shorted lines are added to work as transformers to match the filter to 50 ohm. The prototype s-plane equivalent circuit model now has seven elements.

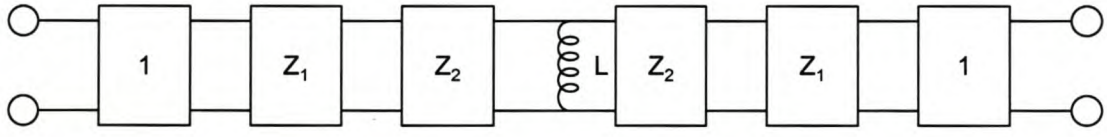

Figure 4-8: The prototype s-plane equivalent circuit model with 7 elements and the Z_1 and Z_2 are made the same in both sides because they are equal

The above s-plane circuit model can be realized by seven lines which are alternately shortened at their end points. See figure 4-2 and letting N equals 7. The capacitance network of such a structure is shown in fig 4-9 [11], after transformation to the simplest form.

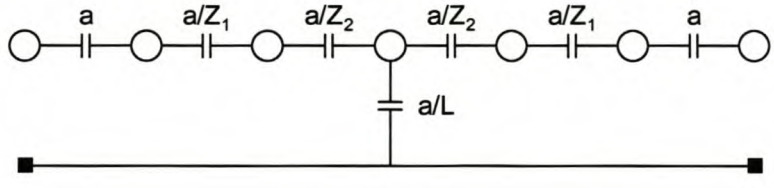

Figure 4-9: The capacitance network equivalent circuit of the seven elements including two transformers.

In figure 4-9, $a = \frac{\eta_o}{50\sqrt{\varepsilon_r}} = \frac{7.54}{\sqrt{\varepsilon_r}}$ (4-6)

This is for use in obtaining 50 ohm designs using s-plane elements normalized to 1 ohm [11]. The capacitance values in figure 4-9 are normalized and therefore dimensionless. A capacitance matrix is constructed with each diagonal element equal to the sum of all capacitance connected to that node (line) and each off-diagonal equals the capacitance connecting two nodes (lines), [13]. Multiplication of each row and column by a constant represent the introduction of transformers at both ends of the specific line, [11] and [13]. In general the capacitance network and its matrix is exactly in the form as provided in figure 4-3 and 4-4, but in this case N equals 7. It gives the capacitance to ground for each line as the sum of that column and the interline capacitance as the negative of the off-diagonals.

	n_1	n_2	n_3	n_4	n_5	n_6	n_7
n_1	a	-a	0	0	0	0	0
n_2	-a	a+a/Z_1	-a/Z_1	0	0	0	0
n_3	0	-a/Z_1	a/Z_1+a/Z_2	-a/Z_2	0	0	0
n_4	0	0	-a/Z_2	2a/Z_2+a/L	-a/Z_2	0	0
n_5	0	0	0	-a/Z_2	a/Z_1+a/Z_2	-a/Z_1	0
n_6	0	0	0	0	-a/Z_1	a+a/Z_1	-a
n_7	0	0	0	0	0	-a	a

Figure 4-10: The capacitance matrix constructed from the capacitance network in figure 3-9, with the rows and columns constant multipliers introduced.

After the multiplication of the matrix in figure 4-10 with constant multipliers and also setting $n_1=n_7=1$, $n_2=n_6$ and $n_3=n_5$ for symmetry reasons, the matrix changes to the one provided in figure 4-11.

n_1^2a	$-n_1n_2a$	0	0	0	0	0
$-n_1n_2a$	$n_2^2(a+a/Z_1)$	$-n_2n_3(a/Z_1)$	0	0	0	0
0	$-n_2n_3(a/Z_1)$	$n_3^2(a/Z_1+a/Z_2)$	$-n_3n_4(a/Z_2)$	0	0	0
0	0	$-n_3n_4(a/Z_2)$	$n_4^2(2a/Z_2+a/L)$	$-n_4n_3(a/Z_2)$	0	0
0	0	0	$-n_4n_3(a/Z_2)$	$n_3^2(a/Z_1+a/Z_2)$	$-n_2n_3(a/Z_1)$	0
0	0	0	0	$-n_2n_3(a/Z_1)$	$n_2^2(a+a/Z_1)$	$-n_1n_2a$
0	0	0	0	0	$-n_1n_2a$	n_1^2a

Figure 4-11: The capacitance matrix transformed from the one in figure 4-10 by using constant multipliers

Using the matrix provided in figure 4-11 and also the conditions of the general capacitance matrix; see figure 4-3 and 4-4, the following equations can be deduced from the general capacitance network of the design of interest in figure 4-12.

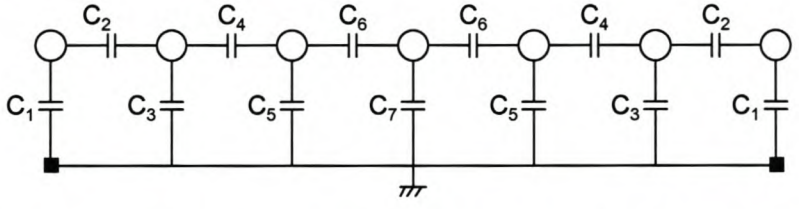

Figure 4-12: General capacitance network of the proposed design with capacitances to ground

The equations are

$$C_1 = n_1^2 a - n_1 n_2 a \tag{4-7}$$

$$C_3 = -n_1 n_2 a + n_1^2 (a + \frac{a}{Z_1}) - n_2 n_3 (\frac{a}{Z_2}) \tag{4-8}$$

$$C_5 = -n_2 n_3 (\frac{a}{Z_1}) + n_3^2 (\frac{a}{Z_1} + \frac{a}{Z_2}) - n_3 n_4 (\frac{a}{Z_2}) \tag{4-9}$$

$$C_7 = -2n_3 n_4 (\frac{a}{Z_2}) + n_4^2 (\frac{2a}{Z_2} + \frac{a}{L}) \tag{4-10}$$

The multipliers n_5, n_6 and n_7 are replaced by their symmetrical equivalents as mentioned earlier, thus leading to have a symmetrical network shown in figure 4-12. Choosing equal capacitance to

ground in both lines helps reduce the number of unknowns. If that is the case then there are four equations with four unknowns, i.e equation (4-7, 4-8, 4-9 and 4-10) and the unknowns are n_2, n_3, n_4 and cg which is representing all the capacitances to ground(C_1, C_3, C_5 and C_7). From equation (4-7), (4-8) and solving for n_3, the following relation is obtained

$$n_3 = \frac{n_2^2(a + \frac{a}{Z_1}) - n_1^2 a}{n_2 \frac{a}{Z_1}} \tag{4-11}$$

Also from equation (4-7) and (4-9) and solving for n_4 the following relation is obtained

$$n_4 = \frac{-n_2 n_3 \frac{a}{Z_1} + n_3^2(\frac{a}{Z_1} + \frac{a}{Z_2}) - n_1^2 a + n_1 n_2 a}{n_3(\frac{a}{Z_1})} \tag{4-12}$$

In actual iteration in equation (4-12), n_3 was replaced by equation (4-11). Thus in equation (4-12) only n_1 and n_2 exist on the right hand side of the equation, leading to only two unknowns. Using equation (4-7) and (4-10), the following relation is obtained

$$n_1 n_2 a - 2n_3 n_4(\frac{a}{Z_2}) + n_4^2(\frac{2a}{Z_2} + \frac{a}{L}) - n_1^2 a = 0 \tag{4-13}$$

From this relation only n_2 is unknown since equation (4-11) is used instead of n_3 and equation (4-12) is used instead of n_4. Inspecting equation (4-11) and (4-12), n_2 has many solutions due to double squared terms. Therefore numerous empirical iterations were used to determine the realizable value of n_2. The solution that satisfied the realizable criterion was $n_2 = 0.1999615$. It was used to determine the rest of the unknowns and were found as follows

$n_1 = n_7 = 1$

$n_2 = n_6 = 0.1999615$

$n_3 = n_5 = 0.00629814286754$

$n_4 = 1.559619304277080 \times 10^{-4}$

giving the values of the capacitance to ground from the general capacitance matrix provided in table 4-1. C_7 can also be approximated to C_1, C_3 and C_5. The negative of the off diagonal elements gives the capacitances between the rods. The obtained capacitance is converted to impedance using equation (4-1) and is used to model the realizable filter response. The dielectric constant, $\varepsilon_r = 2.54$ was used for modeling purposes only.

Capacitance to ground (C_g)		Corresponding Impedance in ohms	
C_1	3.784995	Z_1	62.45
C_3	3.784995	Z_3	62.45
C_5	3.784995	Z_5	62.45
C_7	3.762195	Z_7	62.45
Capacitance between adjacent rods		Corresponding Impedance in ohms	
C_2	0.946021	Z_2	249.87
C_4	0.147706	Z_4	1600.37
C_6	0.099741	Z_6	2369.98

Table 4-1: The table of the capacitances obtained from the Interdigital line analysis program with their respective impedances

The original ideal design was analyzed using microwave office. The filter was implemented using ideal lines called TLIN and TLIN4 which model the coupling between two conductors. The model makes use of the impedance values provided in table 4-1.

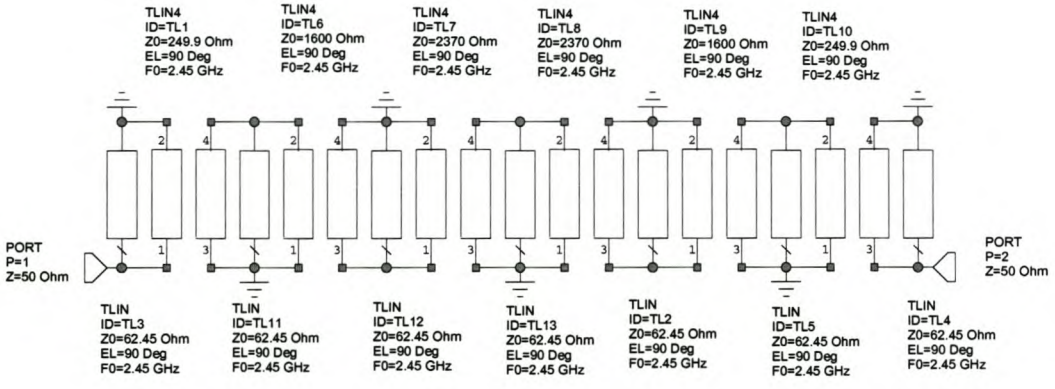

Figure 4-13: The simulated filter schematic from AWR Microwave Office with ideal transmission lines

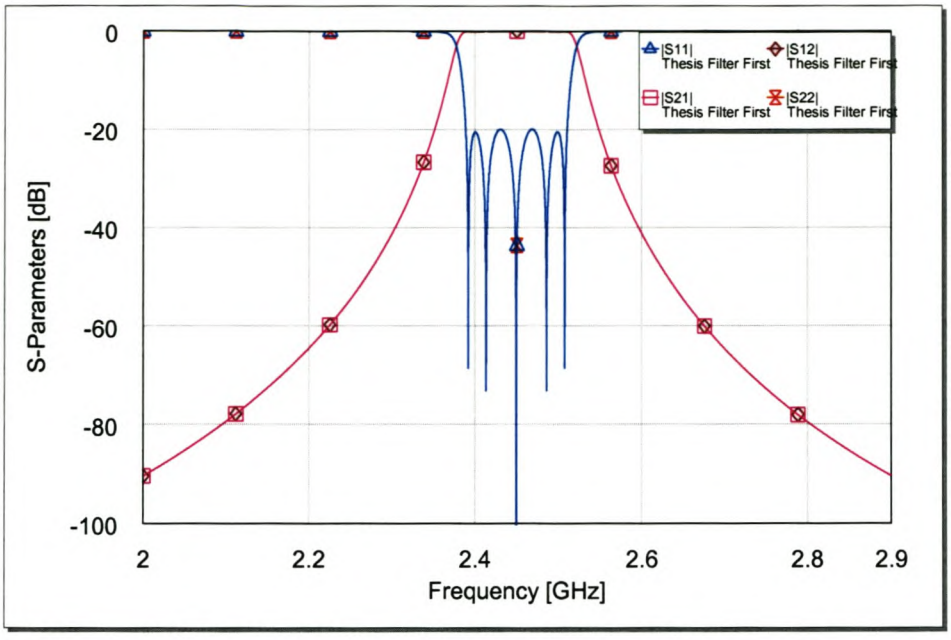

Figure 4-14: Simulated ideal filter response modeled using ideal lines from Microwave Office

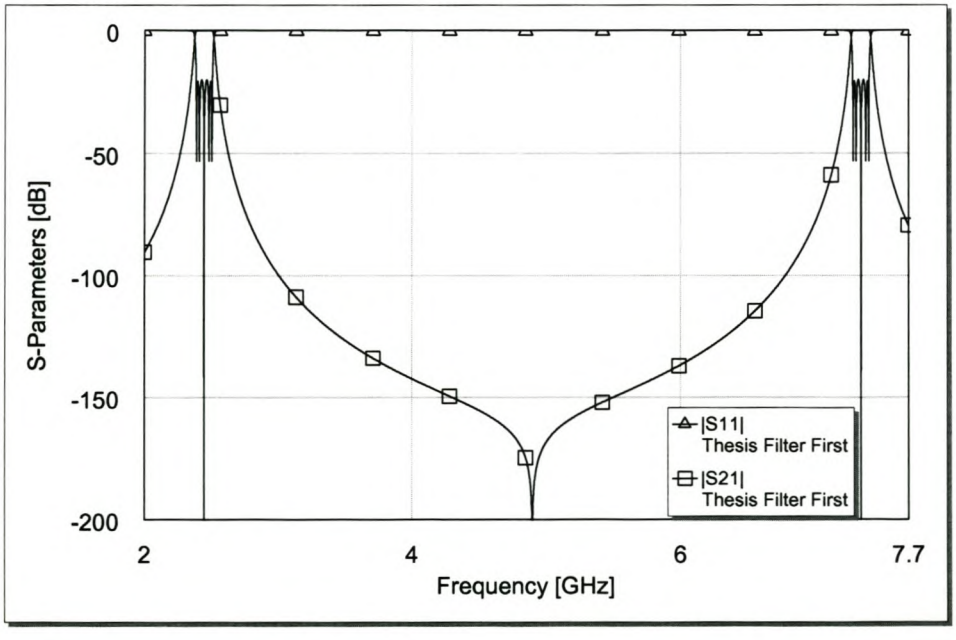

Figure 4-15: A wider span showing a second passband at three times the first passband

The simulations response obtained are exactly as expected and the simulation satisfies the proposed design specifications.

4.3 Prototype 1

The proposed filter prototype was to be fabricated using quarter wavelength cylindrical rods. An in-house code (Fildim) was used to approximate rod diameters and spacings from the capacitance values. This program synthesizes a single rod at one instance. The rods diameters obtained from the capacitance values (table 4-1) were different. The constant multipliers were optimized such that all the rods can have the same diameter. The multipliers were used with caution, to maintain the realizability of the final structure, thus by avoiding negative capacitance. After numerous iterations approximately equal rod diameters were obtained. The Fildim approximated diameters were 5×5.4mm rod diameters and 2×5.3mm rod diameters, with a maximum rod diameter difference of less than 0.2mm. The spacings were 5.467 mm, 14.771 mm and 16.4845 mm for s_1, s_2 and s_3 respectively, see figure 4-16. In-house interdigital line analysis program in Matlab was used to model the complete structure of the filter. The program allows the user to enter the height of the filter box, rod diameter vector (each rod diameter), the spacing vector between the rods and finally the wall spacing vector, which is the distance between the side wall and the first rod on each side. All rods were made equal to 5.4 mm and the rod spacings optimized until their capacitances are close to the ones in table 4-1. The capacitances obtained from the interdigital line analysis program are given in table 4-2, (see figure 4-12 for capacitance positions).

Capacitance to ground (C_g)		Corresponding Impedance in ohms	
C_1	4.050900	Z_1	58.35
C_3	3.714000	Z_3	63.65
C_5	4.277300	Z_5	55.26
C_7	4.318800	Z_7	54.73
Capacitance between adjacent rods		Corresponding Impedance in ohms	
C_2	0.939300	Z_2	251.713
C_4	0.156800	Z_4	1505. 63
C_6	0.114800	Z_6	2059. 09

Table 4-2: The capacitances table obtained from Interdigital line analysis program

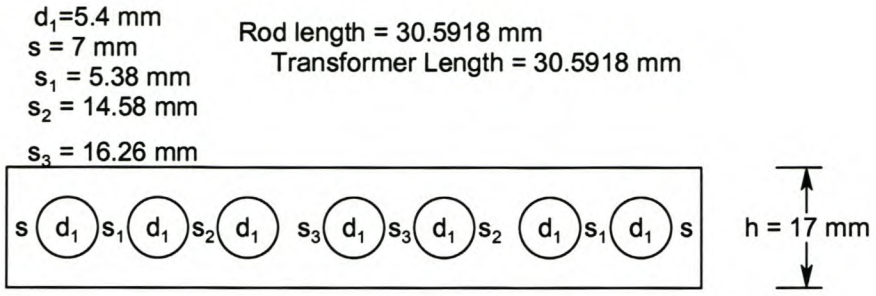

Figure 4-16: The suggested front cross section of the filter with dimension obtained from the interdigital line analysis program

Equation (4-1) was again used to convert capacitances in table 4-2 into their respective impedances. The impedances obtained were used to model the filter in Microwave Office. The impedances are also listed in table 4-2. The filter model was implemented as shown in figure 4-13, with the only difference being in the values of impedances.

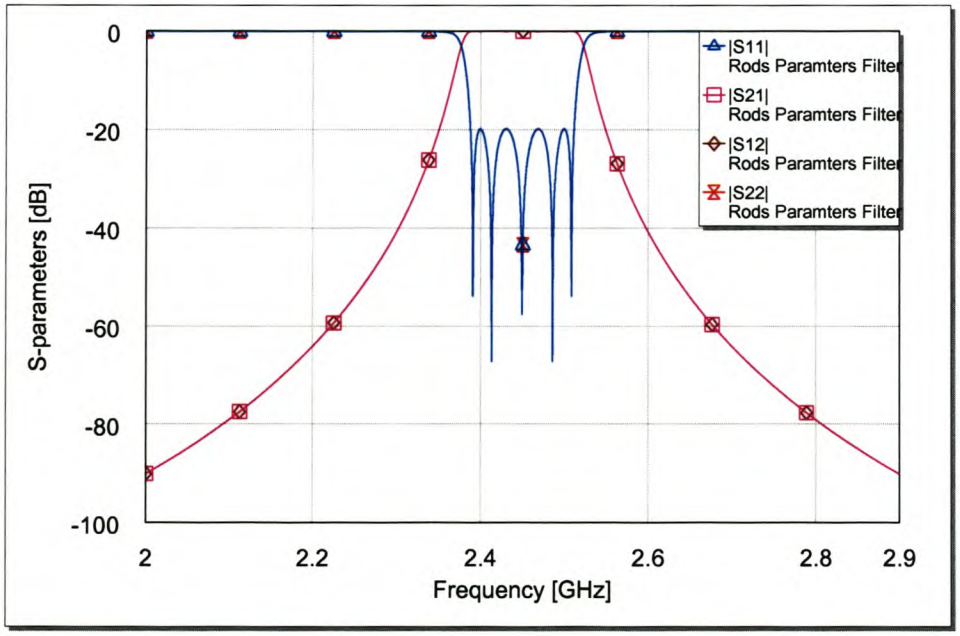

Figure 4-17: The simulated filter response obtained from the Interdigital line Matlab synthesis program

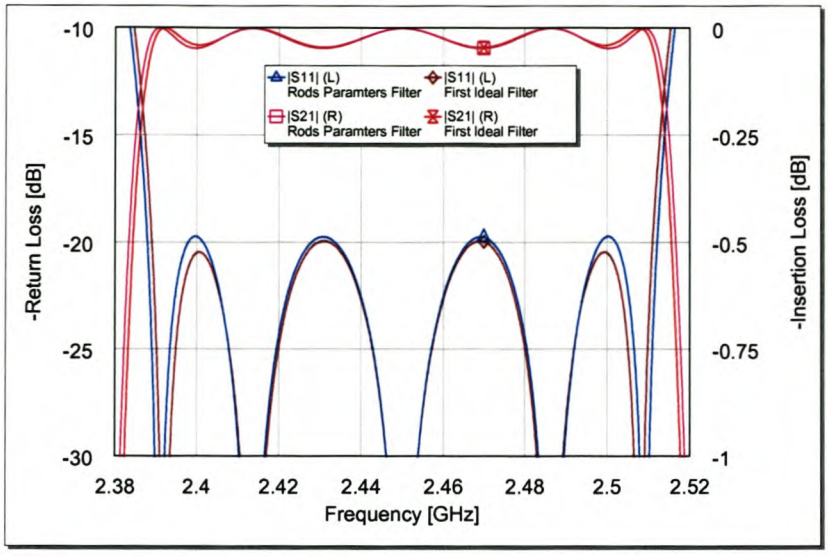

Figure 4-18: The simulated filter response comparison between first ideal filter and a filter modeled from rod diameters

The simulation results obtained using rod diameter capacitances are satisfactory. The filter was constructed and its rods and box were made of brass. Standard SMA Connectors were used as input and output ports. Tuning screws were also mounted on the open circuited side of each rod except the transformers. Figure 4-30 in the chapter appendix contains a picture of the manufactured filter.

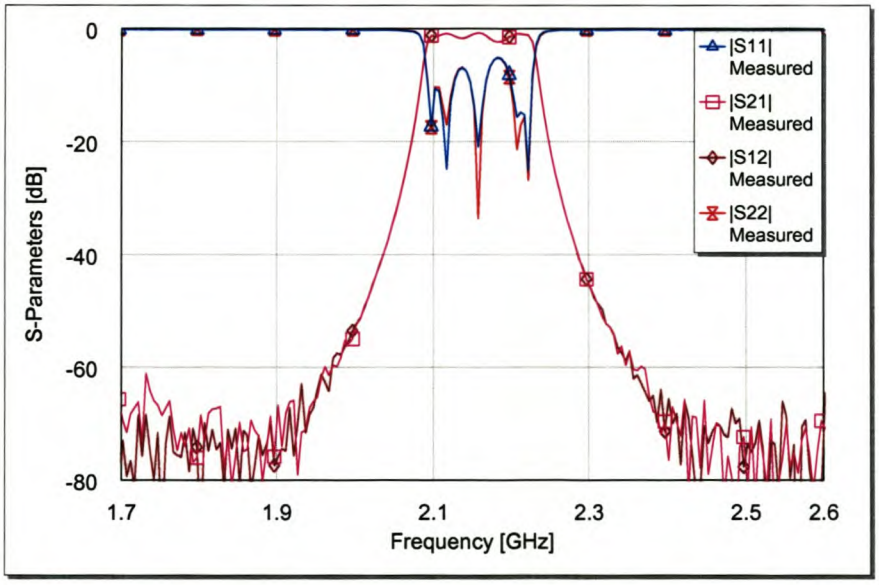

Figure 4-19: The first measured filter response only with tuning the screws to center it at the proposed center frequency.

From the measurements shown in figure 4-19, the reflection of the filter in the passband is not good, -5 dB. The center frequency shifted to lower frequency by about 10% and the insertion loss has a peak which falls to 2.2 dB within the band of interest. The filter had to be modified to shift the proper response to the proposed center frequency. A simple parameter extraction model was created to emulate the measured response using Microwave Office. The model showed that filter lines (rods) were much longer than required, thus creating more capacitance at each open circuited endlines. These lines were shortened by about 10% in response to the frequency shift required. The spacing between the end-lines and the first and last resonator was increased by 1 mm. The measured response after these changes is shown in figure 4-20. It shows an s_{11} improvement to -15 dB and an Insertion loss of 0.85 dB average through out the band of interest.

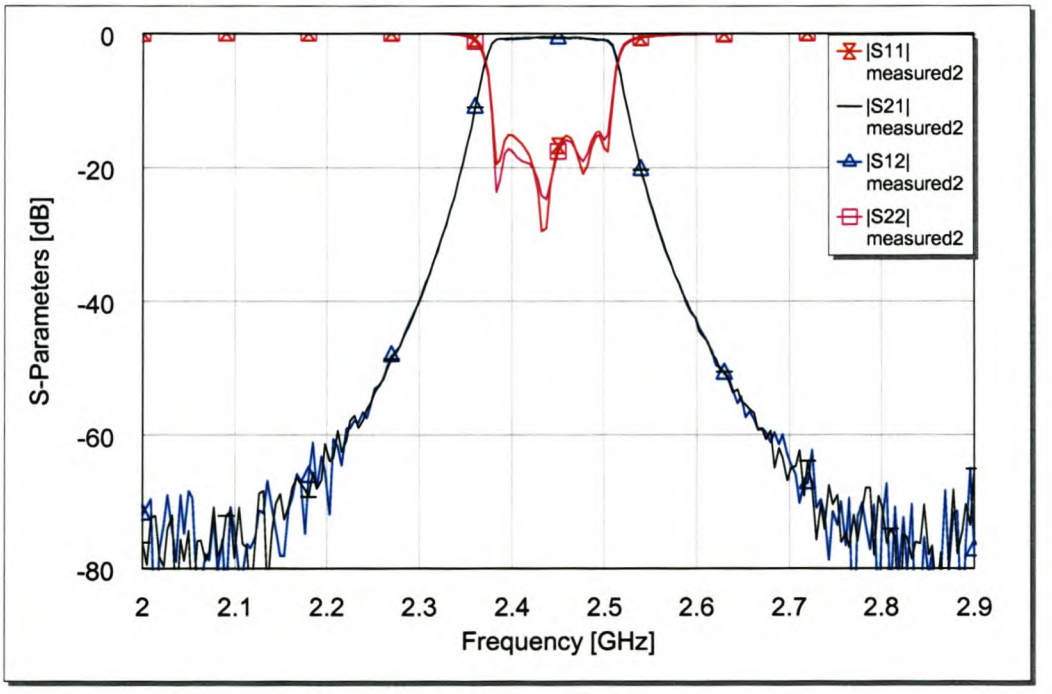

Figure 4-20: The measured filter response after shortening the rods and minor adjustment at the transformer

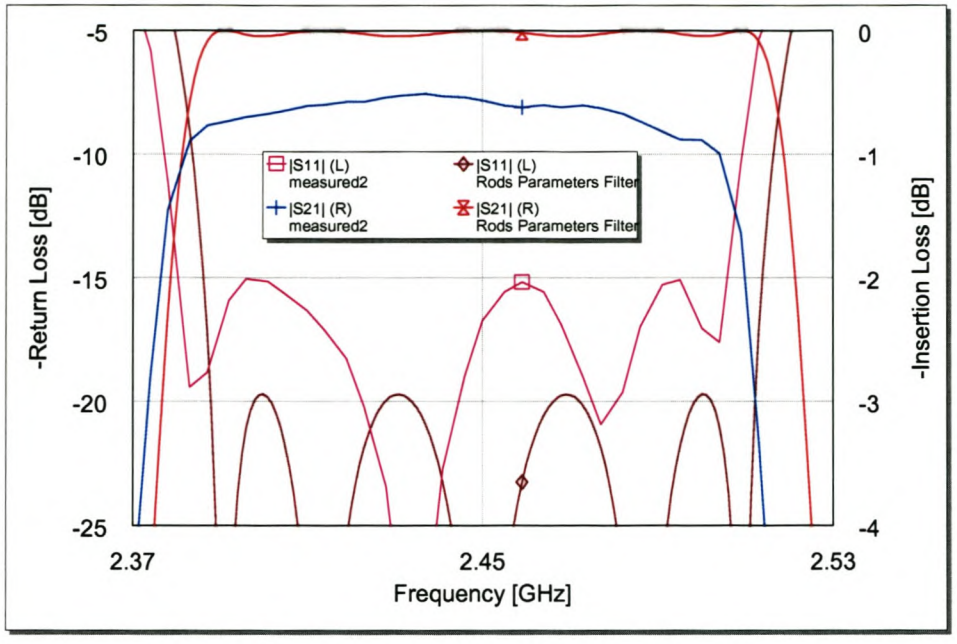

Figure 4-21: The comparison between measured tuned filter and the simulated response from rod parameters

The modification of the first prototype lead to an improved response, the reflections and insertion loss was improved as compared to the one given by figure 4-19. The reflection remained 5 dB bigger than expected from ideal simulations and lead to further investigation into the structure using other analysis software.

4.4 Prototype 2

The original dimensions (see figure 4-16) of prototype 1 were programmed into electromagnetic analysis software, called CST Microwave studio. The response was observed to be similar with the measured results shown in figure 4-19.

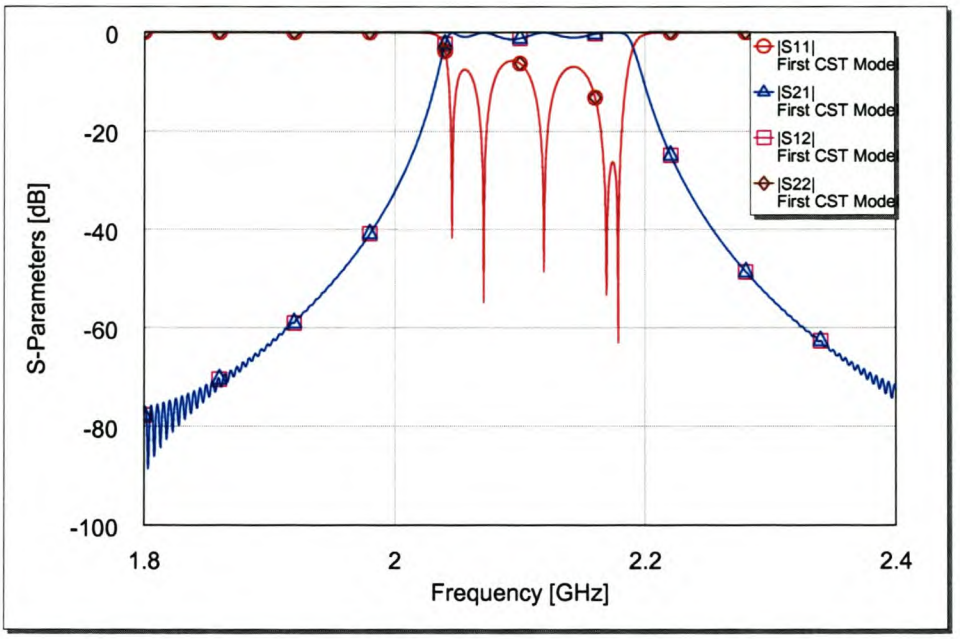

Figure 4-22: The CST microwave studio simulation of the first prototype using parameters from figure 3-16

With the encounter of the results shown in figure 4-22, the filter was optimized to give the expected response. A conical transition from the connector to the rod was also evaluated. From the microwave parameter extraction the length of the transformer also showed great influence in the reflections and also the positions of the two transformers. The lengths of the filter rods were also shortened after observing bigger capacitances at the open circuited endlines than expected. The lengths of the transformers were increased by 0.25mm. The final optimized filter dimensions used in CST are given in figure 4-23. Both the frequency and transient analysis were performed to increase the prediction accuracy. The width, length, height of the box and the diameters of the rods remained unchanged.

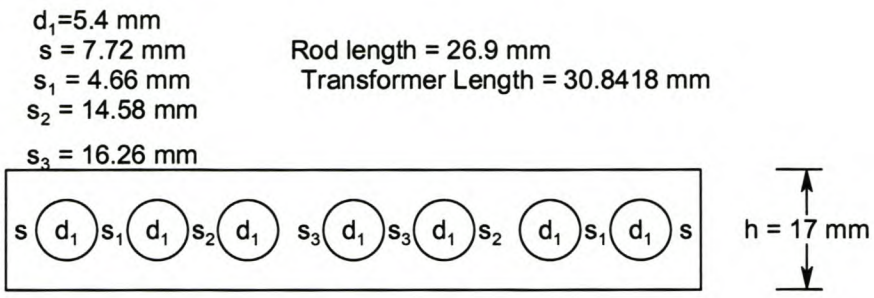

Figure 4-23: The final optimized filter dimensions simulated using CST Microwave studio

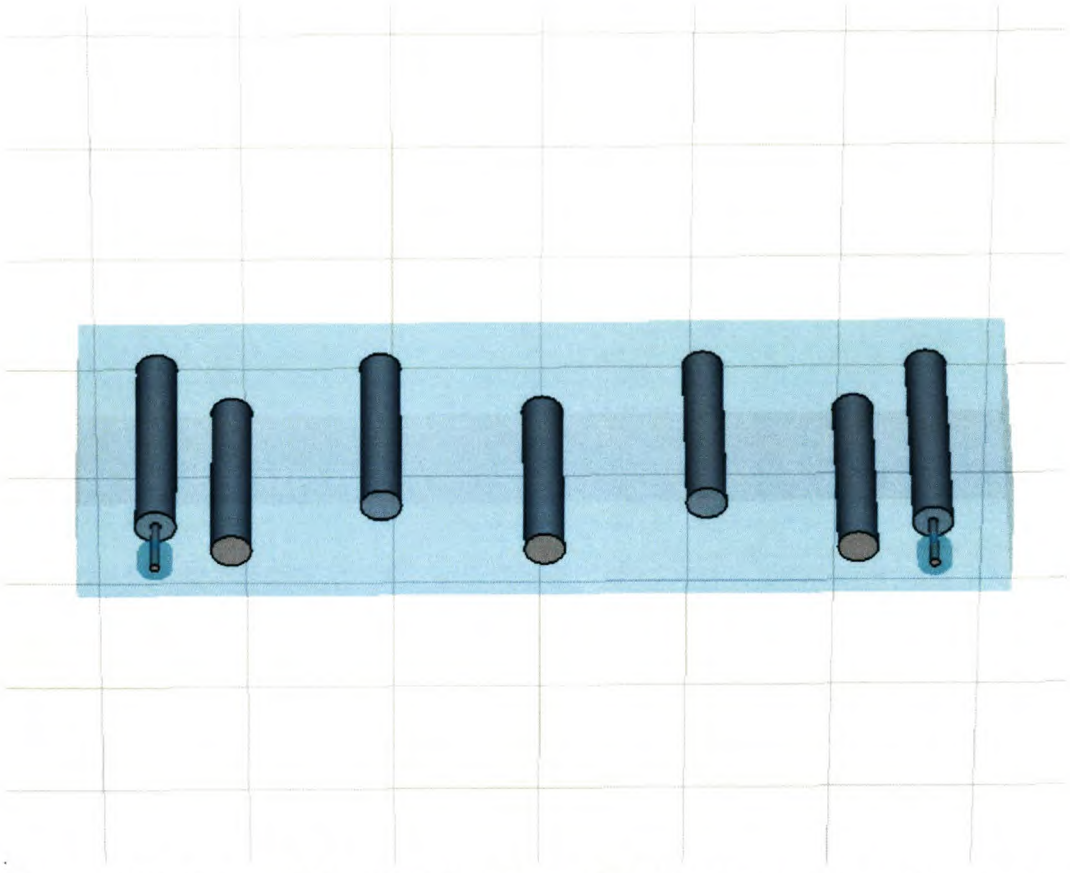

Figure 4-24: The model of the filter from the CST microwave studio software

The simulations results in figure 4-25 were performed with mesh cells at 211968. The frequency analysis shows a very good response, and it provides precise information even for large values of attenuation in s_{21}. The transient analysis seems to have a smaller dynamic range when compared to the frequency domain analysis. This is noted at frequencies where the attenuation is very large ($S_{21} \leq$ -70 dB). The s_{21} trace of the transient analysis shows instability where there is very big attenuation. Both frequency and transient analysis approximate the same response in the band of interest.

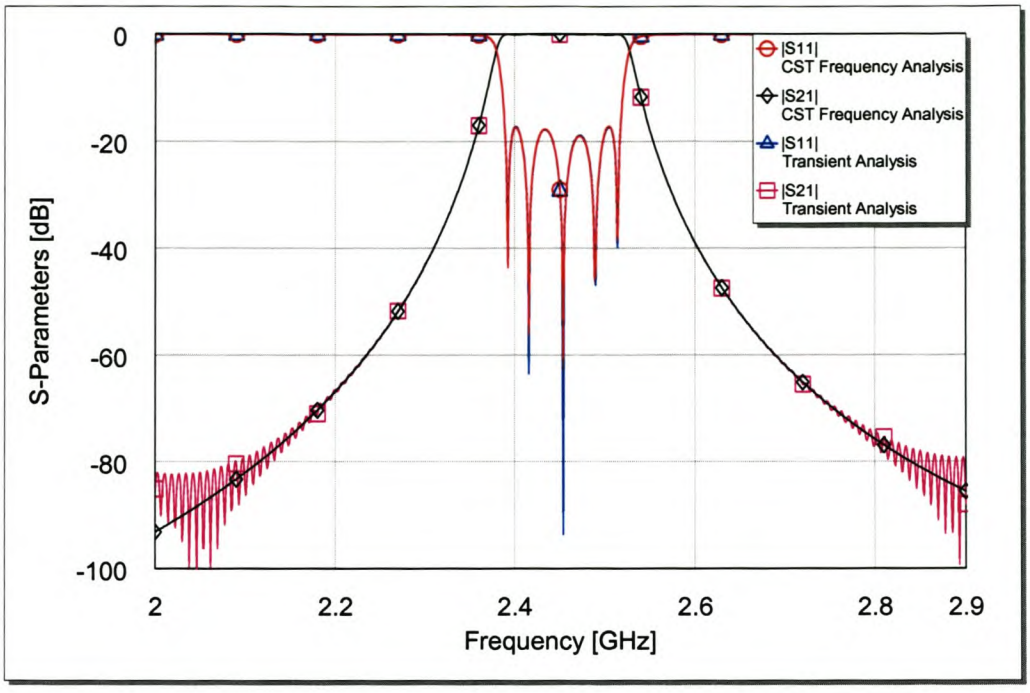

Figure 4-25: The frequency and transient analysis of the optimized filter from CST microwave studio software

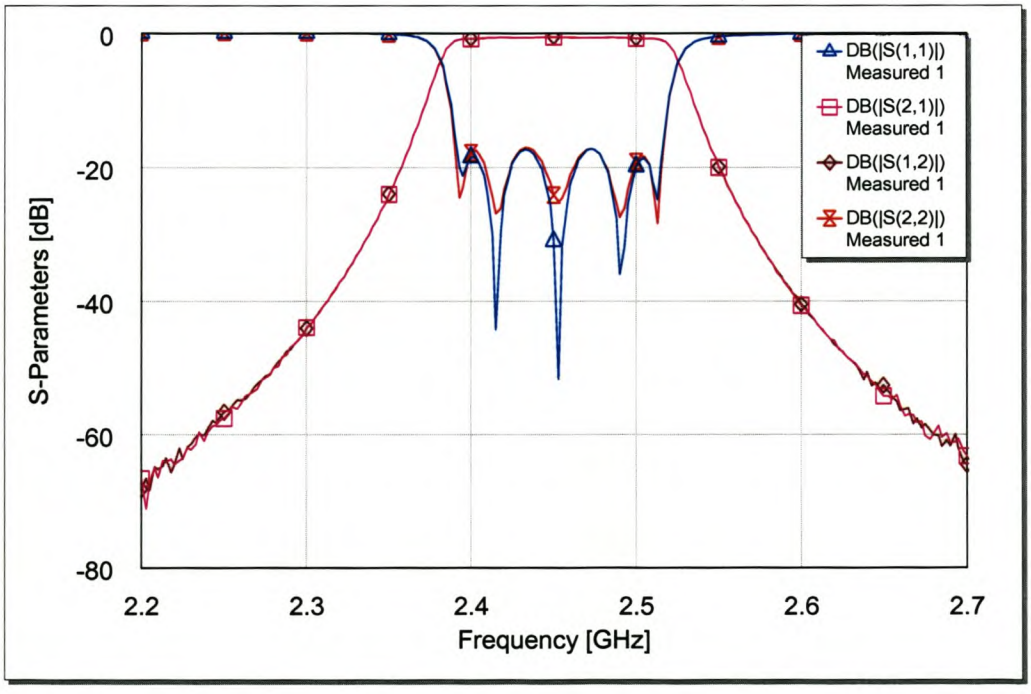

Figure 4-26: The Filter Measurements of the second prototype with all S-parameters

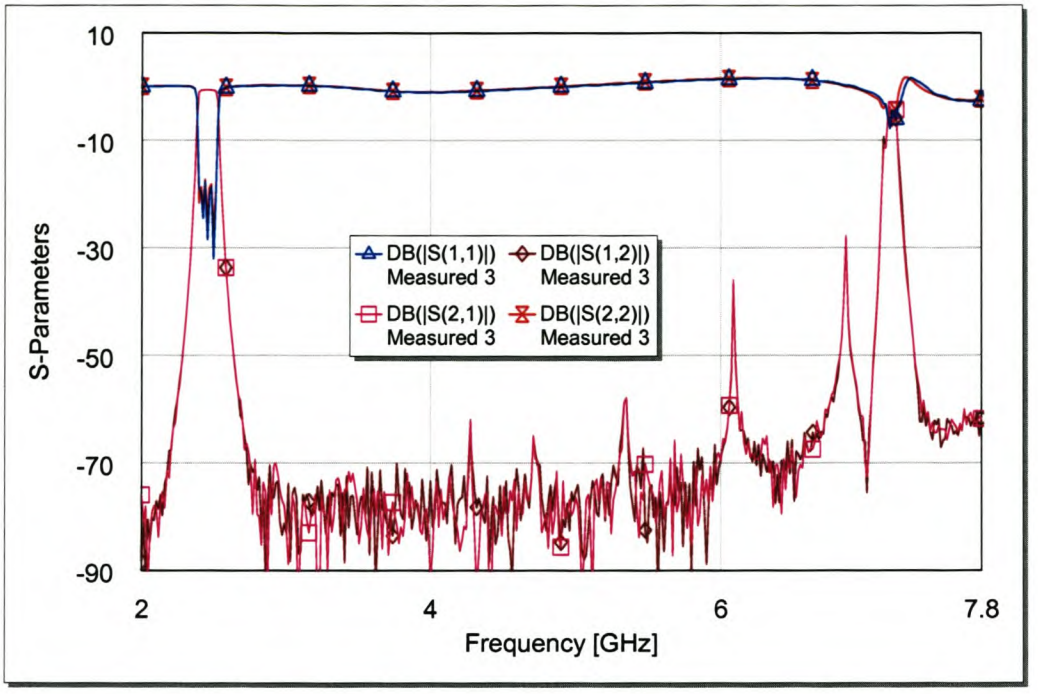

Figure 4-27: The filter response up to 7.8 GHz showing the second passband at approximately 7.35 GHz which can lead to spurious response

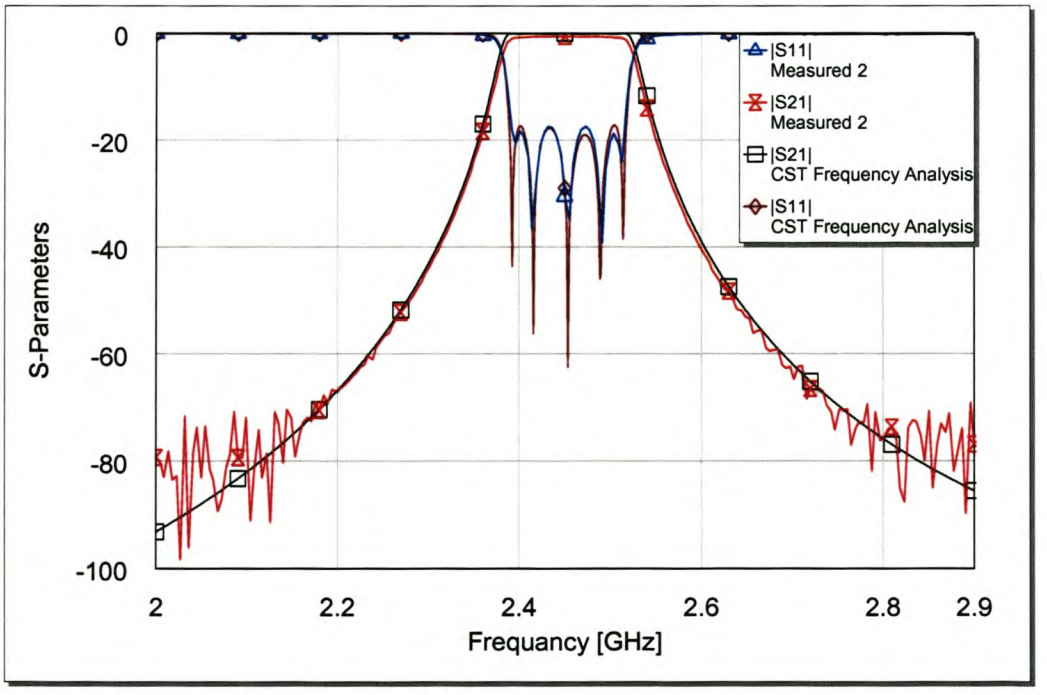

Figure 4-28: The comparison of measured and simulated response in frequency analysis

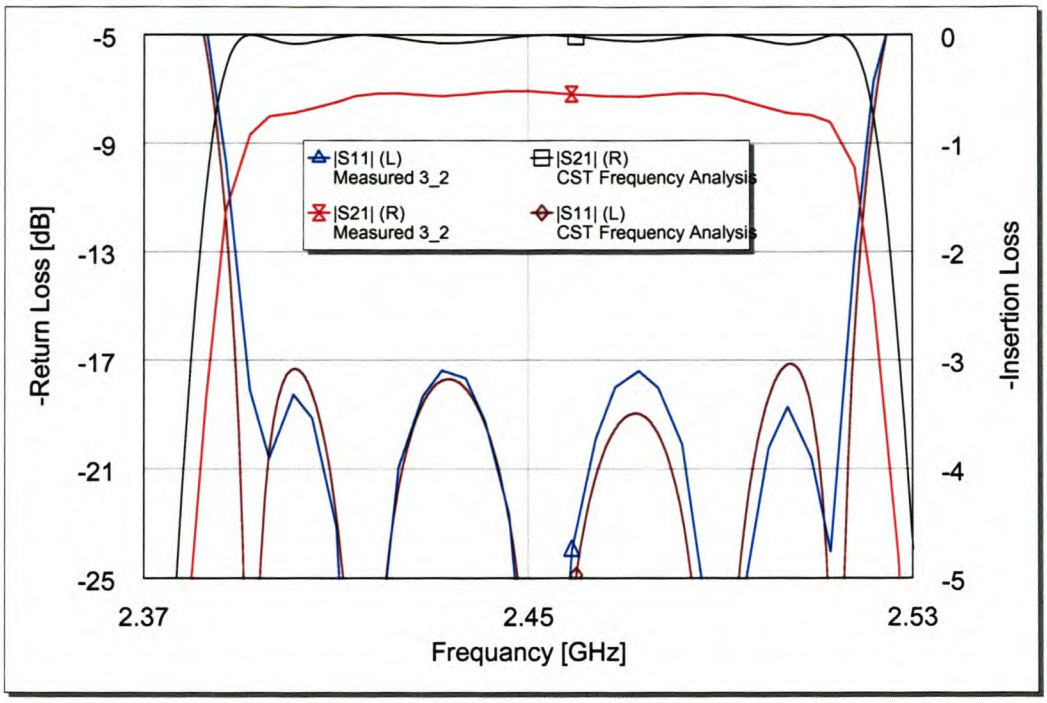

Figure 4-29: The comparison in figure 3-28 at the frequency band of interest

Figure 4-28 and 4-29 compare S_{11} and S_{21} only because the measurements were relatively symmetrical. An average insertion loss of 0.6 dB was obtained through out the frequency band of interest. The forward reflection of the filter is -31 at the center frequency; it remains less than -17 dB in the proposed bandwidth.

4.5 Discussion and Conclusions

The design using the capacitance matrix transformation proved effective. The filter was designed and simulated using two simulation packages. The ideal lines simulation using Microwave Office package was used in the first prototype. The response from prototype 1 built from the ideal simulations was not completely similar to the simulations. It showed bigger capacitance at the open circuited end of each interdigital line. Thick rods were preferred to minimize errors from manufacturing and analysis tolerances. The prototype had to be modified through parameter extraction. After the modifications the filter had a better response. Prototype 1 parameters were modeled using CST to determine the response as compared to the ideal simulation. The response was completely similar to the measured results. The parameter values were optimized to give the

required response. The rod lengths, transformer length and their positions were adjusted in the CST model. A better response, closely matching the proposed specification was obtained from prototype 2 measurements. CST Microwave Studio proved to be good interdigital structures analysis software compared to AWR Microwave Office. The s11 of the filter was higher by 2.5 dB as compared to ideal simulations. It was suggested that discrepancies might have been caused by a small error in each rod. Suppose each rod is coupled to the non adjacent rod by a very small coefficient, violating the technique assumption due to thick rods used. The error introduced could be fairly significant, considering seven elements (including transformers). In practice the filter designed met the minimum requirements of the system.

4.6 Recommendation

There is a dire need for rods spacings and diameter synthesis programs. Presently complete EM analysis software would be preferred in the designs of this nature as it will reduce design time for higher order filters. It can also increase the prediction accuracy. These types of filters are high performance structures and could be implemented in future work.

4.7 Chapter Appendix

4.7.1 Acronyms

c' = total static capacitance per unit length along the conductors

$c = c'/\varepsilon$ = ratio of static capacitance between conductors per unit length to the permittivity of dielectric medium.

η_o = Characteristic impedance of free space

n' = factors used to transform capacitance matrix (Multipliers)

Z_o = Characteristic impedance in ohms

k = integer used to denote position in series

Z = characteristic impedance of the line in the presence of other lines

N = Number of conductors in a parallel array (Integer)

SED = Sentraal Elektroniese Dienste

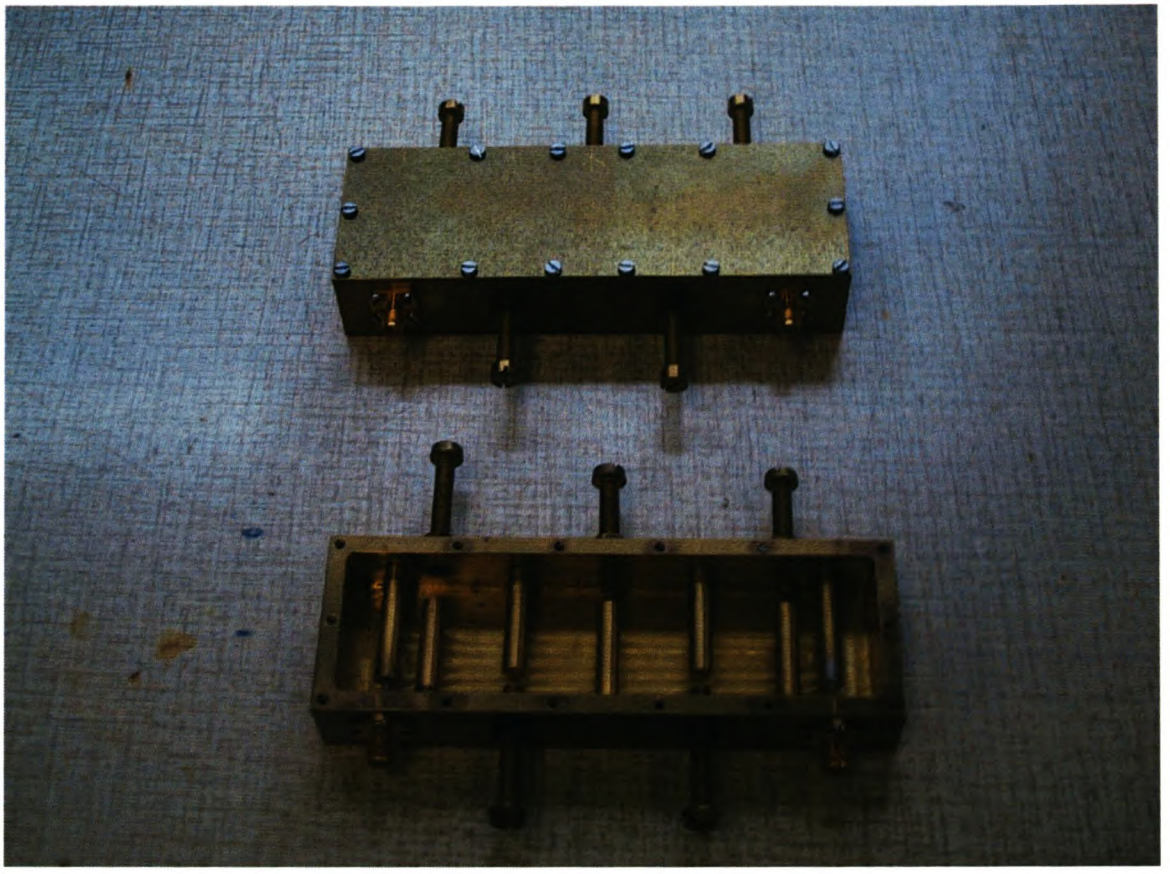

Figure 4-30: The two constructed filter prototypes

5. Oscillator Design

5.1 Introduction

RF and microwave oscillators are found in virtually all modern communications and measurements systems. A solid state oscillator uses an active nonlinear device, such as a diode or a transistor in conjunction with a passive circuit to convert DC-signals to a sinusoidal steady state RF-signals [1]. A Low frequency transistor oscillator can often be designed using a basic oscillator circuit with a crystal to improve frequency stability and low noise. At higher frequency, diodes or transistor biased to a negative resistance operating point can be used with cavity, transmission line or dielectric resonators to produce fundamental frequency oscillations up to very high frequency [1]. It can also be modelled as a feedback circuit providing a nonzero output voltage for zero input voltage [9]. There are numerous oscillator circuits, most of which are still referred to by the name of their originator, including Armstrong, Hartley, Colpitts, Clapp, Pierce and Wien bridge configurations [14]. They can be classified as fixed frequency or voltage controlled. Depending on the operational classification the most important characteristics of an oscillator is its frequency and tuning range, output power, frequency stability and spectral purity [9]. In this section a negative resistance microstrip oscillator is studied, designed and fabricated.

5.2 Design theory

5.2.1 Operational Theory

In the most general sense, an oscillator is a nonlinear circuit that converts DC power to an AC waveform [1]. Most RF oscillators are usually designed to provide sinusoidal output to minimize undesired side bands and phase noise. An oscillator can be described as the feedback system in which the feedback conforms to two criteria called the Barkhausen criteria [14].

- The feedback signal must be exactly in phase with the original input signal at the loop closure point.
- The overall steady state gain around the feedback loop must be exactly equal to unity.

The classical electronic system describing the fundamental operation of a sinusoidal oscillator can be described with a linear feedback circuit shown in figure 5-1.

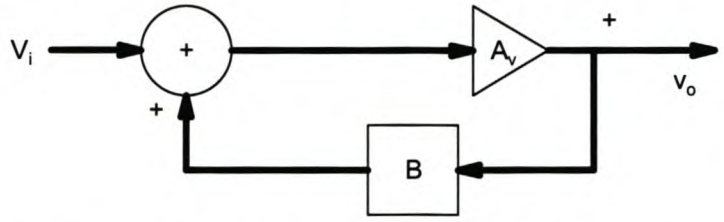

Figure 5-1: Block diagram of a sinusoidal oscillator using an amplifier with a frequency dependent feedback path [14]

An amplifier with a voltage gain A_v has an output voltage V_o. This voltage passes through a feedback network B which is a frequency dependent transfer function, and is added to the input voltage V_i of the circuit. The output voltage of the system including the feedback system can be expressed as [1]

$$V_o = A_v V_i + BA_v V_o \tag{5-1}$$

This can be solved to yield the gain of the closed loop system, A_{CL} as [15]

$$A_{CL} = \frac{A_v}{1 - A_v B} \tag{5-2}$$

If the denominator of equation 5-2 becomes zero at a given frequency, it is possible to achieve an overall system gain of infinity. It implies a possibility to achieve a nonzero output voltage from a zero input voltage [1 and 15]. The oscillator will reach a steady state when the large signal of the amplifier limit the product of $A_v B$ to unity. Unlike the amplifier which requires a stable circuit, an oscillator design depends on an unstable circuit [1].

5.2.2 Design Consideration

There are many design theories that can be used to realize a microwave oscillator. In this work the design consideration provided is the negative resistance method.

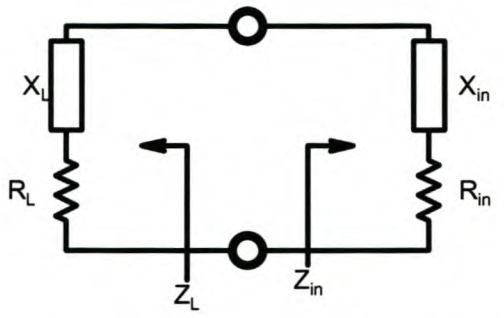

Figure 5-2: A simplified equivalent circuit for one port negative resistance oscillator

Figure 5-2 shows canonical RF circuit for a one port negative resistance oscillator, where Z_{in} is the input impedance of the active device [1]. In general this impedance is current (or voltage) dependent, as well as frequency dependent and it can be written as [9]

$$Z_{in}(I,f) = R_{in}(I,f) + jX_{in}(I,f) \tag{5-3}$$

The active device is terminated with passive load impedance, Z_L which depends on frequency and can be written as [9]

$$Z_L(f) = R_L(f) + jX_L(f) \tag{5-4}$$

Before the oscillation starts, the circuit must be in an unstable state, that is, $R_{in}+R_L<0$. Because the load is passive, then R_L is always positive, R_{in} must be negative. Therefore any disturbance or noise in the circuit may cause oscillation at some frequency f [9]. When the current increases due to oscillation, R_{in} changes to less negative. A properly designed oscillator settles down in a stable operation. From figure 5-2, applying Kirchoff's voltage law gives [1]

$$(Z_L + Z_{in})I = 0. \tag{5-5}$$

If oscillation is occurring, such that the RF current I is nonzero the following conditions must be satisfied [1]

$$R_L + R_{in} = 0 \tag{5-6}$$

$$X_L + X_{in} = 0 \tag{5-7}$$

Oscillation depends on the nonlinear behaviour of Z_{in}. As current I increases, $R_{in}(I,f)$ becomes less negative until the current I_o is reached such that [9]

$$R_L(f_o) + R_{in}(I_o, f_o) = 0 \tag{5-8}$$

$$X_L(f_o) + X_{in}(I_o, f_o) = 0 \tag{5-9}$$

The final stable oscillation frequency f_o is usually different from the original start up frequency because X_{in} is current dependent, so that $X_{in}(I,f) \neq X_{in}(I_o, f_o)$ [1]. In its stable condition any disturbance is damped, and after a disturbance the oscillator rapidly returns to its stable state [9].

Bipolar transistor oscillators are often preferred whenever they are practical because of their low phase noise and high dc-RF efficiency [16]. Field effect transistors replace the bipolar junction transistor at very higher or millimetre wave frequencies. Impatt and Gunn oscillators are capable of operation at frequency well above 100 GHz, but these oscillators often have high noise levels and poor dc-RF efficiency [16].

In designing an oscillator one needs to choose the circuit configuration, i.e. Colpitts or Hartley oscillator. Since a transistor oscillator is more like an unstable amplifier one also need to choose the connection configuration, i.e. common emitter or common collector. The different schematics are shown in figure 5-3 [1] which are the fundamental configuration. Many oscillator configurations can be deduced from the given circuit forms.

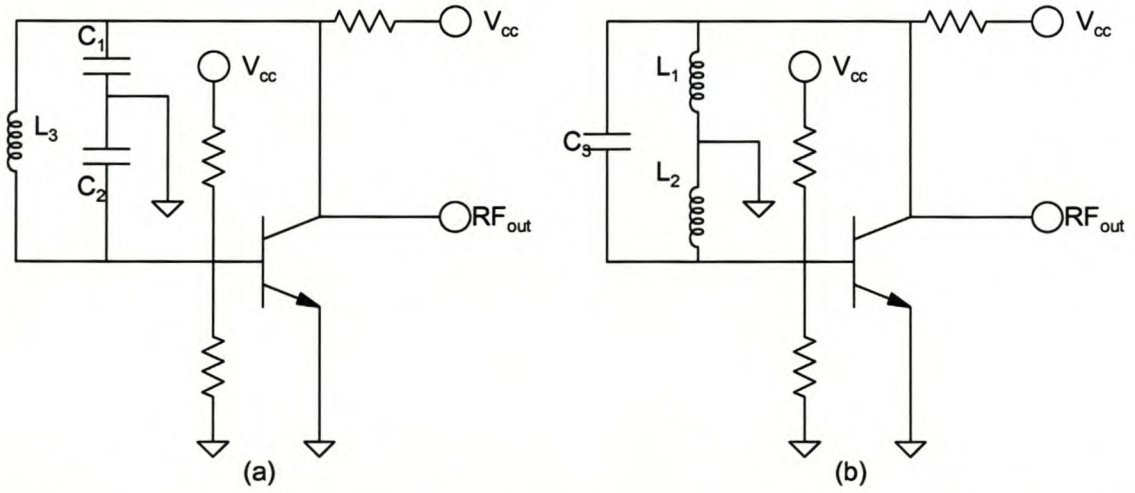

Figure 5-3: Transistor Oscillator circuits using a common-emitter BJT. (a) Colpitts oscillator. (b) Hartley oscillator [1]

From figure 5-3 (a) C_1 and C_2 are feedback capacitors and in (b) L_1 and L_2 are feedback inductors. Given the feedback parameters labelled in the above circuits configurations, it is possible to calculate the oscillation frequency at lower frequency, while at higher frequencies oscillation cease depending on lumped feedback elements. At high frequency the passive part become more dominant in determining the resonant frequency [1]. In the design procedure studied here which is the negative resistance method, the oscillator is modelled as a one-port device in which the real part of the port impedance is negative. The one-port can represent a two terminal solid state device that exhibits negative resistance or a two port that has feedback e.g. a conditionally stable transistor or amplifier, see figure 5-2. In a transistor oscillator, a negative resistance one-port network is effectively created by terminating a potentially unstable transistor with an impedance designed to drive the device into an unstable region.

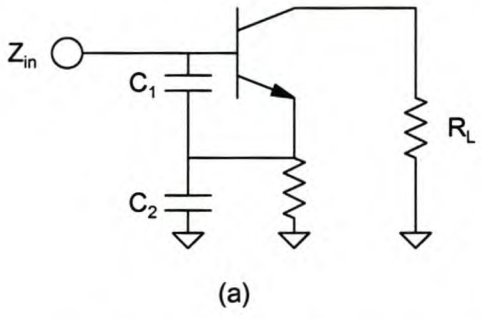

Figure 5-4: The feedback system used to enhance negative resistance, excluding bias

In figure 5-4, Z_{in} is the input impedance in which its real resistance should be negative. The load is included while modelling a one port circuit to increase the accuracy of the circuit model. The load, R_L can be removed, which often requires a more negative resistance compensating for the load to be added. High frequency transistor oscillator design requires a resonator to determine the resonant frequency. A good resonator should have a high quality factor, to minimise phase noise and improve frequency stability. Two fundamental characteristics of an oscillator are its frequency and output power. However other parameters like phase noise, pushing and pulling, thermal stability, harmonic and spurious output have a strong effect on the performance. A few definitions of these parameters are discussed in this work.

Phase Noise

Noise processes in semiconductor devices can modulate the angle and ampliyude of an oscillator output signal and create noise sidebands in the output spectrum. It becomes a big problem in systems where phase information is crucial. Choosing a BJT over a FET helps to reduce the phase noise, as well as using a resonator with a high loaded Q (quality factor) [16].

Harmonics and Spurious outputs

Primarily a well designed oscillator is usually free of spurious outputs that are not harmonically related to the frequency of oscillation [16]. Because the transistor is driven into saturation, most oscillators have significant harmonic outputs. The designer has very little control unless an output filter is used [16].

Thermal Stability

Oscillator temperature variation can affect the resonator's frequency response and also the transistor's input reflection. A very stable bias and resonator is required to compensate for temperature variation. Inconsistent resonators can also lead to post tuning drift which usually occurs in a VCO.

5.2.3 Design Specifications

Parameters	Performance
Fundamental frequency	1.75 GHz
Output Power	5 - 12 dBm
Power Supply Voltage	≤10 V
Power supply current	≤25 mA
Spurious Signal	≥60 dBc

Table 5-1: The proposed operational oscillator specifications

5.3 Bias Circuit and Resonator Design

A general purpose NPN Bipolar Junction Transistor (BJT) form agilent (AT41485) was used in the design. The common emitter Colpitts configuration was chosen.

Symbol	Parameter	Units	Absolute maximum rating
V_{EB}	Emitter Base Voltage	V	1.5
V_{CB}	Collector Base Voltage	V	20
V_{CE}	Collector Emitter Voltage	V	12
I_C	Collector Current	mA	60
P_T	Power Dissipation	mW	500

Table 5-2: Parameters list of the absolute maximum rating of the transistor

5.3.1 Biasing Circuit

The biasing of the oscillator is very important in the oscillator design, since it directly affects the overall design operation. If it is poorly implemented it can negatively affect the oscillator performance. In a fixed frequency oscillator, normally two terminals need to be biased, which in this case are base and collector terminals. The power supply voltage was chosen as, V_{CC}=10V and the collector current I_C to be 20 mA to satisfy the power expected from the design. The BJT is biased in the active region with the base-emitter junction forward bias and the base collector junction reverse biased [17]. The base-emitter voltage is approximately 0.6 volt but increases with a decrease in temperature and with increasing current. The biasing chosen is a one battery biasing [17]. This type of biasing ensures that the bias point is more stable and remains in an active region [17]. This bias is also ideal for the establishment of oscillation since it contains the feedback resistor, R_e, seen in figure 5.5. It helps in controlling the gain.

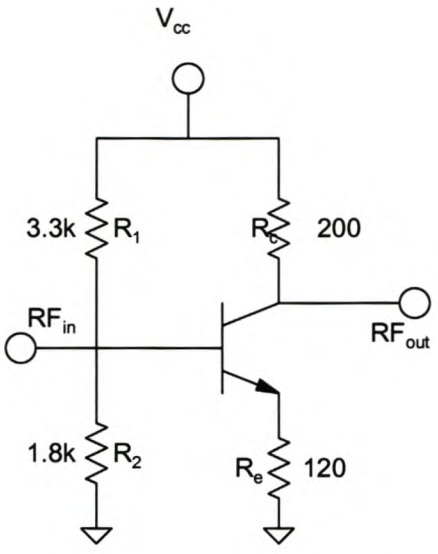

Figure 5-5: The proposed one battery bias network for the oscillator

Using the relations provided below and few empirical assumptions the values of the parameters provided in figure 5-5 were obtained. They were also approximated to practical available values. Few assumptions made were, for $\beta>1$, $I_c \approx I_e$. Stability requires $V_e > V_{be}$. The base voltage is $V_b \approx V_{CC}/3$ or V_e is normally 10% to 20% of V_{CC} [17].

$$R_e = \frac{V_e}{I_c} \tag{5-10}$$

$$R_c = \frac{V_{CC} - V_C}{I_c} = \frac{V_{CC} - V_{ce} - V_e}{I_c} \tag{5-11}$$

$$V_b = V_e + V_{be} \approx V_e + 0.6 \tag{5-12}$$

Selecting $IR_2 = 10I_b = 10I_c/\beta$, thus R_2 and R_1 can now be obtained from

$$R_2 = \frac{\beta V_b}{10 I_c} \tag{5-13}$$

$$R_2 = \frac{\beta(V_{cc} - V_b)}{11 I_c} \tag{5-14}$$

5.3.2 Resonator Design

A resonator is a structure having a natural frequency of oscillation [9]. The fundamental circuit of a resonator is usually modelled by an LC circuit. The resonator has the most direct influence on the frequency stability and phase noise of the oscillator. A resonator is often characterised by its quality factor and its reaction to varying temperature. A quality factor is a measure of the ratio

between the amount of energy stored and the energy dissipated in a circuit [1]. In this work a transmission line resonator is designed. Transmission line resonators can be fabricated as quarter or half wave short circuited or open circuited lines.

A practical resonator that is often used in microstrip consists of an open circuited length of transmission line [1]. These types of circuits behave as a parallel resonant circuit when the length is half or multiples of half wavelengths.

The input impedance of a lossy open circuited line of length l is [1 and 22]

$$Z_{in} = Z_o \coth(\alpha + j\beta)l \tag{5-15}$$

In practice most transmission lines have small loss and assuming its centre frequency is when the line is half wave length, [1] suggests the equivalent resistance, capacitance and inductance of the equivalent RLC circuit can be obtained. The quality factor of the half wavelength transmission line can be approximated as [1]

$$Q = \frac{\beta}{2\alpha} \tag{5-16}$$

where α is the combination of attenuation due to conductor and dielectric loss and β is the propagation constant [1].

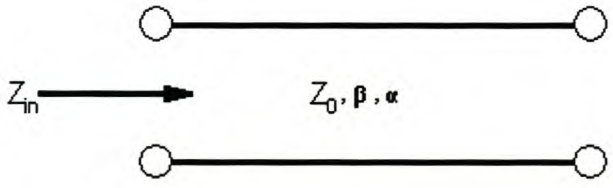

Figure 5-6: An open circuited length of lossy transmission line [1]

The requirements of the resonator are half wavelength (λ/2) of 50 Ω open circuited microstrip line. The substrate is the GIL1000, with a dielectric constant of 3.86, a height of 0.787 mm, a copper thickness of approximately 35 μm and a loss tangent. [18] was used to determine the width and the effective permittivity of the substrate. The width of a 50 ohm microstrip line on this substrate is, W = 1.61918 mm and the effective permittivity is, ε_e = 2.9640 (Using [18]). In equations 5-17 and 5-18, c and f represents speed of light in vacuum and frequency of operation respectively. In equation 5-20, μ_0 is a constant. The resonant length can be calculated from [1]

$$l = \frac{c}{2f\sqrt{\varepsilon_e}} \tag{5-17}$$

The propagation constant is [1],

$$\beta = \frac{2\pi f\sqrt{\varepsilon_e}}{c} \tag{5-18}$$

The attenuation due to conductor loss is [1],

$$\alpha_c = \frac{R_s}{Z_o W} \tag{5-19}$$

Where surface resistance R_s can be found from [1],

$$R_s = \sqrt{\frac{\omega\mu_0}{2\sigma}} \tag{5-20}$$

The attenuation due to dielectric loss is [1],

$$\alpha_d = \frac{k_o\varepsilon_r(\varepsilon_e - 1)\tan\delta}{2\sqrt{\varepsilon_e}(\varepsilon_r - 1)} \tag{5-21}$$

The results obtained using equations (5-16) to (5-21) are provided in the table below

Parameter	Determined Value
Resonant Length, l	49.8 mm
Propagation constant, β	63.1009 Rad/m
Surface Resistance, R_s	0.0109 Ω
Attenuation due to conductor loss, α_c	0.1347 Np/m
Attenuation due to dielectric loss, α_d	0.0806 Np/m
Unloaded quality factor, Q	180.3227

Table 5-3: The table showing the calculated resonator parameters

5.4 Simulations and Measurements

5.4.1 Simulations

The circuit from figure 5-5 is used with decoupling and DC blocking capacitors. The input port is connected to the side of RFin. Another port is connected to the side of RFout which is used to

model a 50 ohm load, see figure 5-7. The decoupling and DC block capacitor must be chosen carefully, with careful attention paid to their impedance at the frequency of operation. A feedback capacitor is placed in parallel with R_e to make the circuit highly unstable. The circuit was modelled using non linear analysis in AWR Microwave Office. Unlike the linear S-parameter model this analysis requires a transistor SPICE model. Thus it also requires the transistor to be biased in the simulation model. Firstly the bias circuit was modelled and the feedback resistor was tuned until the current from the power supply is as required. The resonator and the active circuit were combined and simulated using a harmonic balance simulator. This type of a simulator is able to predict power level, frequency of oscillation and also phase noise of the oscillator.

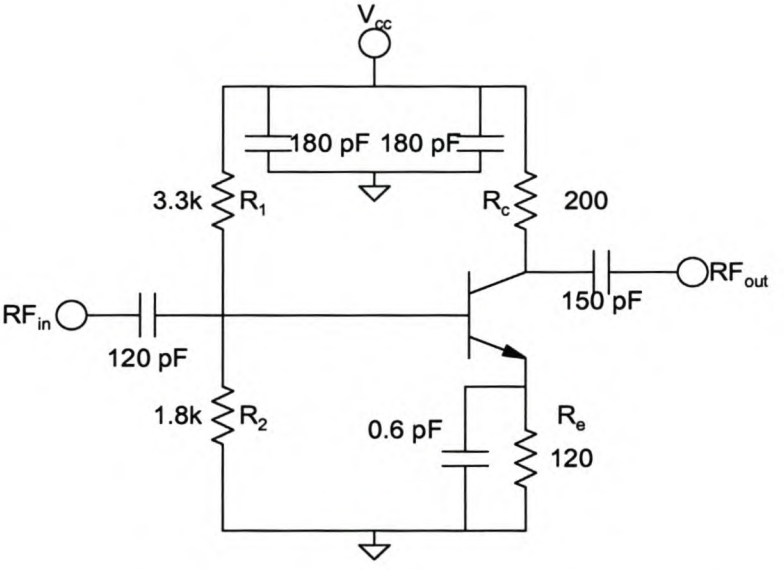

Figure 5-7: The circuit used as a one port circuit with a negative resistance, the RFin and RFout ports were modeled with 50 ohm

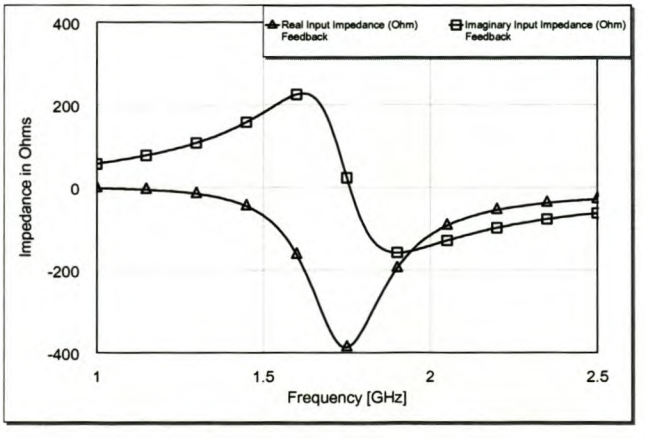

Figure 5-8: Simulated input impedance of the active circuit

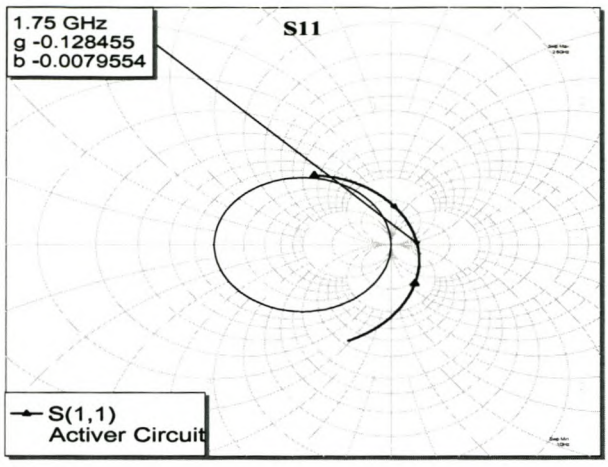

Figure 5-9: The s11 response of the active circuit outside the smith chart

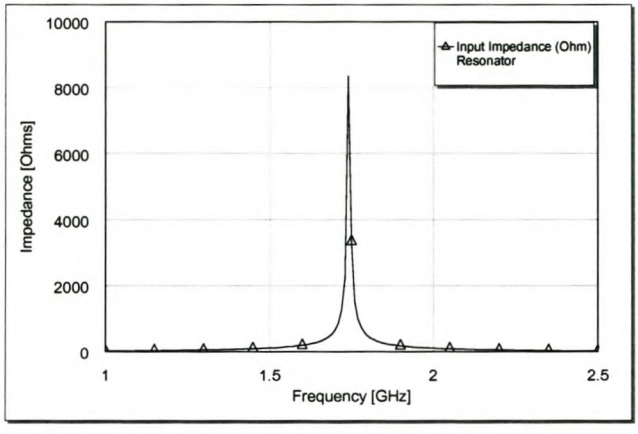

Figure 5-10: The input impedance magnitude of the resonator

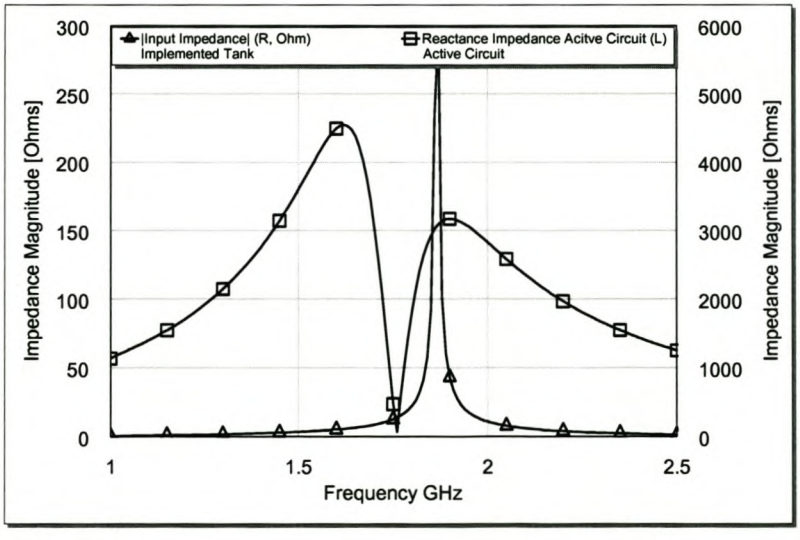

Figure 5-11: The resonant frequency determining graph, showing possibilities of resonance at approximately 1.75 GHz

In figure 5-7 two quarter wave length cascaded transmission line were included to act as RF chokes. These lines were implemented in the feed, from V_{cc} to base and to collector respectively. These lines were made shorter than the normal ¼ wavelength line by 30% to center the most negative resistance at the proposed center frequency. Figure 5-8 shows an input impedance response of the active circuit (without a resonator). It shows a negative resistance which is a prerequisite for oscillation. The reactance of the active circuit passes through zero ohm at a frequency about 1.75 GHz, which also enhance oscillatory condition in that frequency [17]. Figure 5-9 shows the s11 magnitude outside the smith chart (S_{11}>1). Figure 5-10 shows the ½ wavelength open circuited simulated resonator response. Figure 5-11 shows the reactance of the active circuit plotted in the positive half of the graph. It was achieved by using output equations from [18]. It also shows an input impedance of the tank circuit. The point where these two lines cross is approximated as the frequency of oscillation, which is 1.75 GHz. The complete oscillator circuit diagram with the ¼ wavelength feed lines mentioned above connected together with the resonator is given in figure 5-12.

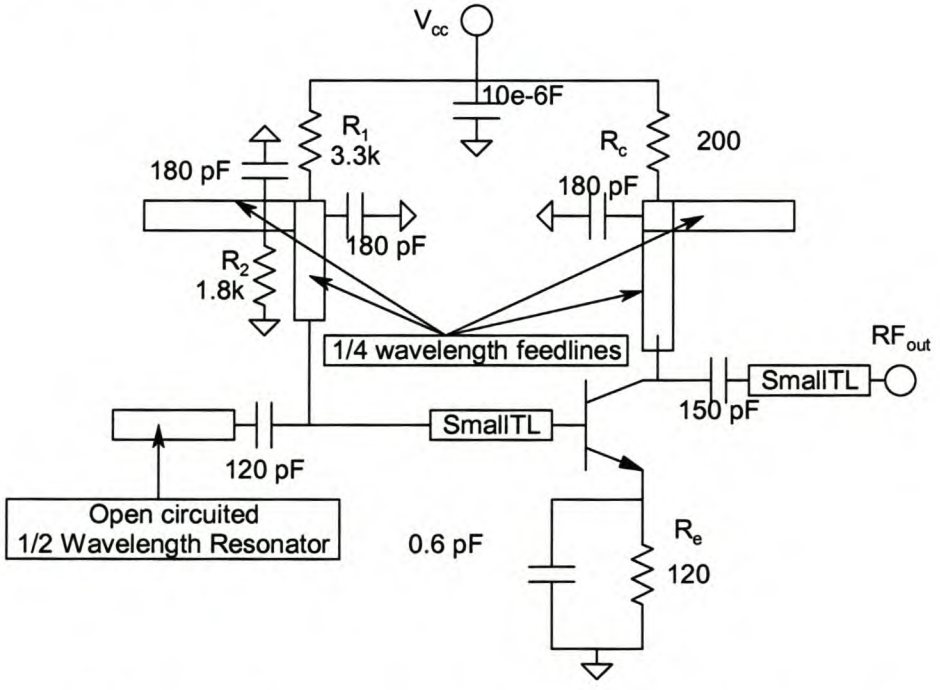

Figure 5-12: The schematic of the fabricated common emitter oscillator

The complete oscillator was modelled in Microwave Office. (See figure 5-12 and Appendix A). The resonator length was reduced by approximately 1% in simulations to center the oscillation frequency at the required frequency.

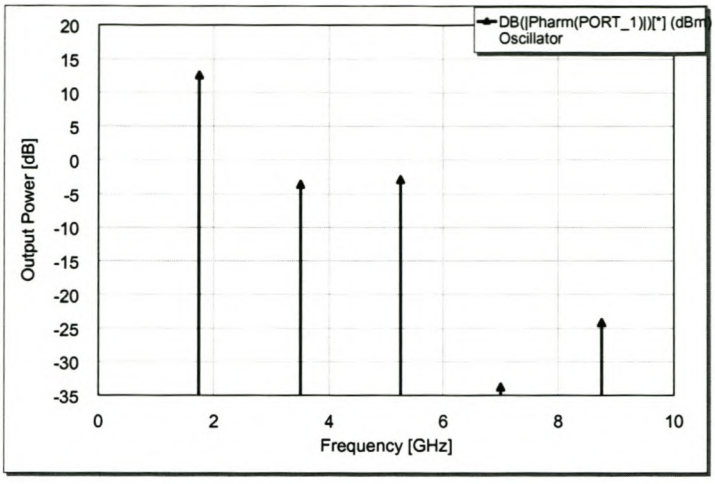

Figure 5-13: The predicted output spectrum of the oscillator

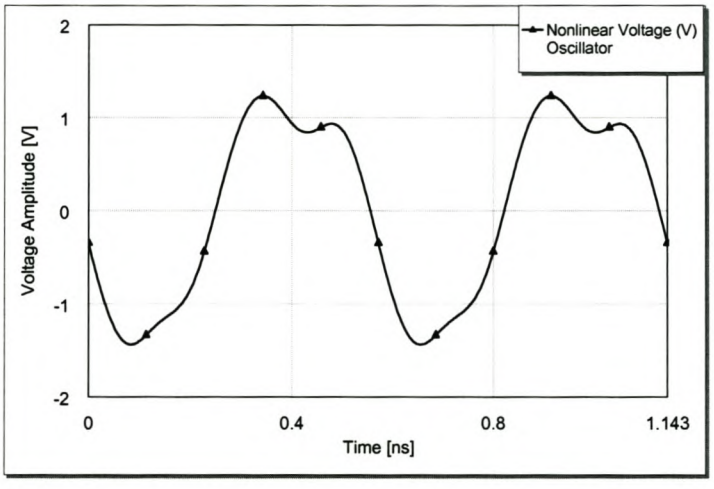

Figure 5-14: The simulated voltage time signal of the oscillator

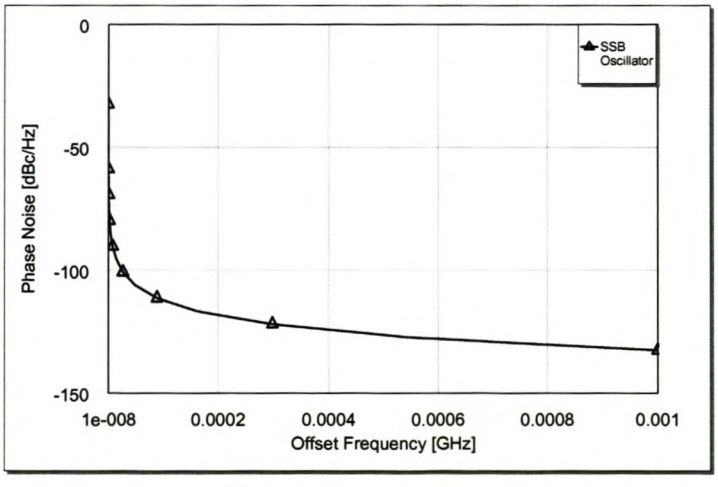

Figure 5-15: The simulated single side band phase noise of the oscillator

Figure 5-13 shows the simulated spectrum of the oscillator. It shows the output power at the proposed fundamental frequency at 12.4 dBm. The second and third harmonics are 15 dBc and 14 dBc respectively. Figure 5-14 shows the voltage time signal of the oscillator. It is roughly 2.5 V peak to peak. Figure 5-15 shows a single sideband of the oscillator phase noise. It is 106 dBc/Hz, 126.2 dBc/Hz and 132.5 dBc/Hz at 0.05, 0.5 and 1MHz respectively.

5.4.2 Measurements

The oscillator was fabricated on a microstrip transmission lines technology using the substrate mentioned in the resonator fabrication. Components used are surface mount capacitors and resistors from Dielectric Laboratories. It was constructed similar to figure 5-12, except the resonator was curled to reduce the space size. The resonator length was again reduced by 4% to make the circuit oscillate at 1.75 GHz. Measurements were performed using an Agilent DC power supply and a Rohde & Schwarz FSEK 30 spectrum analyser.

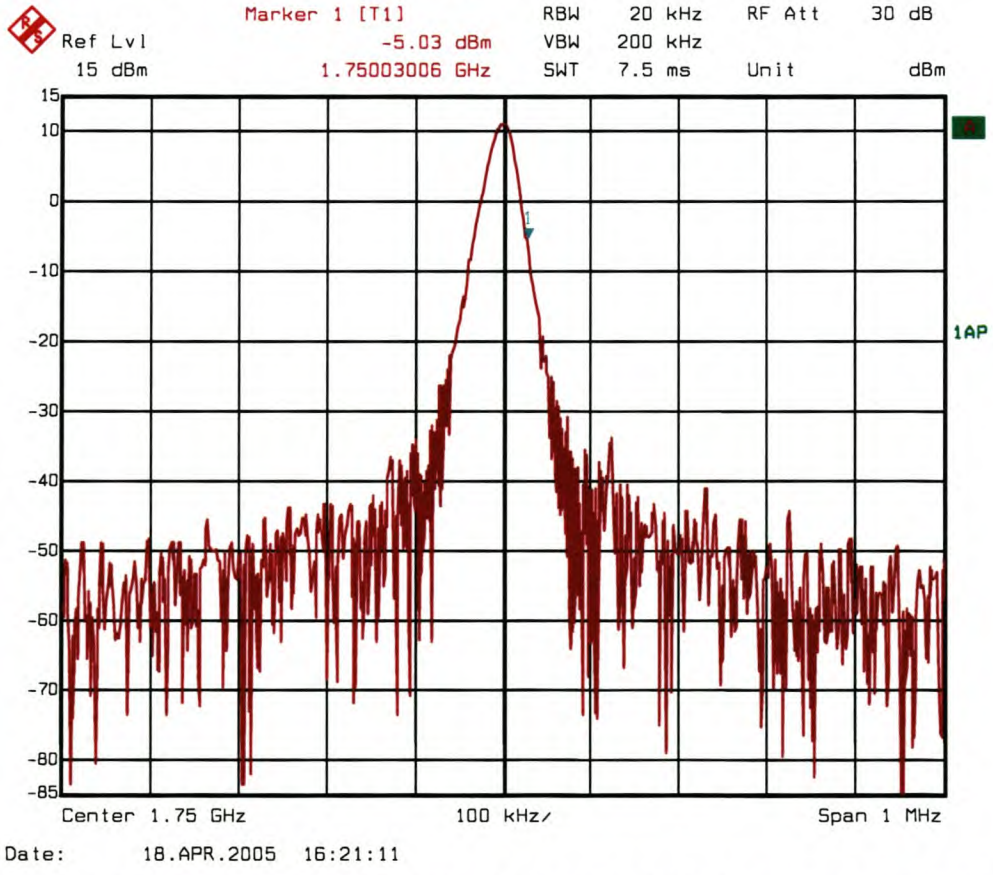

Figure 5-16: The oscillator measured response as seen on the spectrum analyzer

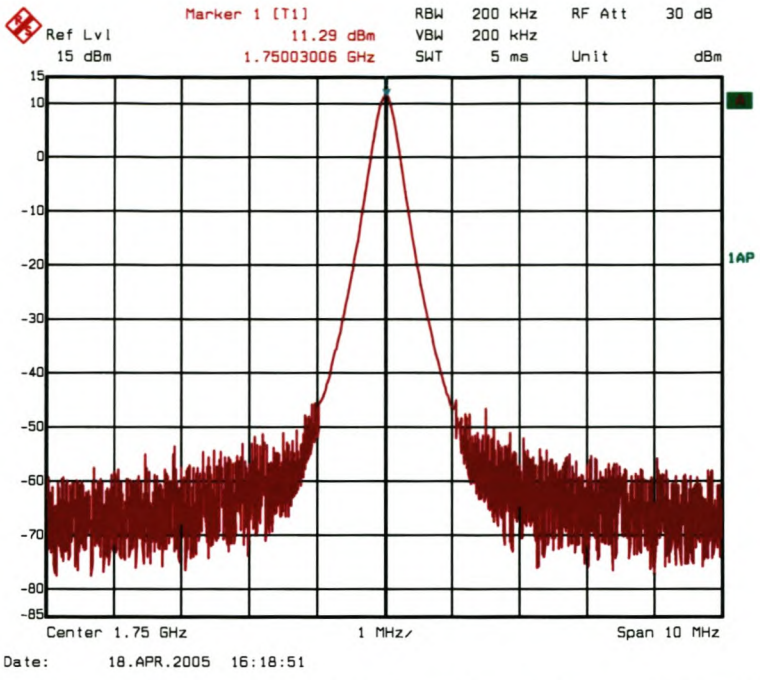

Figure 5-17: The oscillator output with a marker at the peak showing 11.3 dBm

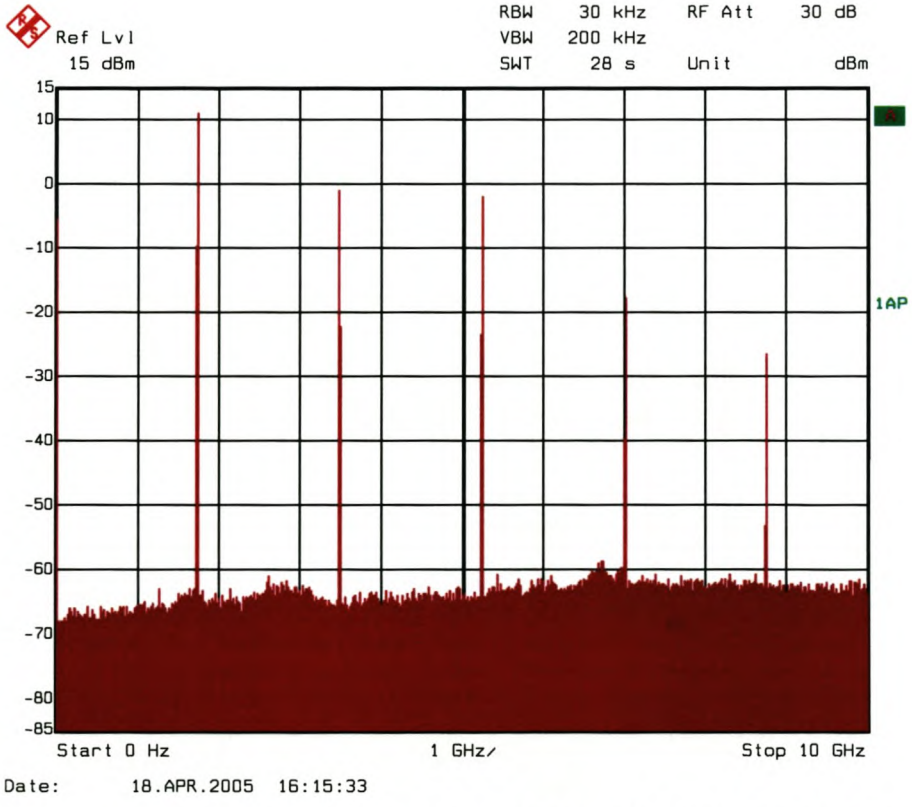

Figure 5-18: The oscillator output showing harmonics which are related to the fundamental signal

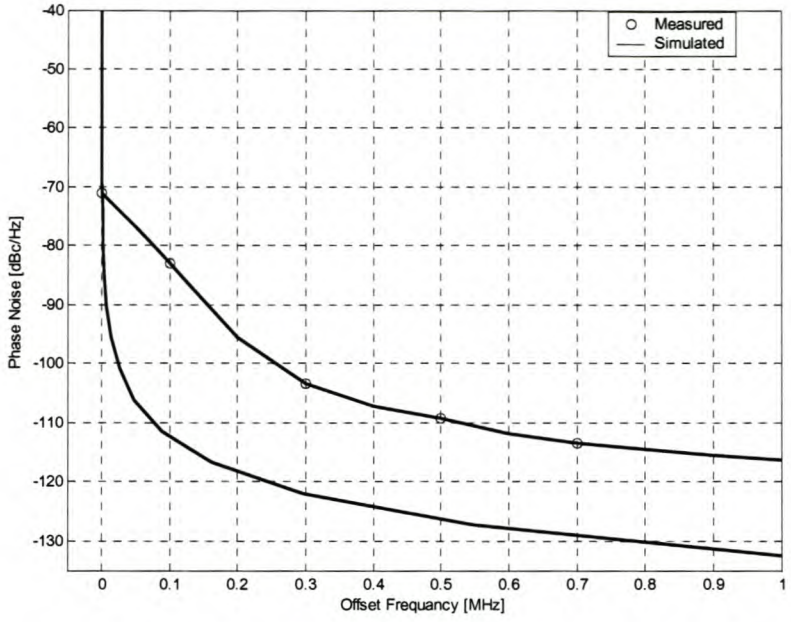

Figure 5-19: The figure showing simulated and measured phase noise from the fabricated oscillator

The fabricated oscillator was biased with 9.6 V DC power supply and it consumed 23.2 mA of current. Figure 5-17 shows the marker at the peak oscillator output power of 11.3 dBm with a 10 MHz span. Figure 5-18 shows the second and third harmonics are 14 dBc and 15 dBc respectively, the measurements were made with 10 GHz span to include other higher order harmonics. The oscillator spectrum is clean when measured with spectrum analyser settings of 30 dB attenuation and 20 dB reference levels. Measured oscillator phase noise is shown in figure 5-19. It shows 77 dBc/Hz, 109 dBc/Hz and 116.6 dBc/Hz for 50, 500 and 1000 KHz respectively. It was also measured using an FSEK 30 spectrum analyser.

5.5 Discussion and Conclusion

A negative resistance oscillator design was implemented. Nonlinear analysis techniques were used to simulate and predict the performance of the design. The open circuited resonator was effectively implemented. The resonator of the oscillator was made smaller than ½ wave-length to compensate for radiation and fringing fields. The bias voltage of the circuit had to be adjusted to tune the oscillator to the required center frequency and compensate for temperature variation effects. The measured fundamental signal output power is 1.1 dB less than the simulated response. The second and third harmonics agrees well with the simulations. The measured phase

noise is different from the simulations by 16 dB at 1 MHz offset frequency. The measured phase noise is higher than predicted, but still low enough to allow proper oscillation frequency. The practical design agrees well with the simulations. The oscillator deviates from the specifications by less than 10 percent, and it met the minimum requirements.

5.6 Recommendations

In future designs all components should be characterised and models used in the modelling programs. High Q resonators are ideal for high performance and stable oscillator and therefore they must be made available. Designing and perhaps testing each component (resonant and active circuit) separately can reduce debugging time.

5.7 Chapter Appendix

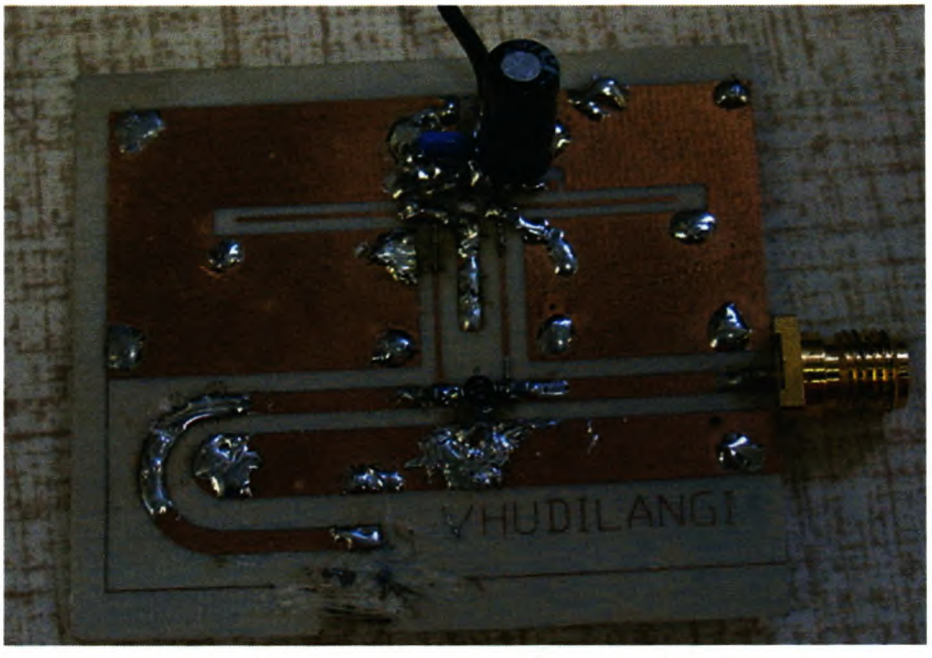

Figure 5-20: The constructed and measured oscillator

6. Mixer Design

6.1 Introduction

A mixer is a three port device that uses a nonlinear or time varying element to achieve signal frequency conversion while preserving the signal information [1, 21 & 23]. It converts a radio frequency signal to intermediate signal or vice versa using the local oscillator signal [9]. Mixers are classified as either down or up conversion, single or dual side band. Up converters are normally used in modulators and transmitters, while down converters are used in heterodyne receivers and demodulators [9]. Mixers are employed because it is easier to work with lower frequency signals as compared to radio frequency signals (which are normally higher). Microwave mixers are often designed containing one or more nonlinear components, which are usually diodes or transistors. The mixer characteristics are also classified as unbalanced or balanced. In this study a single balanced diode mixer is investigated, designed and characterised.

6.2 Design Theory

6.2.1 Operational Theory

In most cases a mixer uses the nonlinearity of a diode or transistor to generate an output spectrum consisting of the sum and difference frequencies of two signals [1]. In a receiver application a low level RF signal and an RF Local oscillator (LO) signal are mixed together to produce an intermediate frequency (IF), $f_{IF} = f_{RF} - f_{LO}$, and a much higher $f_{RF} + f_{LO}$, which is often filtered out[1], see figure 6-1. A mixer operational performance can be approached using different techniques. The two main methods are the small and large signal analysis. The small signal approximation does not give very accurate results in the practical case when the mixer is driven with a relatively high LO power. Small signal analysis is used in this work and complemented with simulations.

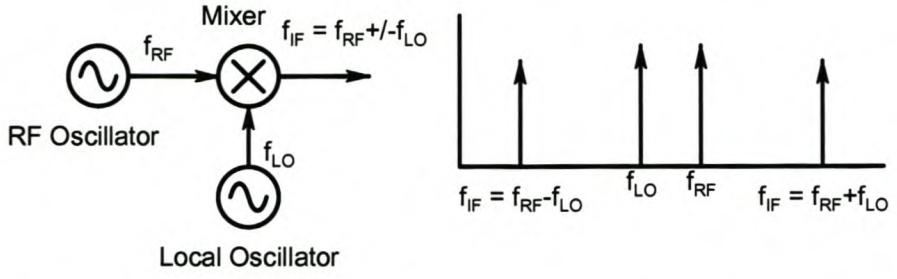

Figure 6-1: The frequency down conversion using a mixer [1]

Figure 6-1 shows an ideal down conversion mixer operation, in real operation the mixer output contain many higher order terms.

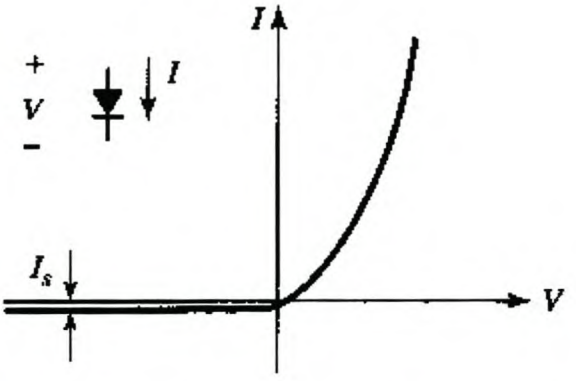

Figure 6-2: A typical illustration of the forward I-V characteristics of the diode [22]

The nonlinear behaviour of a mixing device is used to realise the mixing function. Figure 6-2 shows a typical I-V characteristic of a schottky diode. The IV response of a diode can be written as [21]

$$I(V) = I_s(e^{\alpha V} - 1) \tag{6-1}$$

Where V is the voltage across the diode, I is the current through the diode, and I_s is the reverse saturation current. The constant $\alpha = q/nkT$ where q is the charge of an electron, k is Boltzmann's constant, T is the temperature in Kelvin and n is the diode ideality factor [21]. If the total diode voltage and current consist of small AC signals, *v(t)* and *i(t),* superimposed on a DC bias I_o and V_o, then the total current can be represented as a Taylor series in terms of the applied AC signal voltage [21 and 22]:

$$I(V) = I_o + G_d v(t) + \frac{1}{2} G_d' v^2(t) + \ldots\ldots, \tag{6-2}$$

where G_d is the dynamic conductance of the diode and $G_d^{'}$ is the derivative of the dynamic conductance. The first two terms representing DC bias current and a linear diode response are of little interest to a mixing operation because no frequency conversion occurs through these terms [22]. The third term containing v^2 represents the square law response of the diode. It is responsible for the dominant frequency conversion terms. This theory is briefly explained by a single ended mixer given in the design consideration.

6.2.2 Design Consideration

In this work the design consideration provided is the one used to realize the designed mixer and it is given through the single ended (one diode) mixer operation. The mixer operation model (Small signal model) given is valid for both active and passive cases. The RF and LO inputs are combined in a diplexer, which superimposes the two input voltages to drive the diode. The AC equivalent circuit of the mixer is shown in figure 6-3, where the RF and LO input voltages are represented as two series-connected voltage sources [21]. Assume that that the LO and RF voltages are frequency cosine waves given by the equations (6-3) and (6-4) [21]

$$v_{RF}(t) = V_{RF}\cos\omega_{RF}t \tag{6-3}$$

$$v_{LO}(t) = V_{LO}\cos\omega_{LO}t \tag{6-4}$$

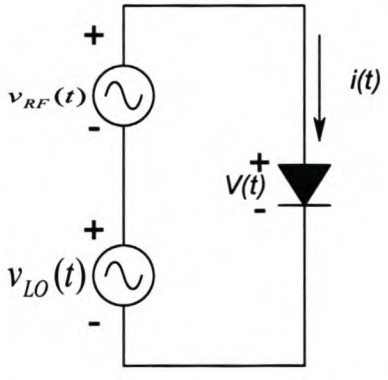

Figure 6-3: Idealized AC equivalent circuit of a single ended mixer [21].

Using the small signal approximation from equation (6-2) gives the total diode current as

$$i(t) = I_o + G_d[v_{RF}(t) + v_{LO}(t)] + \frac{1}{2}G_d^{'}[v_{RF}(t) + v_{LO}(t)]^2 + \ldots\ldots \tag{6-5}$$

The first term in equation (6-5) is the DC bias current, which is normally blocked from the IF output by the DC blocking capacitors [21]. The second term is the replication of the RF and LO input signals, which will be filtered out by the IF filter. Thus only the third term remain which can be written using trigonometric identities as [21]

$$i(t) = \frac{1}{2} G_d' [V_{RF} \cos \omega_{RF} t + V_{LO} \cos \omega_{LO} t]^2 \tag{6-6}$$

$$\begin{aligned} i(t) = {} & \frac{1}{4} G_d' [V_{RF}^2 (1 + \cos 2\omega_{RF} t) + V_{LO}^2 (1 + \cos \omega_{LO} t) \\ & + 2V_{RF} V_{LO} \cos(\omega_{RF} - \omega_{LO}) t + 2V_{RF} V_{LO} \cos(\omega_{RF} + \omega_{LO}) t] \end{aligned} \tag{6-7}$$

The result of equation (6-7) contains several new signal components and one which produces the desired IF difference component. With a proper filtering or harmonic suppressing circuit, only the IF output current will be allowed to pass through which is [21]

$$i(t) = \frac{G_d'}{2} V_{RF} V_{LO} \cos \omega_{IF} t \tag{6-8}$$

where $\omega_{IF} = \omega_{RF} - \omega_{LO}$ is the IF frequency. Using a small signal method the spectrum of a down-converting single ended mixer is identical to that of an idealised mixer which is shown in figure 6-1 [21]. Though the single ended mixer model was used to explain the mixer operation, it suffers from poor isolation between the IF port and the RF and LO ports, no isolation between RF and LO ports, a high level of oscillator noise input to the IF amplifier and the generation of many spurious signals [19].

Balanced mixers are used to improve the characteristics of the mixer and reduce some of the listed shortcomings. A single balance diode mixer requires two diodes to be well matched in their electrical properties in order to achieve a well balanced mixer. For broadband mixers up to 1 GHz, the single balanced mixer can be built using transformers consisting of windings on a ferrite toroidal core [19].

At microwave frequencies the single balanced mixer can be constructed using 180° 3 dB hybrid junction. A 90° hybrid junction can also be used, but the mixer will not be fully balanced with respect to LO and IF port interactions [19]. In a 90° hybrid junction reflected waves at the output port appear at both input ports with a phase that makes the reflected waves add out of phase [19], while in the 180° hybrid the reflected waves add in phase at each port. Therefore using 180° hybrid junction a better balanced mixer is obtained, though the VSWRs (Voltage Standing Wave ratios) is higher than for the 90° hybrid. The180° hybrid Junction was selected for the proposed mixer.

The 180° Hybrid

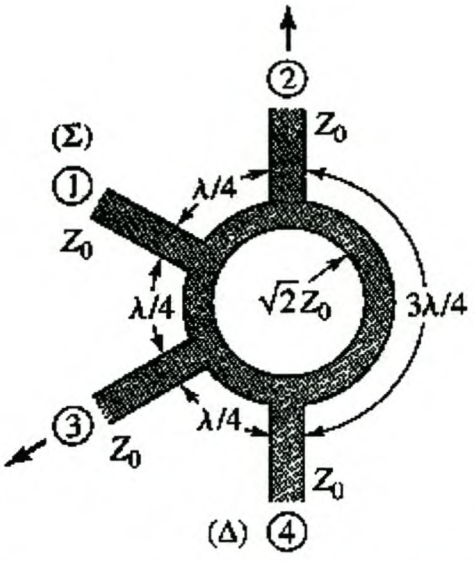

Figure 6-4: A ring or rat-race hybrid junction [22]

The 180° hybrid junction is a four-port network with a 180° phase shift between the two output ports and it can also be operated so that the output ports are in phase [22]. With reference to figure 6-4, a signal applied at port 1 will be evenly split into two in-phase components at ports 2 and 3, and port 4 will be isolated [22]. If the input is applied at port 4, it will be equally split into two components with an 180° phase difference at ports 2 and 3, and port 1 will be isolated [22]. When operated as a combiner, with input signals at port 2 and 3, the sum of the inputs will be formed at port 1, while the difference will be formed at port 4. Therefore ports 1 and 4 are referred to as the sum and difference ports respectively.

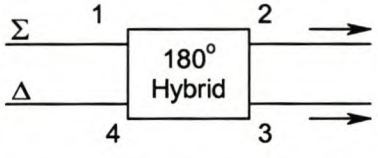

Figure 6-5: The symbol for the 180° hybrid junction [22]

The scattering matrix of the ideal 3 dB 180° hybrid has the form as shown in equation (6-9) [22]

$$S = \frac{-j}{\sqrt{2}} \begin{bmatrix} 0 & 1 & 1 & 0 \\ 1 & 0 & 0 & -1 \\ 1 & 0 & 0 & 1 \\ 0 & -1 & 1 & 0 \end{bmatrix} \tag{6-9}$$

and it is unitary and symmetric [22]. The 180° hybrid can be fabricated in several forms; the ring hybrid shown in figure 6-4 can be fabricated in planar form and can have a bandwidth of between 20 and 30% [1]. Waveguide versions of 180° hybrid junction are also possible like a magic T.

Balanced Mixer

A microwave balanced mixer combines two or more identical single ended mixers with a 3 dB hybrid junction to give either better input SWR or better RF/LO isolation [1 and 22]. In this work a single balanced mixer is investigated which combines two single ended mixers and it consist of two diodes and a hybrid junction. It also rejects AM Local oscillator noise and also some even harmonics [20].

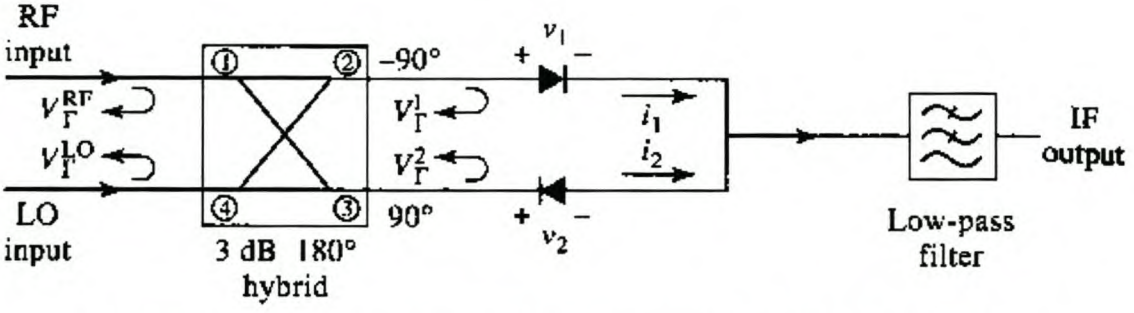

Figure 6-6: A balanced mixer circuit using 180° hybrid junction [21]

The single balanced mixer using a 180° hybrid junction or rat-race is qualitatively investigated. Consider a small random noise voltage, $v_n(t)$, superimposed on the local oscillator signal [22]. Taking ω_r and ω_0 as the RF and LO angular frequency respectively, the RF and LO voltages at the input of the hybrid can be expressed as [21]

$$v_{RF}(t) = v_r \cos \omega_r t \tag{6-10}$$

$$v_{LO}(t) = (v_0 + v_n) \cos \omega_0 t \tag{6-11}$$

assuming $v_r \langle\langle v_0$ and $v_n(t) \langle\langle v_0$. If the RF is applied to the sum port and LO applied to the difference port (refer to figure 6-4, 6-5 and 6-6), the voltages across two diodes are

$$\begin{aligned} v_1(t) &= v_r \cos(\omega_r t - 90) + (v_0 + v_n)\cos(\omega_0 t - 270) \\ &= v_r \sin \omega_r t - (v_0 + v_n)\sin \omega_0 t \\ v_2(t) &= v_r \cos(\omega_r t - 90) + (v_0 + v_n)\cos(\omega_0 t - 90) \end{aligned} \tag{6-12}$$

$$= v_r \sin \omega_r t + (v_0 + v_n) \sin \omega_0 t \tag{6-13}$$

The quadratic term of the diode I-V characteristics (3rd in equation (6-2)) will give rise to the desired mixer products, thus considering only this term and assuming identical diodes then diode currents can be written as

$$i_1 = k v_1^2 \text{ (For diode 1)} \tag{6-14}$$

$$i_2 = -k v_2^2 \text{ (For diode 2)} \tag{6-15}$$

where negative sign in equation(6-16) accounts for reverse polarity, i_1 and i_2 are the first and second diode currents respectively and k is a constant.

$$i_1 = k[v_r \sin \omega_r t - (v_0 + v_n) \sin \omega_0 t]^2 \tag{6-16}$$

$$i_2 = -k[v_r \sin \omega_r t + (v_0 + v_n) \sin \omega_0 t]^2 \tag{6-17}$$

After lowpass the following DC, noise and IF frequency terms remain

$$i_1 = k[\frac{1}{2} v_r^2 + \frac{1}{2}(v_0 + v_n)^2 - v_r (v_0 + v_n) \cos \omega_i t] \tag{6-18}$$

$$i_2 = -k[\frac{1}{2} v_r^2 + \frac{1}{2}(v_0 + v_n)^2 + v_r (v_0 + v_n) \cos \omega_i t] \tag{6-19}$$

where $\omega_i = \omega_r - \omega_0$ is the IF frequency. Adding these currents together gives the IF output as

$$i_{IF} = i_1 + i_2 = -2k v_r (v_0 + v_n) \cos \omega_i t$$

$$\cong -2k v_r v_0 \cos \omega_i t \tag{6-20}$$

since $v_n \langle\langle v_0$ [22]. The result shows that the first order terms in the noise voltage were canceled by the mixer and that the desired IF signals combined in phase [22]. With reference to figure 6-6, the RF waves reflected from the diodes will be zero at the LO port (difference) and they will only appear at the RF port [22].The LO reflected waves from the diodes will be zero at the RF port (sum) and they will only appear at LO port [22]

In both the RF and LO waves the mismatch occurs at the input port at which it was sent and the RF and LO ports are isolated [22]. The small signal method described in the preceding section is not very accurate for predicting realistic results for conversion loss, due to the violation of the small signal approximation by the high level LO port power. Large signal method or simulation is often performed to approximate the desired results. Mixers have several performance parameters and the fundamental ones are briefly described below.

Diode Selection

Diodes are square law devices, leading to a functional description of their nonlinear behaviour which has strong V^2 (3^{rd} term in equation (6-5)) components [20 and 23]. Recently most mixers use schottky diodes, because they have much higher switching speed than p-n junction diodes [9]. Manufactures often specify the intended application of the diode and barrier type. The higher the barrier the higher the breakdown voltage and/or the LO drive.

Mixer Performance Parameters

Also defined in the previous chapters the mixer performance parameters are Conversion loss, one dB compression point, Noise figure, third order intercept point, isolation, image frequency rejection and spurious response

6.2.3 Design Specifications

Parameter	Specified Performance
IF Frequency	700 MHz
RF Frequency	2.45 GHz
LO Frequency	1.75 GHz
LO Power	5-12 dBm
Conversion Loss	$\leq$ 9 dB
LO to RF Rejection	$\geq$ 20 dB
LO to IF Rejection	$\geq$ 30 dB
IF Bandwidth	10 MHz

Table 6-1: The proposed operational mixer specifications

6.3 Mixer Design

A low barrier type silicon schottky diode for mixers, phase detectors and modulator applications called Bat 15-03w from Infineon technologies was selected because of its small capacitance. It has the characteristics outlined in table 6-2.

Symbol	Parameter	Units	Typical Values
I_F	Forward current	mA	110
(VBR)	Breakdown Voltage	V	4
V_F	Forward Voltage	V	0.15-0.23
C_T	Diode capacitance	pF	0.35
R_F	Forward Resistance	Ω	5.5

Table 6-2: Parameters list of the absolute maximum rating of the diode

6.3.1 Rat-race Design

A 50 ohm system impedance 180° ring hybrid at 2.45 GHz frequency was designed using the relations shown in figure 6-4. The characteristic impedance of feed lines and of the ring transmission line are given by [22]

$$Z_o \quad \text{and} \quad \sqrt{2}Z_o \tag{6-21}$$

respectively. The values obtained from these relations are 50 ohm and 70.7107 ohm respecttively. This design was verified using Microwave Office and it was tuned to give the best response. The results of the rat-race simulations are provided in section 6-4.

6.3.2 Mixer Design

The mixer was implemented as shown in figure 6-7. As illustrated in the figure, the two inductors serve as IF return, and in this case they had to be small because the IF frequency is large, 700 MHz. For example a 12 nH (nanohenry) inductor gives 52 ohm impedance with the proposed IF frequency. In terms of the RF and LO bypass capacitor the calculation shows that a capacitor bigger than 10 pF has 10 ohm impedance at 1.75 GHz, but its impedance is 23 ohm for 700 MHz IF signal, the capacitor need to be smaller so that IF wont get grounded. The initial values of the mixer were implemented with regard to the above mentioned estimates.

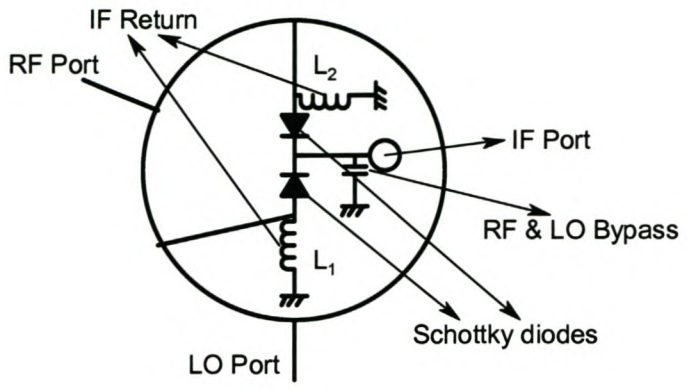

Figure 6-7: The complete illustrated mixer configurations

6.4 Simulations and Measurements

6.4.1 Simulations

The rat-race was first simulated without other components connected to it, as shown in figure 6-4. The results are provided in the following figures.

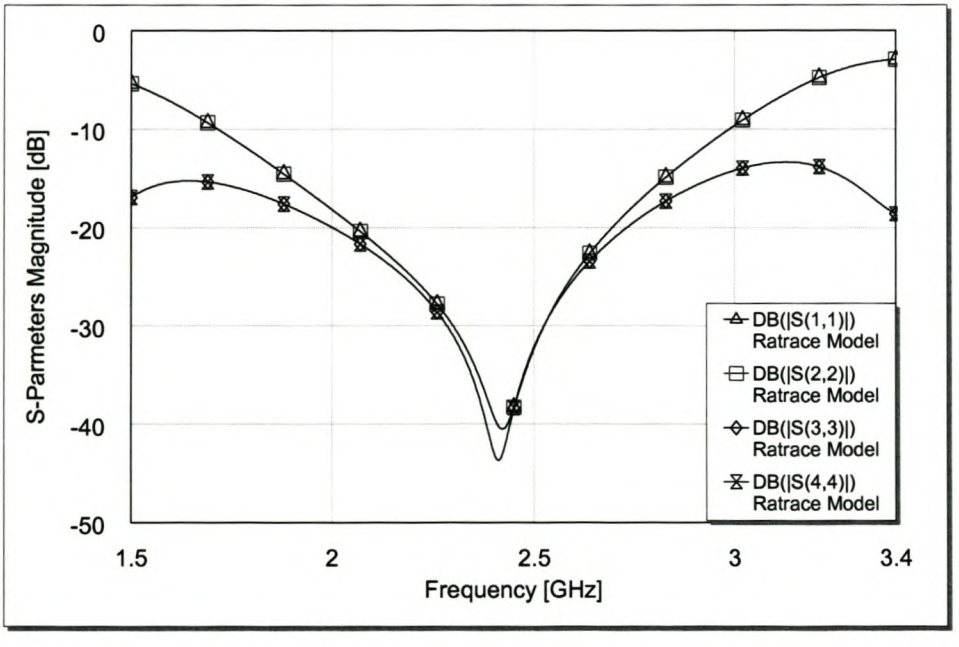

Figure 6-8: The reflection magnitudes of all ports of the rat-race

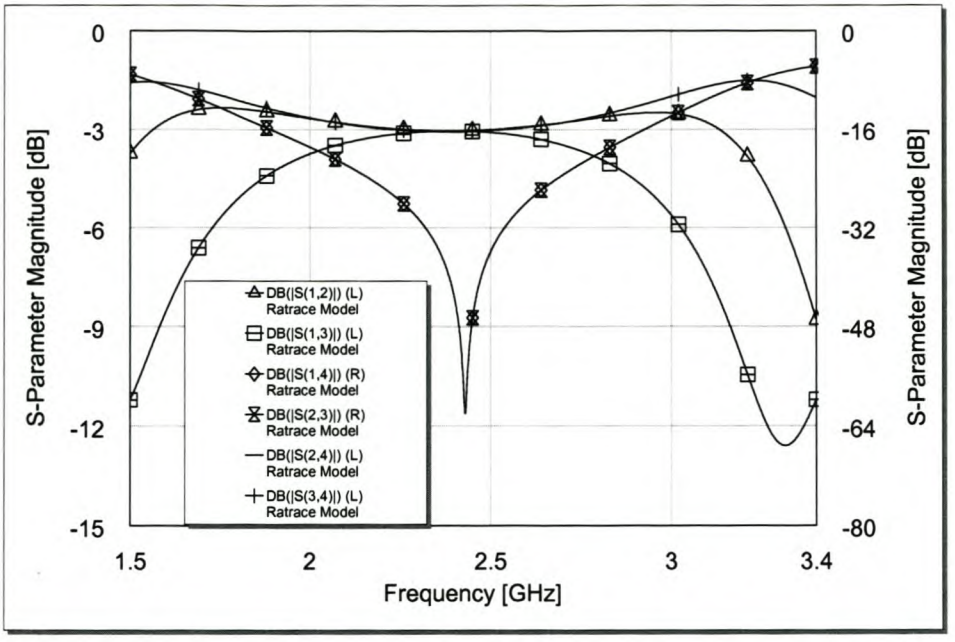

Figure 6-9: The different ports interference with each other of the rat-race

The ports labels were similar to the labels in figure 6-4. Figure 6-8 shows the reflection of each port. Figure 6-9 shows the interference of ports with each other. It shows isolation between port 2 and 3, and also between port 1 and 4. It also shows 3 dB coupling between the rests of the ports with each other at the center frequency.

In mixer implementation the diode used was first modelled before implemented in the rat-race model. The diode SPICE data model was obtained from the manufacturer and the subcircuit was created. The diode nonidealities and packaging parasitic models were also taken into account. The subcircuit model is shown in figure 6-10.

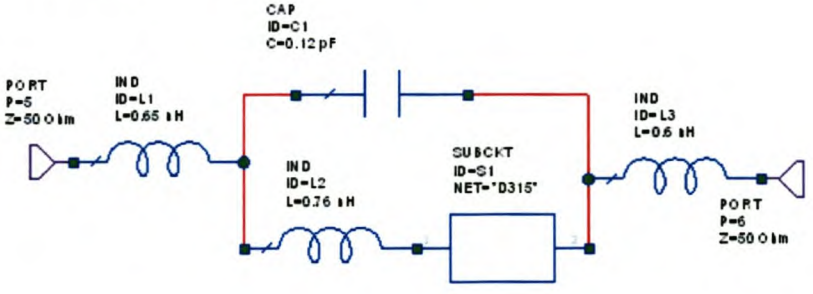

Figure 6-10: The diode sub circuit including parasitic and packaging model non idealities

The diode model included the connecting pins. After obtaining satisfactory response from the rat-race simulations, its model was connected to the diode model with the suggested lumped components. The inductors L_1 and L_2 in fig 6-8 were made 3.9 nH and 11 nH respectively and the bypass capacitor was replaced by LO frequency centred ¼ wavelength open circuited stub.

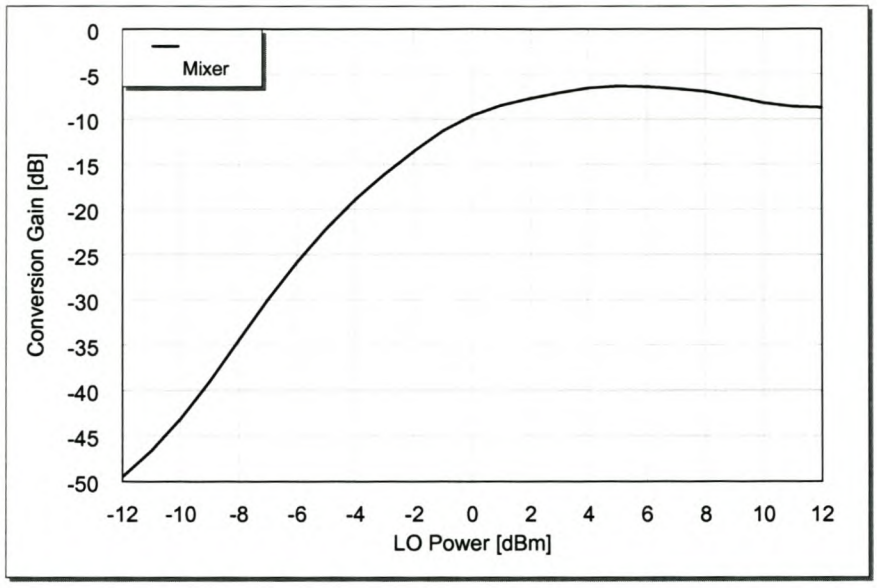

Figure 6-11: The LO power influence on the conversion loss of the mixer

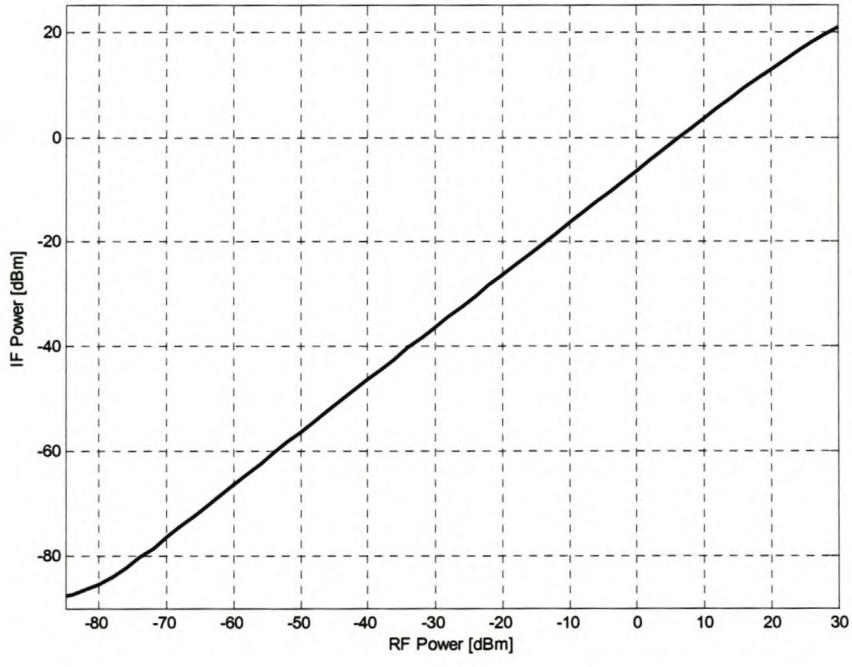

Figure 6-12: The RF versus the IF power from the mixer with 5 dBm LO power

Figure 6-11 shows the LO power influence on the conversion loss of the mixer. The minimum conversion loss is obtained with an LO power between 5 to 6 dBm. Figure 6-12 shows the relation between the RF input power and output IF power of the mixer.

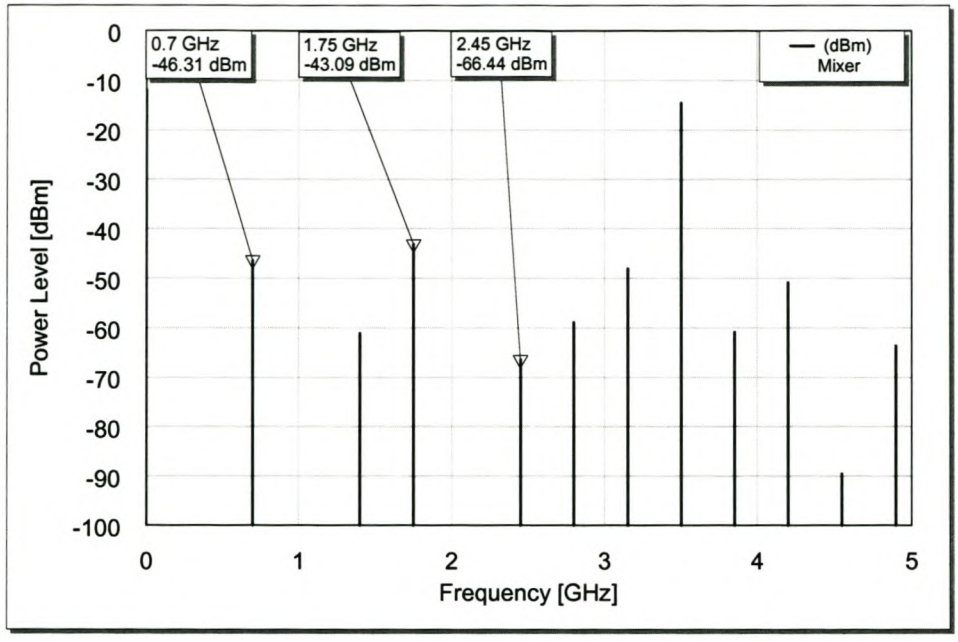

Figure 6-13: The simulated IF port spectrum of the mixer

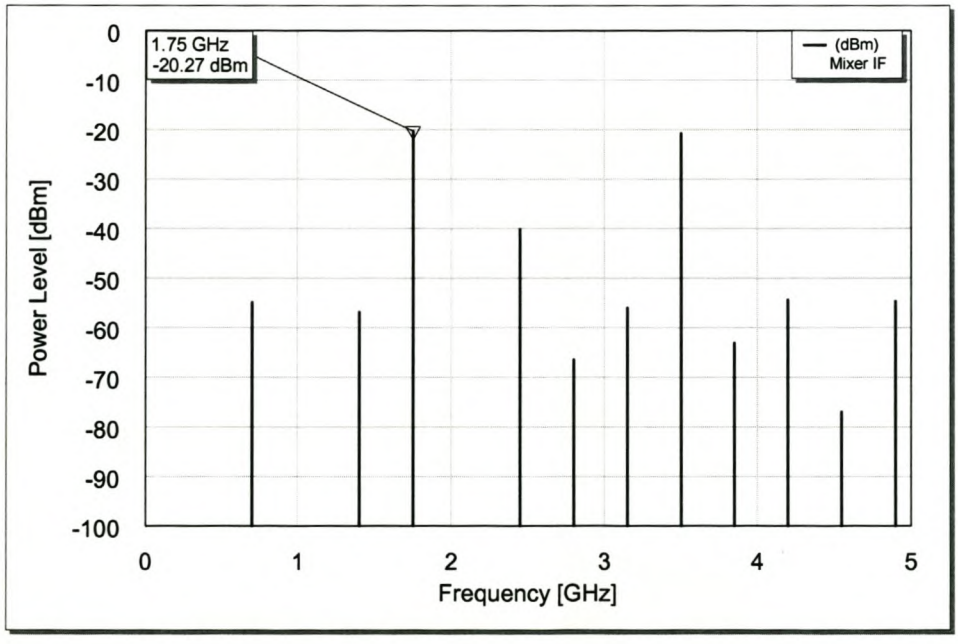

Figure 6-14: The simulated RF ports spectrum of the mixer

Figure 6-14 and 6-15 where obtained with the RF input power of -40 dBm and an LO pump of 5 dBm. The spectrum of figure 6-13 gives the conversion loss of 6.31 dB. The 2nd order harmonic of the oscillator is the strongest signal in the IF port spectrum, it is -14 dBm, while in the RF port spectrum both the fundamental and the 2nd order harmonic signals of the oscillator are about -20 dBm.

6.4.2 Measurements

The mixer was fabricated using microstrip transmission line technology. It was fabricated on GIL1000 substrate with a dielectric constant of 3.86 mm and a height of 0.787. Transmission line bends in Microwave Office were used in implementing the layout of the mixer and later modified with AutoCAD 2000i. The 3.9 nH was replaced by two parallel 8.1 nH inductors and the rest of the components were as simulated. Three standard female SMA connectors were used at the RF input, IF output and LO input ports. The measurements were made using Rhode & Schwarz signal generators and FSEK 30 spectrum analyser.

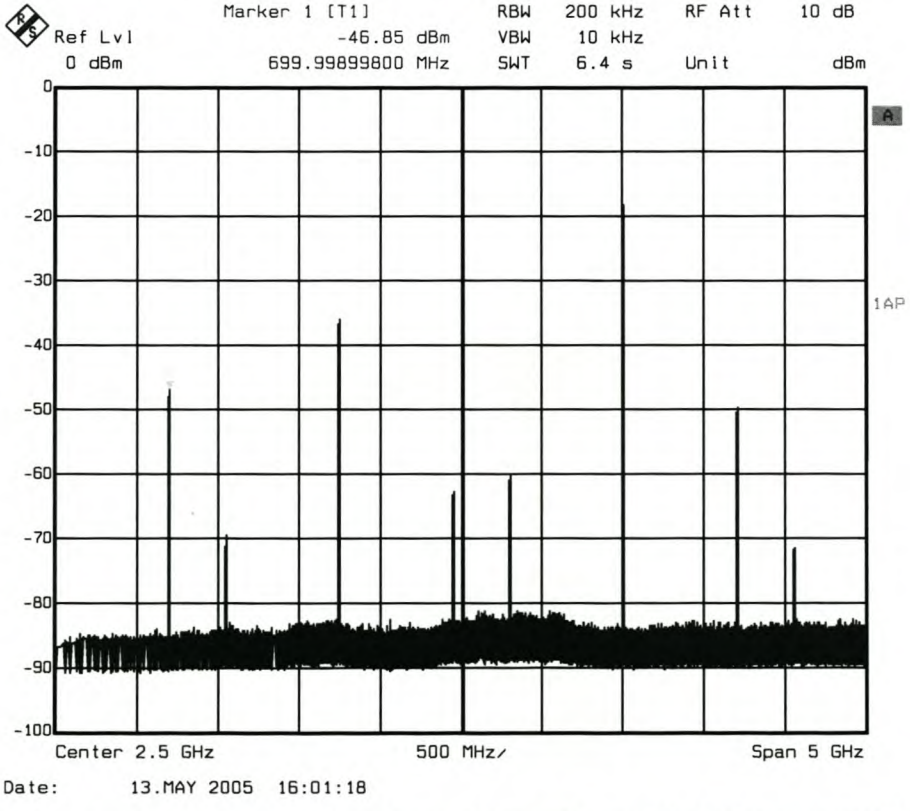

Figure 6-15: The measured IF port spectrum of the mixer with 5 dBm and -40 dBm LO and RF power respectively.

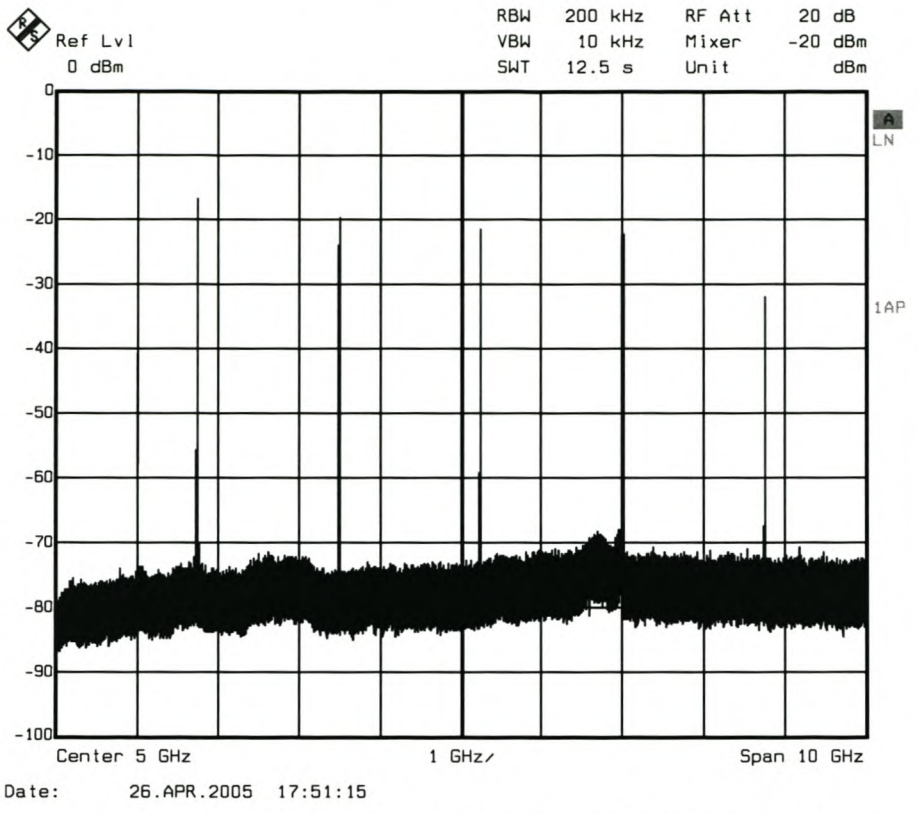

Figure 6-16: The measured RF port spectrum of the mixer with 5 dBm LO power while the IF port is terminated with 50 ohm load

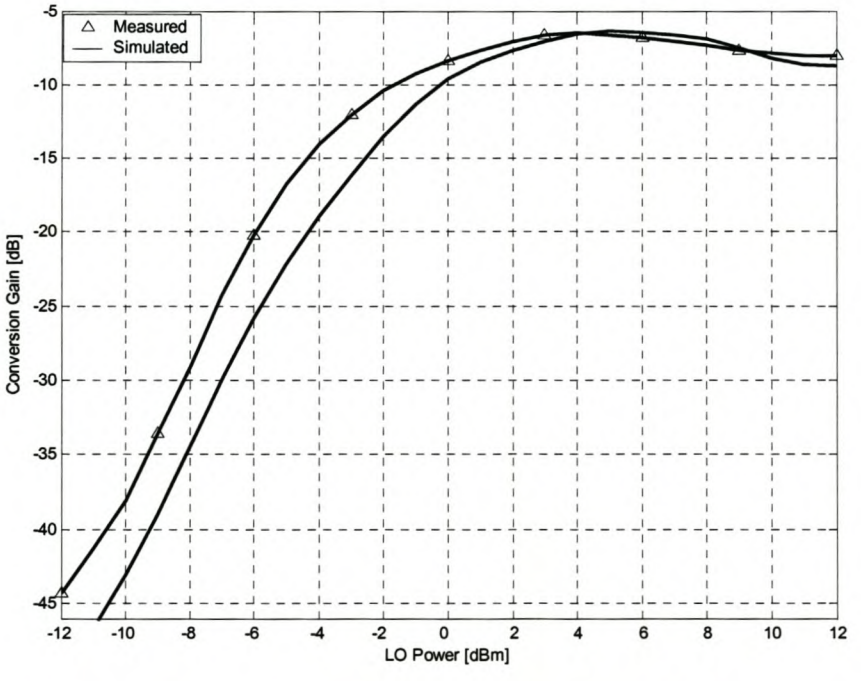

Figure 6-17: The measured LO influence on the conversion loss of the mixer

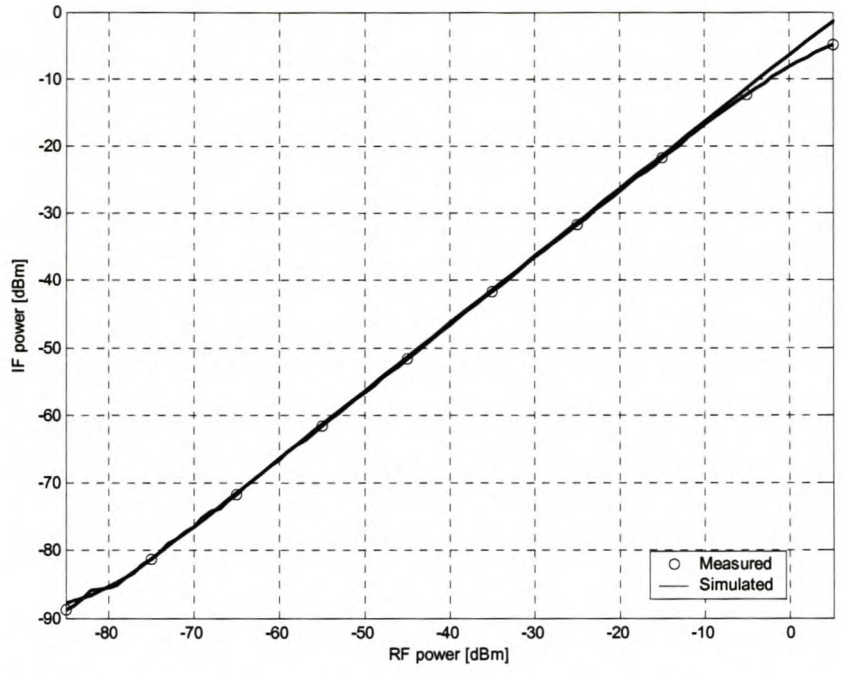

Figure 6-18: The simulated and measured input RF power versus the output IF power

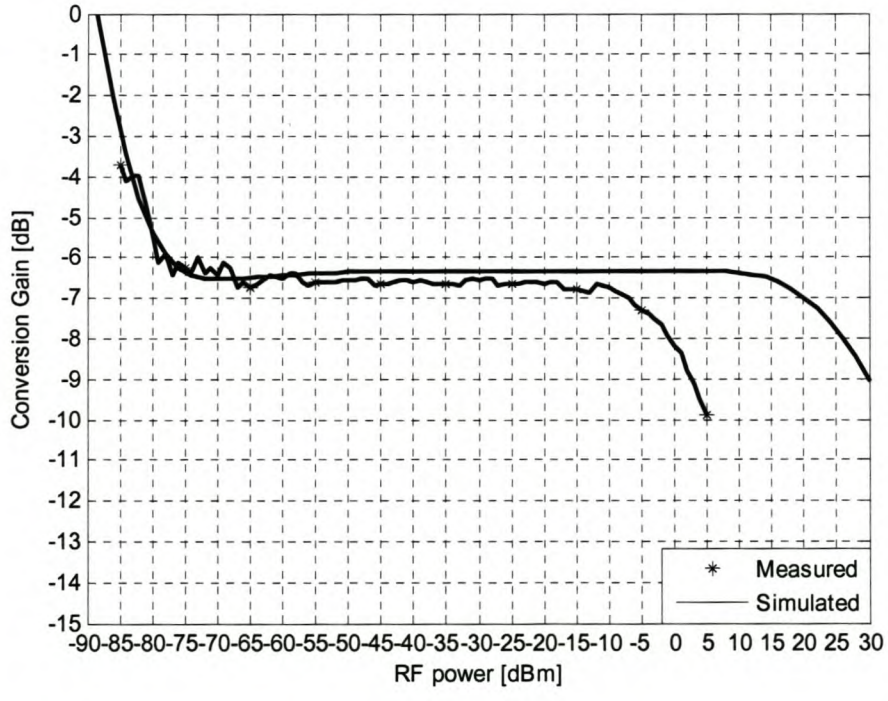

Figure 6-19: The comparison of measured and simulated RF influence on the conversion loss

Figure 6-15 shows the IF spectrum with -40 dBm RF power input and a 5 dBm LO pump. It shows conversion loss of 6.85 dB. The fundamental LO power signal is -38 dBm at the IF port

spectrum and its second harmonic response is -18 dBm. The RF signal is -63.3 at the IF port. In figure 5-16 the RF spectrum is shown and it contains only LO leaking signals up to 10 GHz and the highest signal level is the fundamental LO power at -16 dB. The LO to IF isolation is 43 dB, the LO to RF isolation is 21 dB and the RF to IF isolation is 22.3 dB. Figure 6-17 shows the LO power influence on the mixer's conversion loss and the minimum conversion loss is obtained with LO power between 4 to 6 dBm. Figure 6-18 shows the relationship between the RF and IF power and this relationship is also used to determine the P1dB of the mixer and it was obtained to be -3 dBm with reference to the input. Figure 6-19 also gives the P1dB and RF sweep as compared to Conversion Loss. An average of 6.8 dB conversion loss is obtained from the power sweep in figure 6-19.

6.5 Conclusion

A single balanced diode mixer was designed and fabricated using a 180° hybrid junction, also known as a rat-race. It was selected over a 90° hybrid junction due to its bandwidth and a better balance with respect to isolation. The normal rat-race is known to operate within 30% bandwidth [22] whereas in this case a larger bandwidth was required, where it had to mix 2.45 GHz RF signal and 1.75 GHz LO signal. The mixer was optimised to work with 5 dB LO power. The measured conversion loss is 6.8 dB and is bigger than the simulated response by approximately 0.5 dB. The simulated and measured LO to IF and LO to RF isolations only differed by less than 5 dB. The measured input 1 dB compression point is -3 dBm and compared to about 22 dBm simulated and that is accounted for by the small LO pump signal which lowers the mixer's linear range [20]. The wide bandwidth required also affected the performance of the rat-race mixer, for example the IF return inductors were allowed to be different during optimization and thus leading to non symmetrical mixer. Therefore exchanging the LO and RF ports resulted in a different conversion loss and also the LO to RF isolations is 4 dB less than expected. The constructed mixer satisfied the proposed specifications.

6.6 Recommendations

Larger bandwidth of this mixer may require the use of the two separate baluns in future designs.

6.7 Chapter Appendix

Figure 6-20: The constructed rat-race mixer

7. System Integration

7.1 Components Integration

All the designed components except the antenna were connected together to form a small system. The LNA used is the one used in chapter 2 measurements. The system with measured parameters of the individual components is shown in figure 7-1. A 6 dB attenuator was added to lower the LO signal to around 5 dBm for minimum mixer conversion loss.

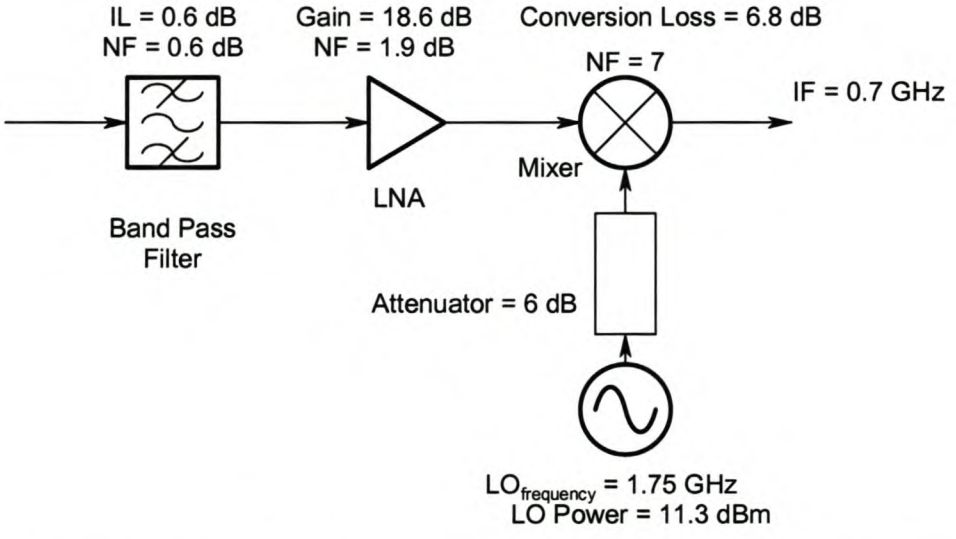

Figure 7-1: The measured systems with their individual performance parameters denoted

Using the system above the system gain, compression point, image and IF rejection, desensitization from external signals, spurious radiation and Noise figure can be measured. The minimum detectable signal can be computed from some of the above mentioned measurements if the minimum SNR is known. In this design -66.23 dBm is expected at the input of the filter [table 1-1]. Theoretically using this predicted signal, the output at the IF port of the mixer is determined as

$$IF_{Level} = -66.23\ dBm - 0.6\ dB + 18.6\ dB - 6.8\ dB = -55.03\ dBm$$

Predicting 11.2 dB system gain. Using equation (1-19) the noise figure is

$$F = 2.6526\ dB$$

7.2 System Measurements

The parameters mentioned above were measured in a similar technique outlined in section 1.3.4, although in this case the system included designed components and a filter.

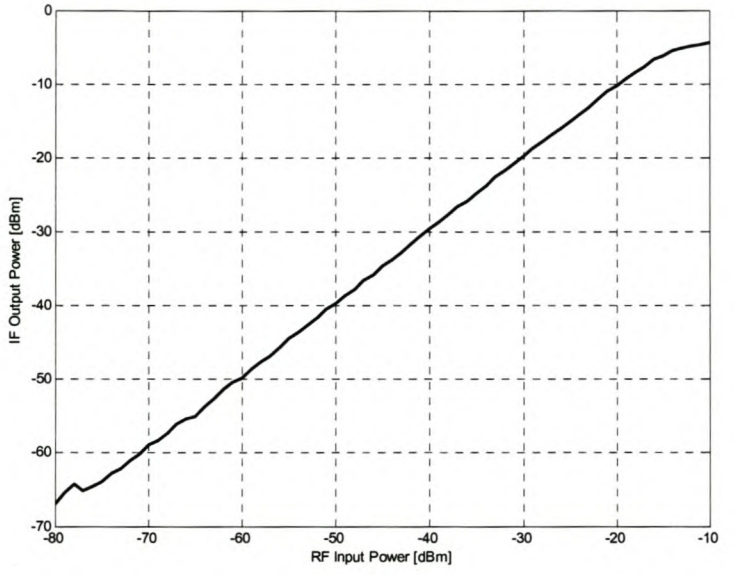

Figure 7-2: The input power versus output power of the complete system with a 20 MHz span and resolution bandwidth of 10 KHz

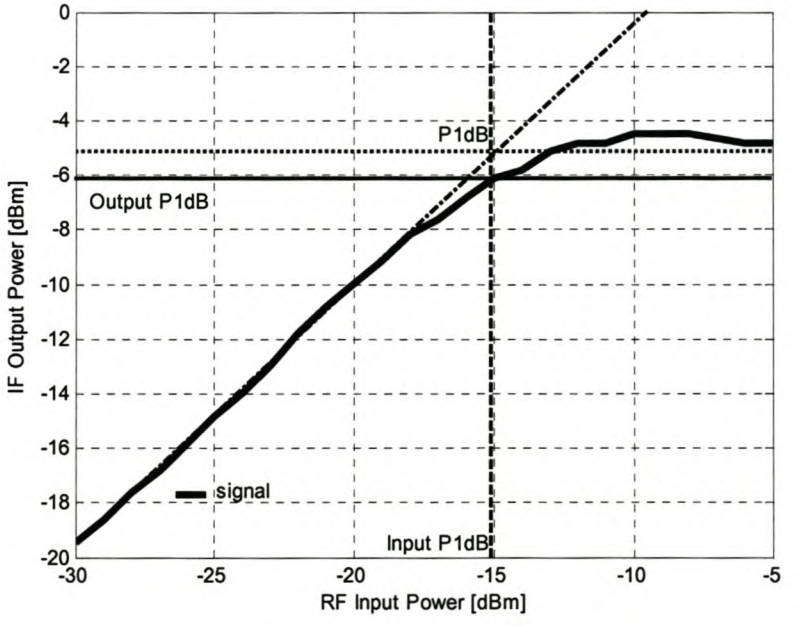

Figure 7-3: The input versus output power of the system with a small range of swept RF power to model the P1dB of the receiver

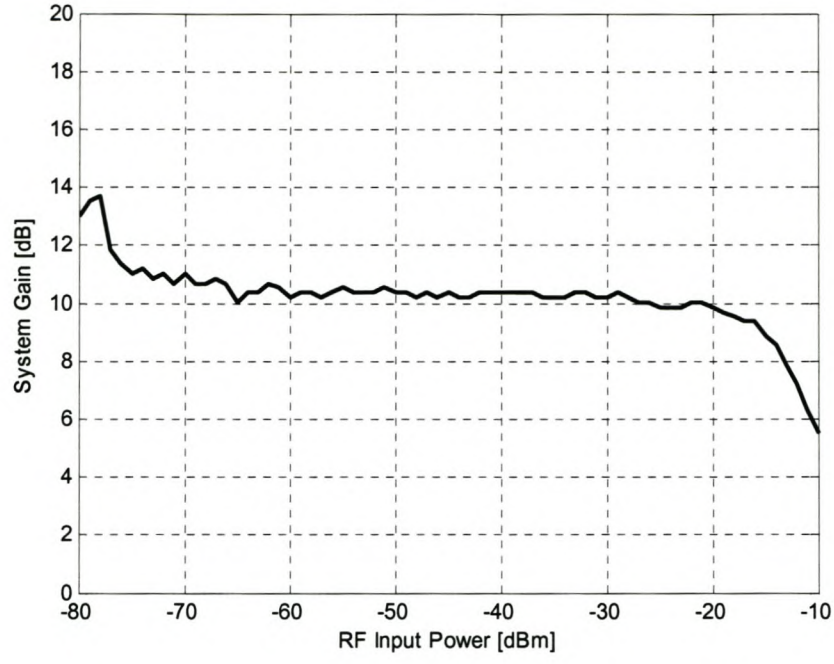

Figure 7-4: The input power versus system gain determined from figure 7-2

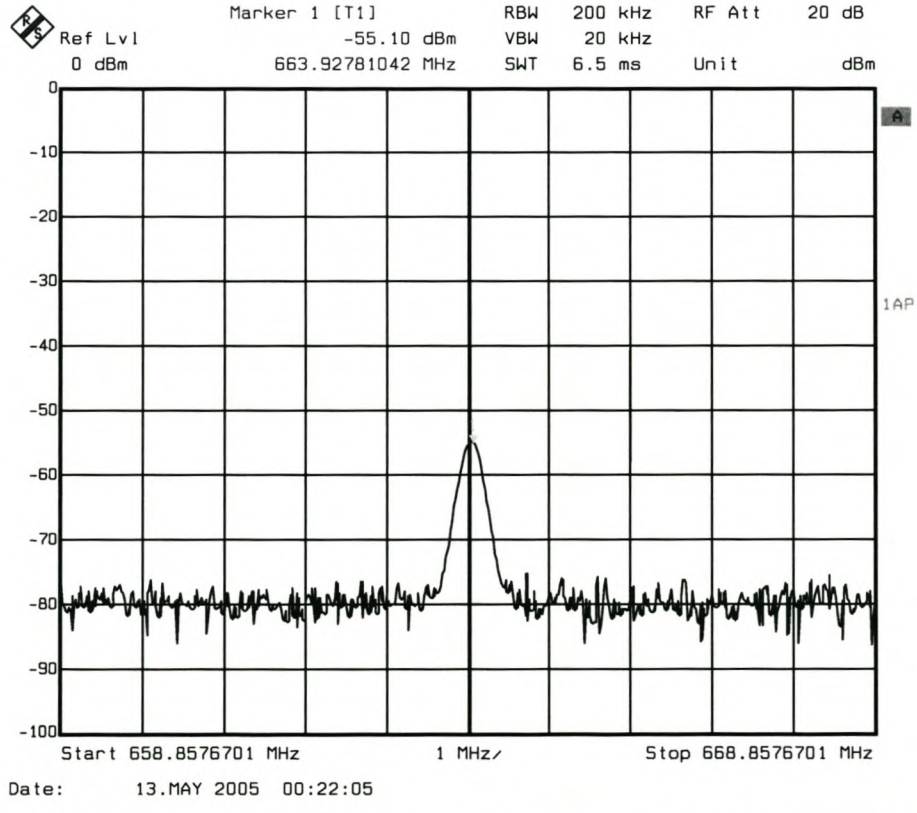

Figure 7-5: The IF signal with 10 MHz span of spectrum analyzer and -65 dBm RF power

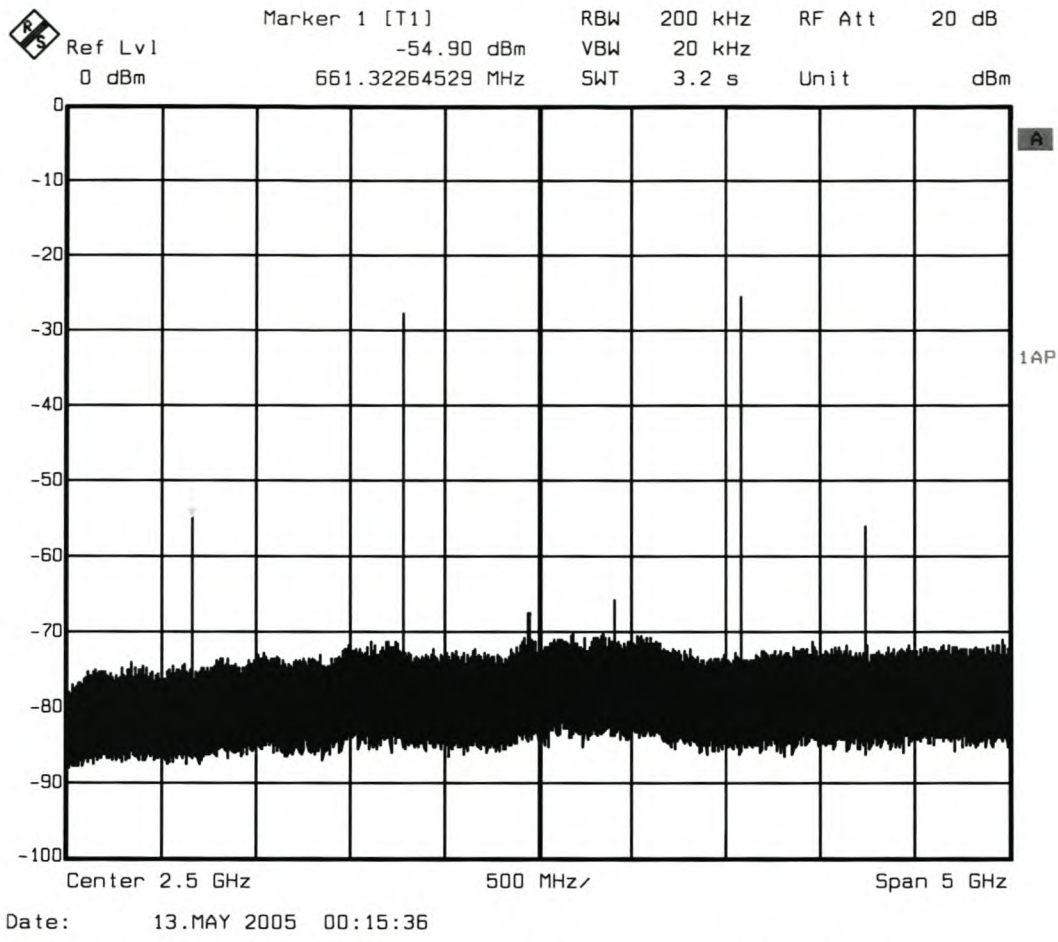

Figure 7-6: The enlarged span of figure 7-5, the IF port is showing the fundamental and second harmonic LO signals at the IF spectrum

The gain of the system is determined by subtracting input power from the output power from the graph of figure 7-2. Figure 7-3 gives the input and output 1 dB compression point of the system. The gain of the system is approximately 10.2 dB. The input and output P1dB of the system are -15.5 dBm and -6.0 dBm respectively. The system noise figure was determined using equation (1-19), and the mixer's noise figure was approximated to 7 dB and the overall noise figure is 2.6526 dB. The receiver contains no inband spurious signal while using an expected signal level from the transmitter. The image and IF rejection measured as illustrated in section 2-5 do not seem to affect the system with a maximum image and IF signal level of 13 dBm. There are no spurious radiations measured with Rhode & Schwarz FSEK 30 spectrum analyzer at the input port of the filter. Using the sensitivity in table 1-1 and equation (1-9), the SNR can be approximated to 41.35 dB.

7.3 Conclusion

The designed system components including commercially selected LNA were integrated together and measured as a single system. Fundamental properties of a receiver were measured and the receiver performs well in comparison to predictions. It has a gain of 1 dB less as compared to practical performance supposed in equation (7-1). The predicted IF frequency moved to a lower frequency by approximately 6%. The oscillator seems to have a load pulling problem with a mixer. The noise figure of the mixer was estimated to 7 dB as compared to its 6.8 dB conversion loss and the complete noise figure of the system is satisfactory. The IF and image rejections are completely out of the RF band and thus the front end is free from image and IF desensitization. There are no spurious radiations from the receiver to the antenna side port within 5 GHz span. The receiver components satisfied the proposed requirements for a data link.

7.4 Chapter Appendix

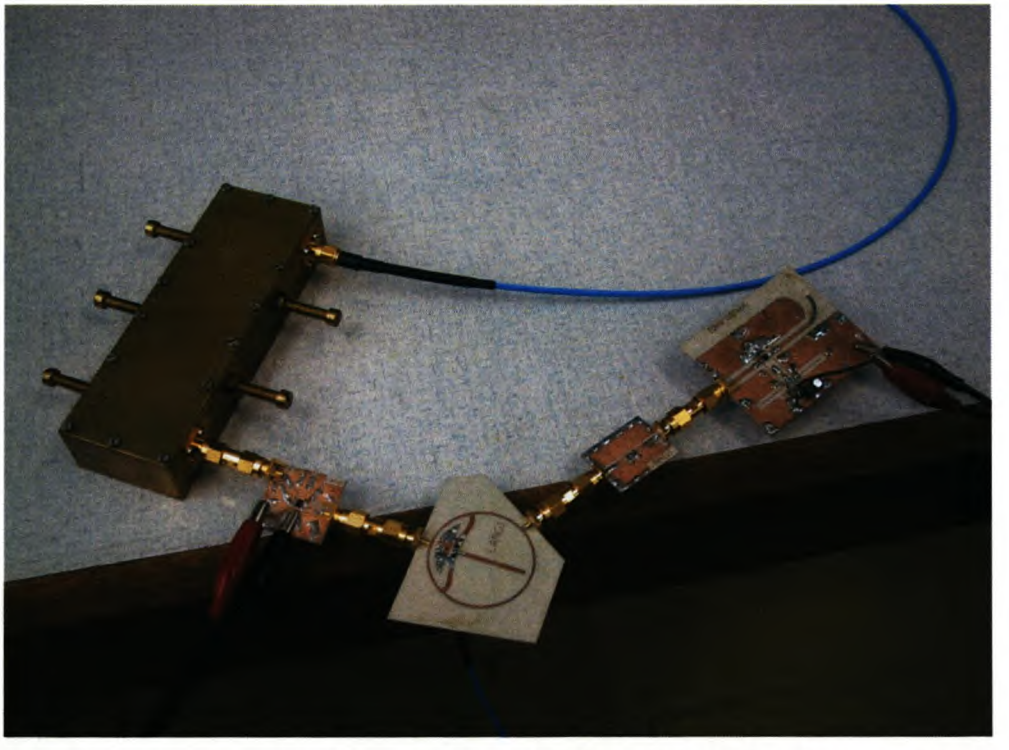

Figure 7-7: The measured system from left to right is filter, LNA, mixer, attenuator and the oscillator

8. Conclusion and Recommendations

8.1 Conclusion

The fundamental operating parameters of the receiver were investigated wich applies mostly to the Superheterodyne receiver. Three commercial components were selected and measured to model their performance parameters. The monofilar axial mode helix antenna was designed, constructed and measured, and it satisfied the high gain specifications of a point to point communications system. The narrow band interdigital filter was successfully designed and worked well. The open circuited resonator Colpitts modeled oscillator was designed and implemented using microstrip technology. It had high output power and worked as predicted from the harmonic balance nonlinear simulations using Microwave Office. The single balanced mixer was designed using 180^{o} hybrid junction and it was also modeled using nonlinear simulations. It was also implemented using a microstrip technology and it worked well though for optimum performance it required much lower power than obtained in the designed oscillator. The complete system was connected together and the commercially selected LNA was used as the RF amplifier, and the LO power was stepped down using a resistive attenuator. The system performed well in comparison to the expected performance and the goal of these studies was achieved.

8.2 Recommendations

The main purpose of this thesis was to design components of a microwave data link receiver front end system, and though achieved better components are needed to design high performance systems.

Bibliography

[1] David M Pozar, Microwave Engineering, third edition, John Wiley and sons, Inc, 2005

[2] Warren L. Stutzman and Gary A. Thiele, Antenna Theory and Design, 1998, John Wiley and sons, Inc.

[3] John D. Kraus, Antennas 2nd Edition, New York, McGraw-Hill, 1988

[4] Constantine A. Balanis, Antenna Theory Analysis and Design, 2nd Edition, Wiley and sons, Inc 1982, 1997.

[5] KD Palmer 2002, some useful equations for working with circularly polarized waves,

[6] P. Delmotte, G.A.E. Vandenbosch, An improved axial mode helix antenna design, Katholieke Universiteit Leuven, ESAT-Telemic, B-3001 Leuven.

[7] Robert Kellerman, The design of FM-CW proximity radar, March 2004,

[8] http://www.ece.mcmaster.ca/faculty/natalia/antenna_dload/
Antenna Measurements

[9] Antti V Raisaen and Arto Lehto, Radio Engineering for wireless Communication and sensor application, 2003 Artech House Inc.

[10] George L. Matthaei, MEMBER, IRE, Interdigital Band-Pass Filters, 1962

[11] R. J. Wenzel, Member, IEEE, Exact Theory of Interdigital Band-Pass Filters and Related Coupled Structures, 1965

[12] R.J. Wenzel, MEMBER, IEEE, Exact Design of TEM Microwave Networks Using quarter-Wave Lines, 1964

[13] Prof Petrie Meyer, 3rd Order Interdigital filter design

[14] Paul H Young, Electronic Communication Techniques, 4th Edition, 1999, 1994 prentice Hall, Inc.

[15] Jason Breitbath, Octave Tuning, High frequency Varactor Oscillator design, Oregon State University, 2001

[16] Stephen A Maas, Non Linear Microwave Circuits

[17] Randall W. Rhea, Oscillator Design and Computer Simulation, Noble Publishing Corporation, 1995, 2000

[18] AWR Microwave office Simulation Software 2003, 2004

[19] Robert E. Collin, Foundations for Microwave Engineering, second Edition, 1992, McGraw-Hill

[20] Stephen A Maas, Microwave Mixers, 2nd Edition, 1993 ARTECH HOUSE, INC.

[21] David M Pozar, Microwave and RF system Design of Wireless System, 2001, John Wiley and sons, Inc.

[22] David M Pozar, Microwave Engineering, 2nd Edition, 1998, John Wiley and sons, Inc.

[23] Liam Devlin, Mixers for Communication Technology, The IEE Event, How to design RF circuits, 2000

[24] JEREMY EVERAD, Fundamentals of RF Circuit Design with Low Noise Oscillator, 2001, John Wiley and Sons, LTD

[25] Stephen J. Erst. Receiving Systems Design, 1984. ARTECH HOUSE, INC.

[26] Mark Hunter, The Basics of Radio System, The IEE Event, How to design RF circuits, 2000

[27] Simon R. Saunders, Antennas and Propagation for Wireless Communication Systems, John Wiley and sons, 1999

[28] David B. Rutledge, The Electronics of Radio, 1999, Cambridge university press.

[29] Ian Hunter, Theory and Design of microwave filters, 2001, The Institution of Electrical Engineers.

[30] JB de Swardt, Notes on Mikrogolf Mengers, 2004

[31] J.O Meilus, M.J.A Smith, Journal of microwaves and optoelectronics Volume 1, number 3, 1998

[32] Peter Vizmuller, RF Design Guide: Systems, Circuits and Equations, 1995 ARTECH HOUSE, INC

[33] Microwave and RF Magazine, a Penton Publication, Semiconductor Issue, January 2005, Vol 44. No 1

Appendix A: Circuit Schematics

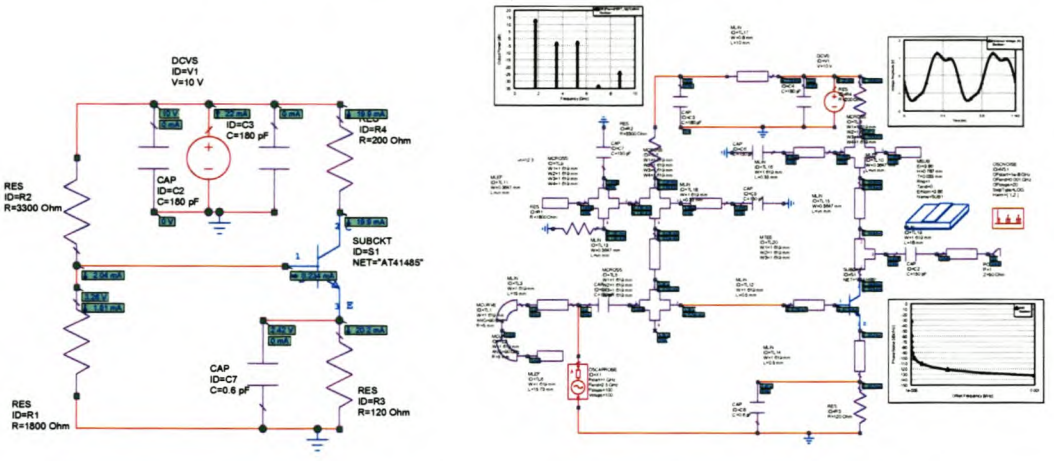

A-1: The Bias and complete oscillator circuit with some results schematics

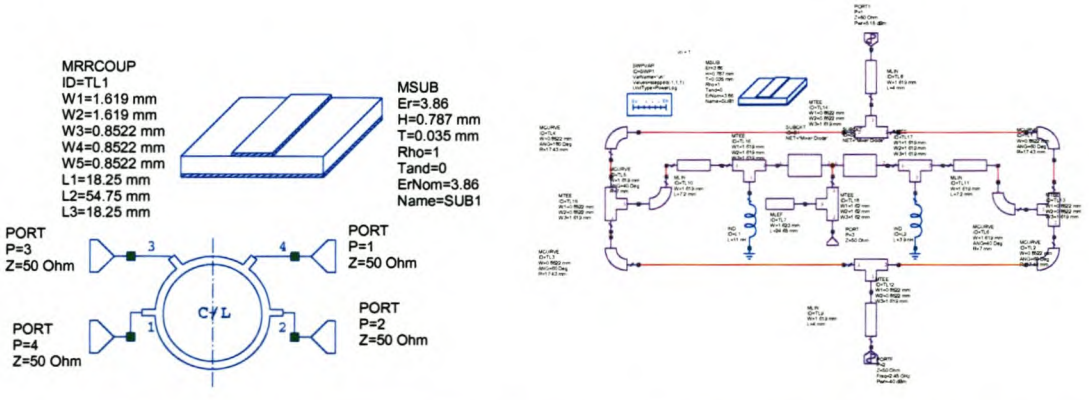

A-2: The Rat-race and bends used in the implementation of the mixer

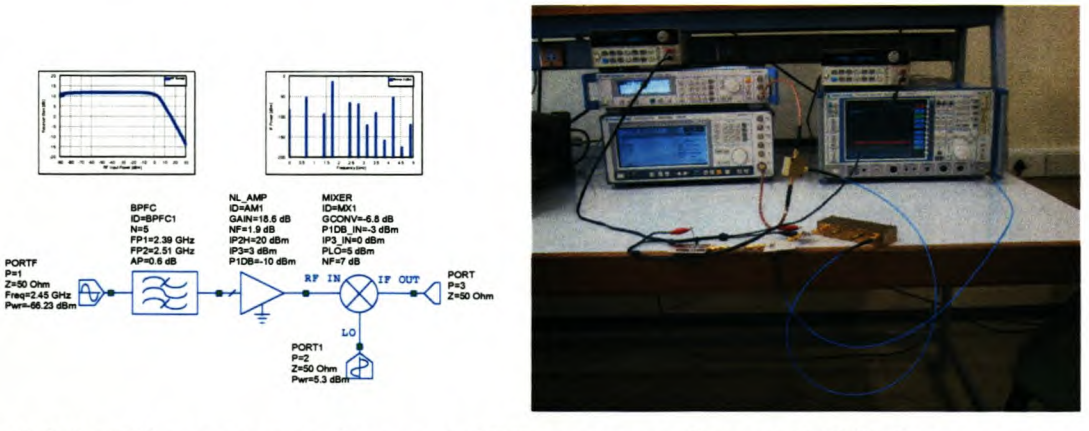

A-3: The Microwave receiver model RF sweep results and 5 GHz frequency span spectrum and the rejection measurements setup of the system

Appendix B: Constants Used

Symbol	description	Value
η_o	Characteristic impedance of free space	376.7 Ω
k	Boltzmann's Constant	8.854×10^{-12} J/°K
q	Charge of Electron	1.602×10^{-19} C
ε_0	Permittivity of free space	8.854×10^{-12} F/m
c	Speed of light in vacuum	2.9978×10^{8} m/s
μ_0	Permeability of free space	$4\pi \times 10^{-7}$ H/m

B-1: The table showing the constants used or explained